UNIVERSITÀ
DI SIENA
1240

Department of Medical Biotechnologies

Doctorate in Genetics, Oncology and Clinical Medicine (GenOMeC)

XXVIII Cycle

Coordinator: Prof.ssa Ilaria Meloni

Characterization of a flavivirus-inhibitory compound implicating Reticulon 3 as a potential host proviral factor

Scientific disciplinary sector: *MED/07 – Microbiology and clinical microbiology*

PhD Candidate
Erika Plicanti
Università di Pisa

Supervisor
Prof.ssa Giulia Freer
Università di Pisa

Co-supervisor
Prof. Leonardo Rossi
Università di Pisa

Academic Year
2024/2025

1. ABSTRACT 4

2. LIST OF ABBREVIATIONS 6

3. INTRODUCTION 8

3.1. *Flaviviridae* 9

3.1.1. Zika Virus 11

3.1.1.1. Virology and pathogenesis 11

3.1.1.2. Transmission 12

3.1.1.3. Clinical Manifestations 14

3.1.1.4. Diagnosis 15

3.1.2. West Nile Virus 16

3.1.3. Usutu virus 19

3.2. Other positive-sense single-stranded RNA viruses 19

3.2.1. SARS-CoV-2 19

3.2.2. Chikungunya virus 21

3.2.3. Coxsackievirus B5 22

3.3. Negative-sense single-stranded RNA viruses 23

3.3.1. Toscana virus 23

3.3.2. Influenza virus H1N1 24

3.3.3. Vesicular stomatitis virus 25

3.4. DNA viruses 26

3.4.1. Herpes simplex 2 26

3.4.2. Vaccinia virus 27

3.5. Single-stranded positive-sense RNA virus replication and replication organelle formation 29

3.5.1. Host proteins involved in RO biogenesis 32

3.5.2. The reticulon family (RTNs) 33

3.5.3. Other proteins involved in ER remodeling 35

3.6. Viruses and autophagy 37

3.7. Antiviral therapy 37

3.7.1. Antiflaviviral compounds 38

3.7.2. Antiviral compound repurposing 40

4. AIM OF THE STUDY 41

5. MATERIALS AND METHODS 43

5.1. Chemical compounds 43
5.2. Cell lines 43
5.3. Viruses 43
5.4. Determination of compound cytotoxicity and Cytotoxic Concentration 50% (CC_{50}) 44
5.5. Determination of viral yield reduction and Effective Concentration 50% (EC_{50}) 45
5.6. Western blotting 46
5.7. Immunostaining 47
5.8. Quantitative reverse transcriptase PCR (qRT-PCR) 48
5.9. Time-of-addition (TOA) experiments 49
5.10. Co-immunoprecipitation assay 49
5.11. Virucidal effect assessment 50
5.12. Cellular Thermal Shift Assay (CETSA) assay 51
5.13. Synergism between PS1097 and SOF 51
5.14. Selection of viral mutants 52
5.15. Proteasome inhibition assay to study RTN3 stability 52
5.16. Determination of RTN3, RTN4, FAM134B and GAPDH half-life 53
5.17. Graphics and statistic 53

6. RESULTS 54

6.1. Antiviral activity against ZIKV by a selection of compounds 54
6.2. Antiviral activity of PS1097 on different cell lines 56
6.3. Antiviral activity of PS1097 on different viruses 57
6.4. Determination of viral protein synthesis during treatment with PS1097 59
6.5. TOA experiments 65
6.6. Co-immunoprecipitation of ZIKV protein NS3 and NS2B 68
6.7. Does PS1097 have a virucidal effect? 70
6.8. CETSA assay 72
6.9. Determination of synergistic effects 75
6.10. Selection of PS1097-resistant variants 77
6.11. PS1097 causes potent downregulation of RTN3 protein 79
6.12. Does PS1097 promotes RTN3 degradation through the proteasomal pathway? 82
6.13. Protein half-life determination using cycloheximide chase assay 85

7. DISCUSSION AND CONCLUSION 87

8. BIBLIOGRAPHY 92

1. ABSTRACT

Viral infections remain among the most formidable challenges to global health, particularly due to the continuous emergence of new or re-emerging viruses. Within this context, the *Flaviviridae* family, which includes major human pathogens such as Zika virus (ZIKV), West Nile virus (WNV), and Dengue virus (DENV), represents a critical threat due to its capacity for rapid evolution, vector-borne transmission, and lack of effective antiviral therapies.

The development of direct-acting antivirals has increased treatment options for a number of RNA viruses, but this approach is often limited by the rapid onset of viral resistance. As an alternative, host-targeted antivirals (HTAs) have gained increasing attention because they interfere with host cellular pathways essential for viral replication, offering the potential for broad-spectrum activity and reduced resistance.

The present work aimed to identify and characterize novel antiviral compounds with activity against flaviviruses and other viruses of medical importance, while identifying possible host factors involved in their mechanism of action. An initial screening of 24 chemically diverse compounds, previously reported to inhibit other RNA viruses, was performed using ZIKV as a model flavivirus. Among these, the pyrido[2,3-g] quinoxalinone derivative (PS1097) emerged as the most potent antiviral candidate, exhibiting high selectivity and low cytotoxicity. Subsequent assays demonstrated that PS1097 inhibited viral replication across multiple virus families, indicating a potentially broad-spectrum effect.

To determine the mechanism of action of PS1097, a series of virological and biochemical assays were performed, including time-of-addition (TOA) experiments, virucidal tests, and protein interaction studies. These analyses revealed that PS1097 does not act directly on viral particles but rather interferes with intracellular replication stages, suggesting a host-targeted mechanism. Further investigation identified significant and selective downregulation of the endoplasmic reticulum (ER)-associated protein Reticulon 3 (RTN3) following PS1097 treatment. RTN3

belongs to a conserved family of ER-shaping proteins involved in the formation of replication organelles (ROs), specialized membrane structures induced by many positive-sense RNA viruses to facilitate replication and shield viral RNA from immune detection.

Functional assays and protein stability studies indicated that PS1097 does not promote RTN3 degradation through the proteasomal pathway. PS1097 did not exhibit virucidal properties nor interfere with viral entry, further supporting the hypothesis that its target lies within host cellular machinery. Collectively, these findings suggest that RTN3 may act as a proviral host factor exploited by flaviviruses to remodel ER membranes and establish replication organelles. The modulation of RTN3 expression by PS1097 provides a novel insight into the interplay between viral replication and ER dynamics, identifying a previously underexplored therapeutic target. Future directions include generating RTN3-overexpressing and RTN3-knockout cell lines to validate its functional role and to confirm whether PS1097-mediated RTN3 downregulation is the primary determinant of its antiviral effect.

In conclusion, this study contributes to the understanding of virus–host interactions centered on ER remodeling and establishes PS1097 as a promising lead compound for the development of host-directed, broad-spectrum antivirals. By uncovering the potential proviral role of RTN3, this research highlights a new cellular vulnerability that could be exploited for future antiviral strategies, particularly against flaviviruses and other emerging RNA pathogens.

2. LIST OF ABBREVIATIONS

ARF	ADP-ribosylation factors
ATL	Atlastin proteins
BVDV	Bovine Viral Diarrhea Virus
CC_{50}	Citotoxic Concentration 50%
CETSA	Cellular Thermal Shift Assay
CHIKV	Chikungunya Virus
CMC	Carboxymethyl cellulose
CNS	Central Nervous System
CO-IP	Co-immunoprecipitation
CV	Capsid protein
CV-B5	Coxsackie B5
DAA	Direct-Acting Antivirals
DENV	Dengue Virus
DMEM	Dulbecco's Modified Eagle Medium
DMSO	Dimethyl Sulfoxide
DMV	Double Membrane Vescicle
E	Envelope protein
EC_{50}	Effective Concentration 50%
EMEM	Eagle Minimum Essential Medium
ER	Endoplasmic Reticulum
FBS	Fetal Bovine Serum
h	hours
HCV	Hepatitis C virus
HSV-2	Herpes Simplex 2 Virus
HTA	Host-Targeted Antivirals
IAV	Influenza A Virus
MOI	Multiplicity Of Infection
NS	Nonstructural

OD	Optical Density
ORF	Open Reading Frame
p.i.	post infection
PBS	Phosphate Buffered Saline
PFA	Paraformaldehyde
PFU	Plaque Forming Unit
prM	precursor Membrane protein
RBV	Ribavirin
RdRp	RNA-dependent RNA-polymerase
REEP	Receptor Expression-Enhancing Proteins
ROs	Replication organelles
RT	Room Temperature
RT-PCR	Reverse transcription PCR
RTN	Reticulon
SD	Standard Deviation
SI	Selectivity Index
SOF	Sofosbuvir
$TCID_{50}$	Tissue Culture Infectious Dose 50%
TOA	Time Of Addition
TOSV	Toscana Virus
UTR	Untranslated Region
VACV	Vaccinia Virus
VACV-IND-G	Recombinant VACV with G of VSV Indiana strain
VSV	Vesicular Stomatitis Virus
WNV	West Nile Virus
ZIKV	Zika Virus

3. INTRODUCTION

Viral diseases remain one of the most pressing challenges to global health. Despite remarkable advances in medicine have been recently achieved, the continuous emergence and re-emergence of viral pathogens demonstrate the dynamic nature of host–pathogen interactions and the vulnerability of human societies to epidemic and pandemic threats. Over the past century, viral outbreaks have repeatedly highlighted the profound impact of these pathogens on public health, social stability, and economic development. From influenza pandemics in the early 1900s to more recent ones such as the spread of Zika virus (ZIKV) [1], the resurgence of West Nile virus (WNV) [2], and the unprecedented COVID-19 crisis, it has become increasingly evident that viral infections are not isolated medical problems, but global concerns shaped by ecological, demographic, and environmental factors. In this respect, the rapid adaptability of RNA viruses poses a unique threat. Their high mutation rates and capacity to exploit diverse hosts and vectors allow them to cross species barriers, expand into new geographic regions, and resist immune responses or therapeutic interventions.

Vector-borne viruses, transmitted by mosquitoes or other arthropods, are an example of emerging public health threats: globalization, climate change, and urbanization contribute to the widening distribution of competent vectors, facilitating the circulation of arboviruses in areas previously considered unaffected. At the same time, modern patterns of mobility and trade accelerate the international spread of pathogens, transforming local outbreaks into global health emergencies.

These challenges underscore the urgent need for deeper understanding of viral biology, mechanisms of transmission, and host interactions. Advances in molecular virology, genomics, and cell biology have provided powerful tools to investigate how viruses replicate, manipulate host pathways, and evade immune surveillance. Such knowledge not only clarifies the pathogenic potential of individual viruses but also reveals common strategies shared across viral families, opening the way for the development of broad-spectrum antiviral therapies. While vaccines remain an

essential preventive measure, the absence of effective vaccines for many viruses, combined with the threat of emerging pathogens, makes the discovery of safe and versatile antiviral compounds a critical research priority. Within this framework, the present dissertation focuses on the study of different RNA viruses of medical relevance, with particular attention to flaviviruses, their replication mechanisms, and the potential identification of antiviral compounds. By situating these viruses in the broader context of global health and antiviral research, this dissertation aims to contribute to the scientific effort of understanding viral pathogenesis and exploring new strategies to combat viral diseases.

3.1. *Flaviviridae*

The world has faced devastating pandemics caused by emerging or mutating viruses, with arboviruses posing significant challenges due to their rapid evolution and host range expansion. The flavivirus genome is approximately 10,794 nucleotides in length and encodes a single open reading frame (ORF) that translates into a polyprotein composed of 3,419 amino acids. This ORF is flanked by two untranslated regions (UTRs) at the 5' and 3' ends, which play essential roles in viral replication and interaction with host cell machinery. The flavivirus genome encodes a single polyprotein that is cleaved into three structural and seven non-structural (NS) proteins. The structural proteins comprise the capsid (CV), which encapsulates the viral RNA and contributes to uncoating and apoptosis; the precursor membrane protein (prM/M), which assists in virion assembly and prevents premature membrane fusion; and the envelope (E) glycoprotein, which mediates receptor binding and membrane fusion and represents the principal target for neutralizing antibodies and vaccine development. The non-structural proteins play equally critical roles in viral replication and immune modulation: NS1 supports replication and immune evasion and is secreted at high levels during infection, serving also as a diagnostic marker; NS2A and NS2B contribute to replication and immune suppression, with NS2B acting as a cofactor for the NS3 protease; NS3 is a

multifunctional enzyme with protease and helicase activity essential for genome replication; NS4A and NS4B remodel host membranes and antagonize interferon responses; and NS5, the largest non-structural protein, possesses RNA-dependent RNA polymerase (RdRp) and methyltransferase activities and functions as a key interferon antagonist (Fig.1) [3].

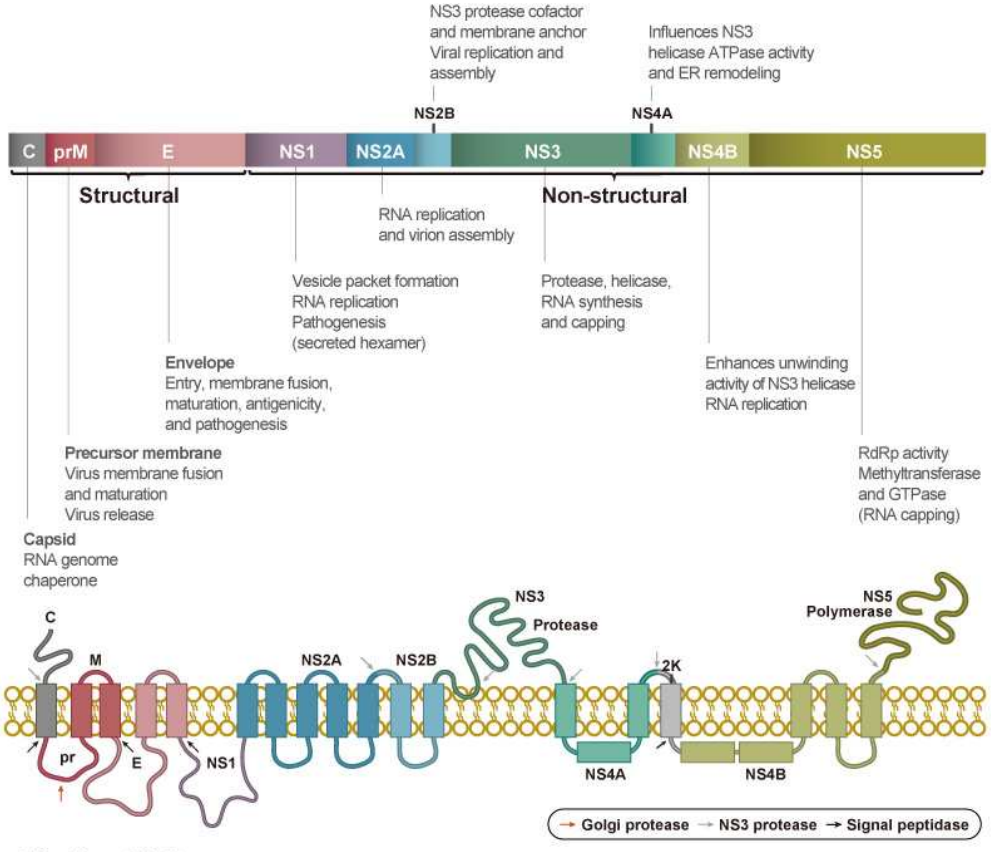

Figure 1: Schematic overview of the proteins encoded by flaviviruses genome, in particular ZIKV [4].

The UTR at both genome ends regulate replication and translation. Some protein features, such as glycosylation of the E protein, influence viral virulence and host adaptation, though their roles remain under study.

The UTRs in ZIKV exhibit secondary structures that are conserved among flaviviruses and necessary for efficient viral RNA replication [5].

In vertebrates, the virus enters host cells through receptor-mediated endocytosis, primarily via DC-SIGNR, followed by membrane fusion at low pH (6.3–6.9). After

fusion, viral RNA is released into the cytoplasm, where replication and assembly occur. New virions bud into the endoplasmic reticulum, mature through prM cleavage, and are released by exocytosis. Mosquito saliva contributes to immune evasion at the infection site by suppressing T-cell responses, facilitating early viral spread [6].

3.1.1. Zika Virus

A notable example is ZIKV (family *Flaviviridae,* genus *Orthoflavivirus*), discovered in 1947 as the cause of a mild disease spread by *Aedes aegypti* mosquitoes in monkeys [7]. In 1954, the first 3 cases of human infection were reported in Nigeria [8], after which symptomatic ZIKV infections were limited to isolated cases or small, self-limiting clusters. This epidemiological pattern shifted dramatically in 2007 with the first large-scale outbreak documented in Yap Island, part of the Federated States of Micronesia. During this event, approximately 73% of the island's population was estimated to have been infected, although only about 18% of those infected developed symptomatic disease, highlighting ZIKV high rate of subclinical infection [9]. Following the Yap outbreak, ZIKV began to spread rapidly across the Pacific region and beyond. Significant outbreaks were subsequently reported in French Polynesia, the Cook Islands, Easter Island, and New Caledonia, each associated with increasing clinical awareness and surveillance capacity. The virus ultimately reached the Americas, where it caused a major public health crisis beginning in 2015 [10]. Sporadic cases have also been recorded in Europe, typically linked to travelers returning from endemic regions, underscoring the virus capacity for global dissemination through human mobility and competent vectors.

3.1.1.1. Virology and pathogenesis

ZIKV stands out among flaviviruses for several distinctive features in both virology and pathogenesis. Unlike most members of its genus, ZIKV has evolved a

pronounced tropism for placental and neural tissues. The envelope protein E, while structurally homologous to that of other flaviviruses, contains determinants that allow efficient infection of neural progenitor cells and placental cell types, including trophoblasts and Hoffbauer cells. This unique cellular targeting underpins two hallmarks of ZIKV pathogenesis: congenital transmission and disruption of fetal neurodevelopment [11].

3.1.1.2. Transmission

ZIKV, like other members of the *Flaviviridae* family, is primarily transmitted to humans through the bite of infected mosquitoes belonging to the genus *Aedes*—specifically within the subgenus *Stegomyia*. Several *Aedes* species have been implicated in ZIKV transmission, including *Ae. aegypti*, *Ae. africanus*, *Ae. hensilli*, and *Ae. albopictus* [12]. Among these, *Ae. aegypti* is widely regarded as the principal vector in urban and peri-urban settings, particularly across Asia, and was identified as the likely primary vector during the 2013–2014 outbreak in French Polynesia [13]. Field studies have confirmed the presence of ZIKV RNA in wild-caught *Ae. aegypti* mosquitoes, while laboratory-based vector competence experiments have demonstrated their efficiency in acquiring, replicating, and transmitting the virus [14]. Although *Ae. hensilli* mosquitoes were epidemiologically linked to the 2007 outbreak on Yap Island, ZIKV has never been successfully isolated from this species in nature, raising questions about its role as a competent vector under natural conditions [15].

In African regions, the situation is more complex. While *Ae. africanus* is a known sylvatic vector involved in the enzootic transmission cycle of ZIKV among non-human primates, the identity of the primary vector responsible for human infections remains uncertain. *Ae. albopictus* was suggested as the probable vector during the 2007 outbreak in Gabon, based on viral detection in field-collected specimens [13]. This species, known for its ecological plasticity and invasive capacity, poses a

growing concern due to its expanding geographic range and ability to transmit multiple arboviruses, including ZIKV.

ZIKV is primarily acquired by *Aedes* mosquitoes during a blood meal from a viremic host. Following ingestion, the virus undergoes replication within the mosquito midgut, disseminates through the hemocoel, and eventually reaches the salivary glands, enabling transmission to a new host during subsequent feeding [16]. Experimental studies using blood-feeding membrane systems have demonstrated that ZIKV is present in high concentrations in mosquitoes immediately after ingestion, becomes undetectable around day 10, and reemerges with high viral loads by day 15, remaining detectable through at least day 60. These findings indicate an extrinsic incubation period of approximately 10 days in *Ae. aegypti* mosquitoes [17].

In addition to mosquito-borne transmission, ZIKV can spread through several non-vectorial routes. Vertical transmission has been well documented, both intrauterine and peripartum. Intrauterine transmission is supported by the detection of ZIKV RNA in the amniotic fluid of symptomatic pregnant women whose fetuses subsequently developed microcephaly [18]. ZIKV RNA has also been identified in fetal tissues and in the brains of two live-born infants with congenital microcephaly who died within 20 hours of birth. Intrapartum transmission is further suggested by cases in which neonates were found to be viremic within four days of birth to infected mothers. Although ZIKV RNA has been detected in breast milk, no cases of transmission through breastfeeding have been reported to date [19].

Sexual transmission of ZIKV has also been well documented, with infectious virus detected in semen up to several weeks post-infection [20]. Although less frequent, probable transmission *via* blood transfusion has been reported. During the 2013–2014 French Polynesia outbreak, ZIKV RNA was detected in 2.8% (42/1,505) of asymptomatic blood donors, some of whom developed Zika-like symptoms days after donation [21].

3.1.1.3. Clinical Manifestations

In humans, the incubation period of ZIKV infection, from mosquito bite to symptom onset, is approximately 3 to 12 days. The majority of infections are asymptomatic, with estimates suggesting that up to 80% of individuals may not exhibit any clinical signs [9]. ZIKV can affect individuals of all ages, ranging from neonates to the elderly (4 days to 76 years), with a slight predominance among females.

When symptomatic, ZIKV infection typically presents as a mild, self-limiting illness with nonspecific features that often overlap with other arboviral infections such as Dengue virus (DENV) and Chikungunya virus (CHIKV), complicating clinical diagnosis. The most reported symptoms include maculopapular and pruritic rash, low-grade fever, arthralgia, myalgia, fatigue, headache, and nonpurulent conjunctivitis. Rash is a prominent finding, usually beginning on the face or trunk and spreading centrifugally to the extremities. It typically resolves spontaneously within 1–4 days. Most symptoms subside within two weeks, although rare cases of prolonged illness have been reported [22].

In recent outbreaks, particularly in Brazil, ZIKV has been increasingly associated with serious complications. Reports of congenital anomalies, such as microcephaly, rose sharply during the 2015–2016 outbreak. Similarly, during the 2013–2014 outbreak in French Polynesia, health officials noted an apparent rise in congenital central nervous system malformations.

Experimental evidence supports a potential neurotropic effect of ZIKV. One proposed mechanism for ZIKV-induced microcephaly involves disruption of autophagy pathways, which are critical for centrosome stability. Centrosome dysregulation has been implicated in abnormal brain development, and mouse studies have shown that increased centrosome numbers can result in microcephaly. This suggests a plausible cellular mechanism through which ZIKV might impair neurodevelopment during pregnancy (Fig .2) [23].

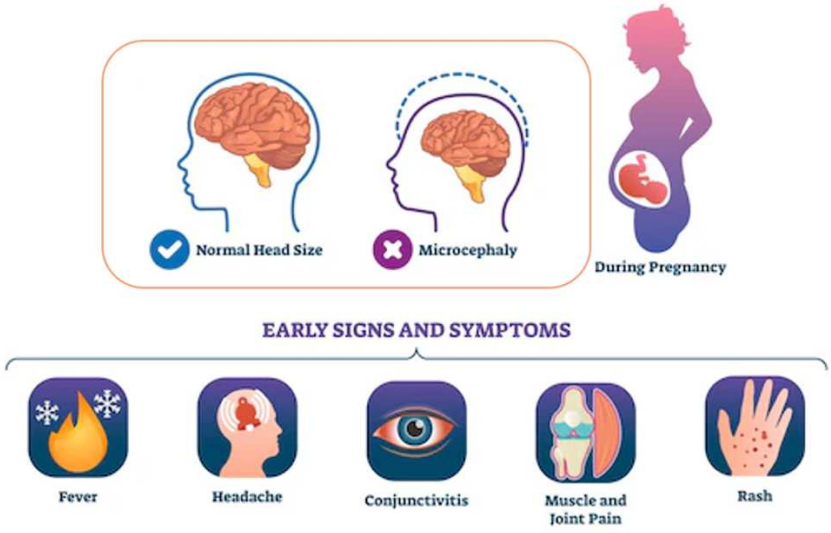

Figure 2: Schematic representation of the symptoms and clinical manifestations of ZIKV infection [Image generated with FreePik.com].

ZIKV has also been linked to severe neurological outcomes in adults, including meningitis, meningoencephalitis, and Guillain-Barré syndrome. Although ZIKV infection was confirmed in some of these cases, a definitive causal relationship remains under investigation [24].

3.1.1.4. Diagnosis

Clinical evaluation alone is insufficient to reliably diagnose ZIKV infection due to symptom overlap with other arboviruses. As a result, laboratory testing is essential. Patients presenting with acute fever, rash, myalgia, or arthralgia within two weeks of travel to areas with active ZIKV transmission should be evaluated for ZIKV, CHIKV and DENV simultaneously.

Molecular amplification techniques like Real-Time PCR (RT-PCR) on various specimens remain the most specific and preferred diagnostic tools for ZIKV during the acute phase (within 7 days of symptom onset) [25]. Serologic testing is generally not recommended during this early period because ZIKV IgM antibodies may not yet be detectable. RT-PCR testing must occur during the viremic phase of the illness, which may be as short as five days [20]. When RT-PCR results are negative after this

window, serologic testing should be considered. The choice of specimen also affects diagnostic accuracy. While serum and cerebrospinal fluid are commonly used, alternative specimens such as urine, saliva, amniotic fluid, and tissue are being evaluated [25]. Urine and saliva are particularly useful when blood samples are difficult to obtain, such as in pediatric or remote settings. Viral RNA can be detected in urine for up to 20 days; after this, it is no longer present in the blood. Therefore, urine RT-PCR should be considered for suspected ZIKV cases with negative serum results [26]. Similarly, saliva testing may improve detection rates during the acute phase, although it does not extend the diagnostic window beyond that of blood testing. For this reason, blood remains the preferred specimen for diagnosis [27].

3.1.2. West Nile Virus

WNV is another mosquito-borne member of the *Flaviviridae* family [28]. The virus was first identified in 1937 in a febrile patient from the West Nile Province of Uganda. Initially considered of limited significance to human health due to its typically mild and subclinical presentation, WNV has since been implicated in substantial morbidity and mortality across a range of animal species. WNV has been documented to cause disease in birds, horses, sheep, reptiles, cats, and rodents in addition to humans. Over the past two decades, there has been a marked increase in reported cases among humans and equines in industrialized countries [3]. Based on seroprevalence surveys, approximately 80% of human WNV infections are asymptomatic, 20% cause a febrile illness, and less than 1% cause neuroinvasive disease (eg, meningitis, encephalitis, acute flaccid myelitis). Mortality of patients with neuroinvasive disease is approximately 10% overall but it is 20% in individuals 70 years old or older and 30% to 40% in patients with hematologic malignancies, solid organ transplants, and those receiving B-cell–depleting monoclonal antibodies [29].

The 1999 New York City outbreak marked the first detection of WNV in the Western hemisphere. Initially mistaken for St. Louis encephalitis, the epidemic was linked to concurrent bird die-offs and later confirmed as WNV. Active surveillance identified 59 hospitalized cases, mostly elderly. Clinical features included fever, encephalitis (63%), meningitis (29%), and, unusually, profound muscle weakness (27%) and flaccid paralysis (10%), associated with axonal polyneuropathy. Mortality reached 12%, higher among patients ≥75 years and those with diabetes (Fig .3A) [30,31].

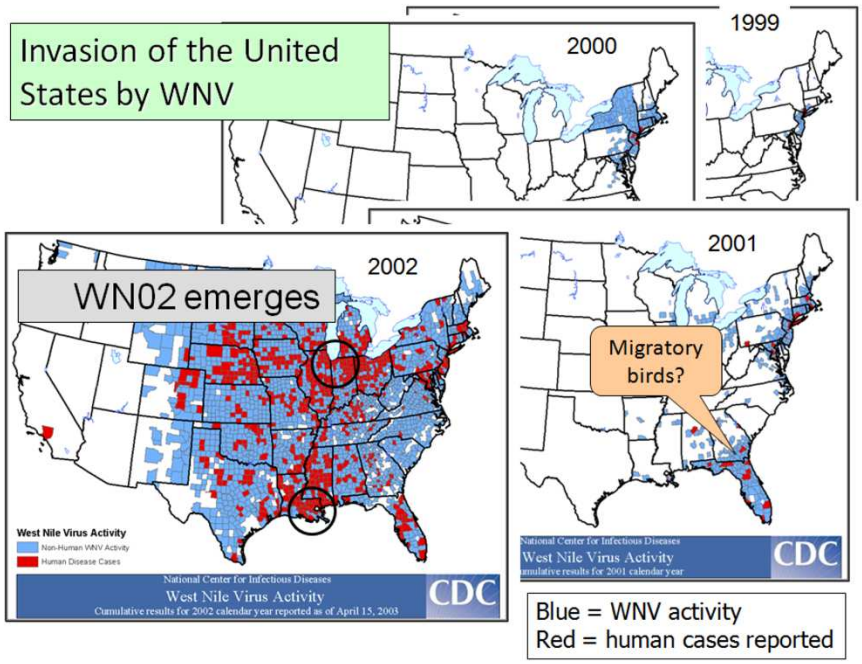

Figure 3: Sequence of maps showing the rapid expansion in the distribution of WNV activity and human cases in the eastern United States from 1999 through 2002. Circles roughly circumscribe epicenter [30].

WNV in Italy was first detected in horses in Tuscany in 1998 without any human cases. After a period of apparent silence, the virus re-emerged in 2008 in the Po Valley and northern regions, marking the first confirmed human neuroinvasive infections. Since then, WNV has become endemic in Italy, with circulation detected every summer in mosquitoes, birds, horses, and people, especially in the north but increasingly extending southward. Different viral lineages have been found over time: Lineage 1 dominated early outbreaks, while Lineage 2 established itself from

around 2011 and became widespread, though recent years have seen both lineages co-circulating. Outbreak intensity varies considerably year by year, with 2018 standing out as the worst season on record, when hundreds of human cases and multiple deaths were reported. More recently, Italy still is one of the European countries most affected by WNV, with dozens of human cases in 2025. Indeed, the latest national bulletin reports 718 confirmed human cases of WNV infection, of which 341 developed the neuroinvasive form and 49 resulted in death [32].

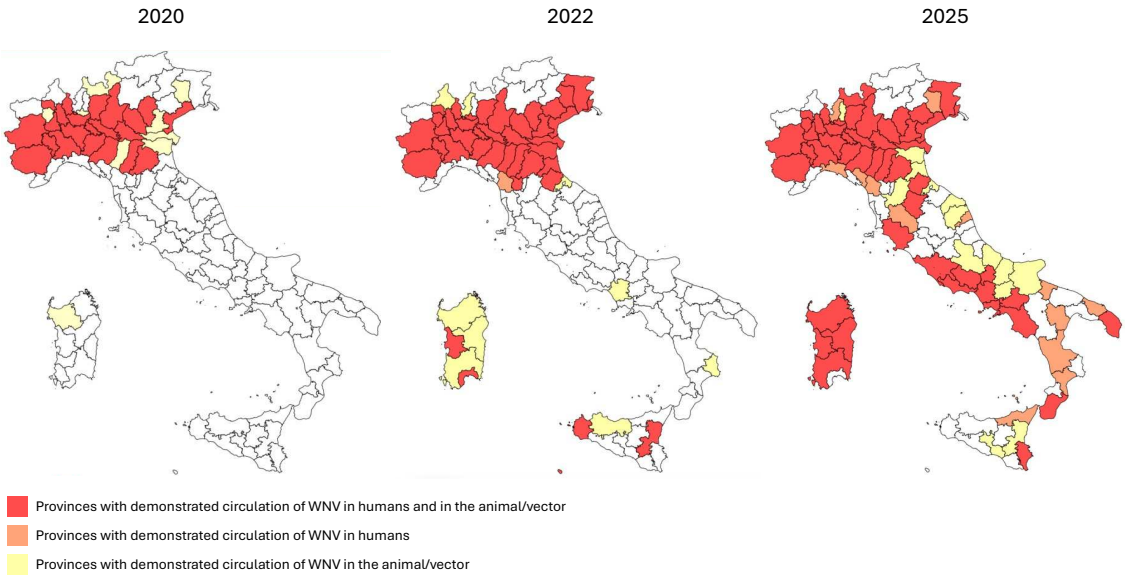

Figure 4: Geographical spread of WNV circulation across Italian provinces from 2020 to October 2025, highlighting areas with confirmed human and vector cases [32].

Transmission primarily occurs *via* the bite of infected mosquitoes of the *Culex* genus [33]. However, alternative routes have been observed under experimental conditions and in real-world cases, including ingestion, aerosol exposure, and direct contact [34].

Despite ongoing efforts, no licensed vaccine is currently available for human use against WNV. WNV maintains its zoonotic cycle primarily between birds (reservoir hosts) and mosquitoes (vectors). Birds often show no symptoms but sustain viremia sufficient to infect mosquitoes. Culex mosquitoes acquire the virus during a blood meal, allow it to replicate in their midgut, and eventually transmit it via saliva during

subsequent feeding. The virus reaches the salivary glands through the hemolymph. Despite systemic infection, mosquitoes do not develop disease. Incidental or final hosts, including humans, horses, and other mammals, become infected via mosquito bites but typically do not sustain viremia high enough to transmit the virus, thus acting as dead-end hosts [3].

3.1.3. Usutu virus

Usutu virus (USUV) is an emerging mosquito-borne flavivirus originally discovered in South Africa in 1959. In recent years, it has spread across much of Europe, where it has been associated with significant avian mortality and, less frequently, human infections. USUV circulates mainly between birds and *Culex* mosquitoes, with humans considered incidental hosts.

Although most human infections are asymptomatic or mild, several cases of serious neurological disease, such as encephalitis, have been reported especially in immunocompromised individuals. The virus shares many similarities with WNV, both genetically and ecologically, which can complicate diagnosis due to serological cross-reactions. In some cases, infections are only discovered incidentally during blood donation screening. The growing presence of USUV in Europe, often overlapping with WNV, raises concerns about public health surveillance and diagnostic capacity [35].

3.2. Other positive-sense single-stranded RNA viruses

3.2.1. SARS-CoV-2

In December 2019, several cases of pneumonia of unknown etiology were reported in Wuhan, China. Many were linked to a seafood and live animal market. A novel coronavirus was isolated and initially named 2019-nCoV, later renamed SARS-CoV-

2. This virus is responsible for the third major zoonotic coronavirus outbreak (COVID19) in 20 years, following SARS-CoV in 2002 and MERS-CoV in 2012 [36]. SARS-CoV-2 infection spread rapidly across the globe in early 2020. On March 11, 2020, the WHO declared a global pandemic. Bioinformatic studies confirmed that SARS-CoV-2 belongs to the *Betacoronavirus* genus and shares 96% genetic identity with the bat coronavirus RaTG13, suggesting a natural origin, with bats as the likely reservoir. Pangolin may have served as an intermediate host, due to strong genetic similarities of SARS-CoV-2 with several pangolin coronaviruses [37]. Transmission occurs mainly through respiratory droplets and aerosols, but indirect contact via contaminated surfaces and a possible fecal-oral route have also been suggested. Clinically, infection ranges from asymptomatic to COVID19, a severe illness, including pneumonia, respiratory failure, and death. SARS-CoV-2 targets ACE2-expressing cells, especially in the lungs, aided by the host protease TMPRSS2 [38]. The virus has a positive-sense RNA genome encoding structural and non-structural proteins. The spike (S) protein, crucial for cell entry, binds to ACE2 and must be cleaved by proteases like TMPRSS2 or furin to become active. After entry, the virus hijacks the machinery of the host to replicate, assemble, and release new virions (Fig. 5) [39].

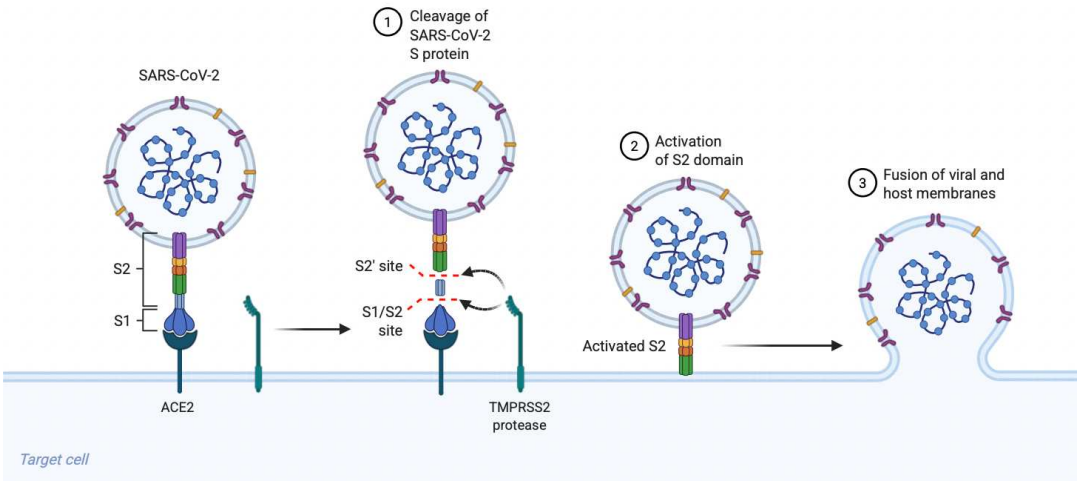

Figure 5: Mechanism of SARS-CoV-2 viral entry [Image created in BioRender.com]

SARS-CoV-2 can trigger a strong inflammatory response, particularly in severe cases, leading to cytokine storm, vascular damage, and organ failure. Elevated

levels of IL-6 and IL-8, neutrophil activation, and endothelial dysfunction are common findings in critical patients [40]. At the start of the pandemic, treatment focused on repurposed antivirals (e.g., remdesivir), anti-inflammatory agents (e.g., dexamethasone), and supportive care. Monoclonal antibodies were later developed to neutralize the virus. New antivirals such as paxlovid (nirmatrelvir + ritonavir) and molnupiravir were authorized for emergency use only later [41]. Vaccination became the primary tool for prevention. mRNA vaccines and viral vector vaccines target the S protein, eliciting both antibody and T-cell responses. However, ongoing viral mutations challenge vaccine efficacy, reinforcing the need for booster doses and updated formulations [42,43].

3.2.2. Chikungunya virus

CHIKV is an arthropod-borne virus belonging to the *Alphavirus* genus in the *Togaviridae* family. It was first identified in Tanzania in the early 1950s and has since caused several outbreaks around the world. CHIKV is primarily transmitted to humans through the bite of infected *Ae. aegypti* and *Ae. albopictus* mosquitoes. The virus is enveloped, with structural and non-structural proteins that facilitate replication, entry into host cells, and evasion of the immune response.

In recent years, the virus has re-emerged globally, causing significant outbreaks in Africa, Asia, the Americas, and even parts of Europe. Climate change, global travel, and the expansion of mosquito habitats have all contributed to this resurgence. CHIKV infection typically causes a sudden onset of high fever, rash, headache, and is characterized by severe joint pain, particularly in the hands, wrists, ankles, and knees. While most cases resolve within a few days to a week, some patients, especially older adults or those with pre-existing conditions, experience prolonged joint pain and fatigue that can last for weeks or months. Although rarely fatal, the disease can severely impact quality of life and productivity.

The pathogenesis of CHIKV involves both viral replication and the host immune response. Upon entry into the host, the virus rapidly spreads to various tissues,

including joints, where it infects synovial fibroblasts and macrophages. This triggers a strong innate immune response, characterized by the production of pro-inflammatory cytokines such as IL-6 and TNF-α. These cytokines help control viral replication but also contribute to the inflammation and pain commonly observed during infection. In some cases, the immune response becomes dysregulated, leading to chronic inflammation and persistent arthralgia. Additionally, although less common, CHIKV infection has been associated with neurological complications, such as encephalitis and Guillain–Barré syndrome, particularly in infants and immunocompromised individuals. Vertical transmission from mother to child during childbirth has also been documented, with potential for serious neonatal illness [44].

3.2.3. Coxsackievirus B5

Coxsackievirus B5 (CV-B5) is a serotype of the Enterovirus betacoxsackie species within the *Picornaviridae* family. It is a small, non-enveloped virus which, like other enteroviruses, is acid-stable and resilient in the environment, capable of surviving in water, on surfaces, and within the human gastrointestinal tract. The virus is primarily transmitted via the fecal-oral route, although respiratory transmission is also possible. It tends to infect children more frequently, especially during the summer and early autumn months in temperate regions [45].

Epidemiologically, CV-B5 has been implicated in both sporadic cases and regional outbreaks across Europe, Asia, and South America. While it often causes mild febrile illness or gastrointestinal symptoms, CV-B5 is also recognized for its ability to cause more serious complications. These include aseptic meningitis, encephalitis, and myocarditis. In neonates and immunocompromised individuals, the virus can lead to severe systemic illness that may mimic bacterial sepsis. Furthermore, CV-B5 has been studied in relation to the onset of autoimmune conditions, particularly type 1 diabetes, although a definitive causal link remains under investigation [46].

The pathogenesis of CV-B5 begins with viral replication in the lymphoid tissue of the oropharynx and gut. The virus then spreads through the bloodstream, potentially reaching secondary target organs such as the central nervous system, heart, and pancreas. In the brain, it can cause inflammation of the meninges or brain parenchyma, while in the heart, it may result in myocarditis, an inflammation that can lead to cardiac dysfunction. Despite most infections being self-limiting, the ability of the virus to invade critical tissues underscores its clinical importance [47]. Currently, there is no specific antiviral treatment or vaccine for CV-B5 [48]. Management is supportive, and preventive strategies rely on good hygiene practices, especially in settings such as childcare centers and schools. Surveillance and molecular typing are crucial for monitoring the circulation of this virus and detecting outbreaks early. Given its potential to cause serious disease and its global spread, CV-B5 continues to be an important public health concern, particularly in pediatric populations [49].

3.3. Negative-sense single-stranded RNA viruses

3.3.1. Toscana virus

Toscana virus (TOSV) is a sand fly–borne *phlebovirus* endemic to the Mediterranean region. As a negative-sense RNA arbovirus in the *Phenuiviridae* family, TOSV possesses a segmented genome encoding the L (polymerase), M (glycoproteins), and S (nucleoprotein) segments and is enveloped and spherical in shape, measuring approximately 80–120 nm [50]. While many infections result in mild or asymptomatic febrile illness, TOSV is noteworthy for its neurotropic potential. It is recognized as a leading cause of summer aseptic meningitis and meningoencephalitis in southern Europe, particularly in Italy, Spain, France, and Croatia. Humans are incidental ("dead-end") hosts, and although most infections do not lead to central nervous system (CNS) involvement, a small but significant proportion do, with a median incubation period of around 12 days for neuroinvasive

disease [51]. Recent national surveillance data from Italy demonstrate a notable rise in neuroinvasive TOSV cases, with 276 confirmed cases reported in 2022–2023, nearly 2.6 times the incidence observed in 2016–2021. Cases were increasingly reported across 12 of Italy's 21 regions during this period, expanding beyond traditional hotspots such as Emilia-Romagna and Tuscany into previously unaffected areas like Sardinia, Umbria, Molise, and Trento [52]. Pathogenesis involves the virus entering through the bite of an infected Phlebotomus species sand fly. After initial infection and replication, TOSV may disseminate to the CNS, causing inflammation of the meninges or brain parenchyma. Though most cases remain benign, neuroinvasive forms of the disease can include meningitis, encephalitis, and even peripheral neuropathies such as Guillain–Barré syndrome. Diagnosis requires laboratory testing such as RT-PCR or serology, due to clinical overlap with other arboviral neuroinfections. There are no specific antiviral treatments or vaccines; management remains supportive, and prevention relies primarily on vector control and personal protection against sand fly bites [52].

3.3.2. Influenza virus H1N1

The Influenza A virus (IAV) A/Puerto Rico/8/1934 (PR8) strain is a laboratory-adapted H1N1 subtype of Influenza A virus, first isolated from a human patient during the 1934 influenza season. It has since become a model strain for experimental virology due to its high adaptability and stability in laboratory settings. PR8 is a negative-sense single-stranded RNA virus with a segmented genome (8 segments), encoding proteins such as hemagglutinin, neuraminidase, and internal proteins including nucleoprotein, matrix proteins (M1/M2), nonstructural proteins (NS1/NS2), and the RNA polymerase complex. The hemagglutinin and neuraminidase proteins define its subtype as H1N1.

This strain is mouse-adapted, capable of replicating efficiently in murine respiratory tissues, causing consistent infection characterized by weight loss, lung inflammation, and immune activation; it is used as a backbone for reassortant

vaccine production, providing internal genes that support high-yield growth in embryonated chicken eggs. PR8 is stable and well-characterized, allowing reproducibility in studies of pathogenesis, immunology, and vaccine efficacy. PR8 does not reflect the full pathogenicity of seasonal or pandemic influenza in humans but is invaluable in controlled experiments due to its predictable replication and immunological behavior in animal models [53].

3.3.3. Vesicular stomatitis virus

Vesicular stomatitis virus (VSV), a member of the *Rhabdoviridae* family, genus *Vesiculovirus*, includes three species (Alagoas, New Jersey, and Indiana) which are all enveloped with helical capsids. VSV primarily affects livestock such as cattle, pigs, and horses, but it also has zoonotic potential and is transmitted through various routes. Natural transmission occurs via arthropod vectors (e.g., sandflies, mosquitoes, and biting flies) or through direct contact between infected animals.

The viral entry mechanism is mediated by the glycoprotein G, which facilitates two critical stages of infection: attachment to the host cell surface and membrane fusion. Following attachment, the virus is internalized via clathrin-mediated endocytosis, and the acidic pH of the endosome triggers fusion of the viral envelope with the endosomal membrane, allowing release of the viral nucleocapsid into the cytoplasm [54]. Replication occurs entirely in the cytoplasm, followed by viral egress through budding. This process is regulated by the viral matrix protein (M), which interacts with various cellular components and leads to rapid disassembly of host cell architecture [55].

Although VSV infection in humans is typically mild and self-limiting, the virus biological properties, such as its strong immunogenicity, high replication efficiency, and simple genome, have made it an attractive tool in virology research [56].

3.4. DNA viruses

3.4.1. Herpes simplex 2

Herpes simplex virus 2 (HSV-2) belongs to the *Herpesviridae* family. It has large, double-stranded DNA genome enclosed in a capsid, surrounded by a protein layer called the tegument, and wrapped in a lipid envelope containing viral glycoproteins. Infection begins when these glycoproteins help the virus attach to molecules on the surface of host cells. Several specific receptors and viral proteins are involved in allowing the virus to enter cells, and this process varies depending on the type of tissue the virus is infecting (some receptors are more important than others in the nervous system). Once inside the cell, the viral envelope fuses with the host cell membrane, releasing the capsid and tegument proteins. Some of these proteins travel to the cell's nucleus, guiding the viral DNA along microtubules using the host transport machinery. Once the DNA enters the nucleus, the virus begins its replication cycle. Viral genes are expressed in a specific order: first immediate early genes that prepare the cell for infection, then early genes involved in DNA replication, and finally late genes that help build new viral particles. All of this occurs in the nucleus. After replication, newly formed viral capsids exit the nucleus through a complex process involving temporary wrapping and unwrapping by nuclear membranes. Once in the cytoplasm, they acquire more proteins and a final envelope at specialized membrane sites such as the Golgi apparatus. These mature, fully assembled viral particles are then transported to the cell surface, often in vesicles, and released by fusion with the plasma membrane [57].

HSV-2 initially infects skin or mucosal epithelial cells, typically in the genital area, then travels to peripheral neurons where it establishes lifelong latency. It can occasionally reach the central nervous system, causing serious diseases like encephalitis. During latency, the virus remains dormant with minimal gene expression, thanks to host immune defenses and low levels of key viral proteins like VP16. Specific viral and cellular RNAs help maintain this silent state. Reactivation

occurs in response to stress, inflammation, or immune changes (e.g. UV light, fever, cytokines like IL-1β). This triggers viral gene expression and production of new virus particles, which travel back to the skin or mucosa, causing recurrent lesions [58].

3.4.2. Vaccinia virus

Vaccinia virus (VACV) is a large, enveloped poxvirus with a linear double-stranded DNA genome of about 190 kb encoding roughly 250 genes. Its genome has a conserved central region that mainly encodes late proteins and variable terminal regions that contain mostly non-essential early genes. VACV carries its own transcriptional machinery, including DNA-dependent RNA polymerases and associated enzymes, which allows it to produce mRNA independently of the host cell's RNA polymerase II. Gene expression occurs in a tightly regulated cascade: early genes are transcribed before DNA replication and are thought to initiate replication, while intermediate and late genes are expressed after replication, encoding enzymes and structural proteins necessary for virion assembly [59]. As a notable exception for a DNA virus, replication takes place entirely in the cytoplasm. The virus enters cells either by membrane fusion or macropinocytosis, after which the core is transported to the perinuclear region and activated. Early mRNAs are transcribed by the viral polymerase and translated on host ribosomes. As uncoating progresses, the DNA genome is released and associates with endoplasmic reticulum membranes and viral proteins to form pre-replication centers, which expand into viral factories. After DNA replication and late gene expression, genomes are packaged into immature virions that mature into intracellular mature viruses, the first infectious form (Fig. 6) [59].

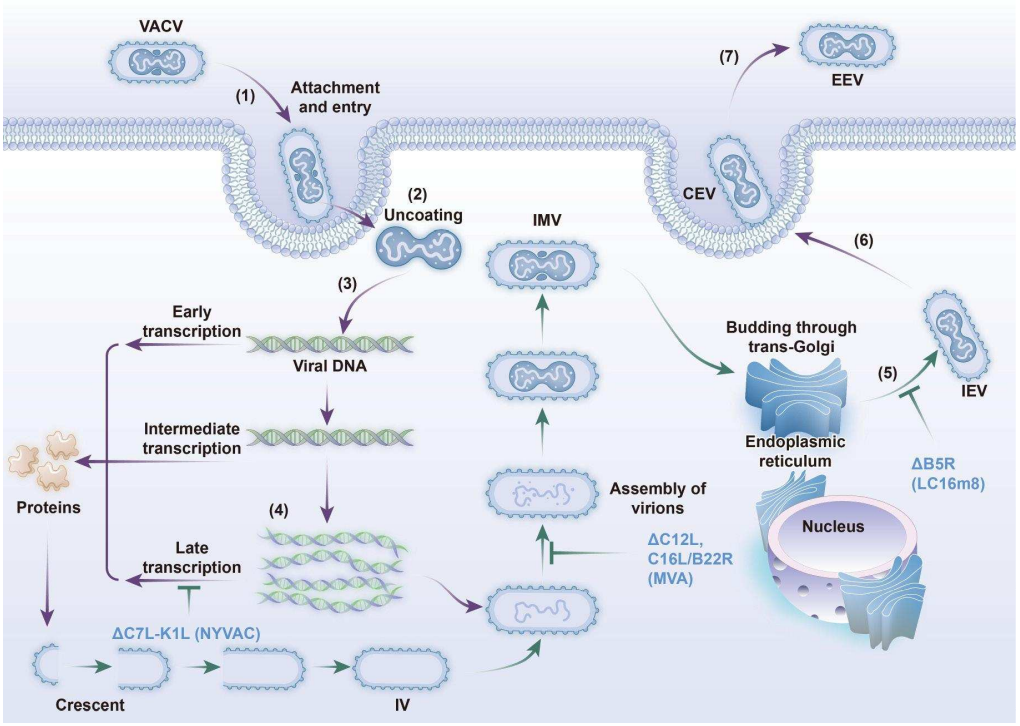

Figure 6: Schematic illustration of the VACV life cycle and key viral proteins. (1) Viral cell entry occurs through membrane fusion or endosomal uptake. (2) The core is released in the cytoplasm through the uncoating step. (3) Early gene expression produces non-structural proteins mediating the synthesis of dsDNA. (4) The transcription and translation of intermediate genes lead to the expression of enzymes and structural proteins for the assembly of virions and the production of IMVs in viral factories. (5) IMVs travel to the Golgi compartment and undergo envelopment to produce IEVs. (6) IEVs are propelled to the cell surface and fuse with the plasma membrane to form CEVs, which remain attached to the cell. (7) CEVs are then released from the cell and form EEVs. CEVs, cell-associated enveloped virions; EEVs, extracellular enveloped virions; IEVs, intracellular enveloped virions; IMVs, intracellular mature virions; IVs, immature virions; VACV, vaccinia virus

The virus we used in our laboratory was a recombinant VACV expressing the glycoprotein (G) of vesicular stomatitis virus Indiana strain (VACV-IND-G), engineered using homologous recombination techniques. The resulting virus retained the replication capabilities of VACV but expressed VSV-G on the surface of infected host cells without incorporating it into its own viral envelope [60].

3.5. Single-stranded positive-sense RNA virus replication and replication organelle formation

As mentioned in par 1.1, ssRNA(+) viruses have a single-stranded messenger-sense RNA genome that is replicated in the cytoplasm through a double-stranded RNA intermediate by viral RNA-dependent RNA polymerases. This occurs within specialized organelle-like structures called RNA replication organelles (ROs), which are virus-induced membrane vesicles in the cytoplasm (Fig. 7). These ROs serve several functions: they concentrate viral replication machinery, protect viral RNA from host immune responses, and facilitate high levels of RNA replication, sometimes amplifying viral RNA up to a million-fold within hours. Interestingly, ROs promote viral evolution by enabling RNA recombination and supporting the high mutation rates of viral RNA polymerases that drive the emergence of new viral strains and variants [61]. ssRNA(+) viruses typically induce one of two major RO morphotypes: membrane invaginations (spherules) or vesico-tubular protrusions that develop into single-, double- or multi-membrane vesicles (Fig. 7). For example, electron tomography of DENV-infected cells revealed invaginated vesicles (~90 nm) within the ER, connected to the cytosol via a narrow neck (~10 nm) (Fig. 7C). These vesicles cluster into vesicle packets, which are associated with convoluted membrane, structures possibly involved in polyprotein processing or immune evasion [62,63].

Flaviviral RO biogenesis occurs in the endoplasmic reticulum (ER) and is driven primarily by the non-structural proteins NS4A and NS4B. These proteins shape the ER membranes through their transmembrane domains and oligomerization abilities. However, additional viral factors such as NS1 (involved in lipid remodeling) and NS2A (which may assist genome transport and alter membrane permeability) are also implicated. These proteins, along with host factors and RNA elements in the viral 3'UTR, coordinate the formation and function of DENV ROs [64]. The double-membrane vesicles generated during coronavirus infection in the ER measure approximately 150–320 nm (Fig. 7F). They emerge very early in infection, within 2–4

h post-entry, and their numbers rapidly expand as infection progresses, often forming clusters in the perinuclear region. Unlike the double membrane vesicles (DMVs) induced by other positive-sense RNA viruses, coronavirus-induced double membrane vesicles typically lack visible openings to the cytosol. Recent cryo-EM studies, however, have revealed the presence of a molecular pore complex spanning the two membranes, enabling the export of newly synthesized viral RNA into the cytosol [65]. As for flaviviruses, the formation of these DMVs is driven by coronavirus nonstructural proteins: *in vitro* experiments have shown that Nsp3 and Nsp4 are sufficient to induce DMV biogenesis and establish the primary sites of RNA replication, while Nsp6 contributes by generating zippered ER membranes that connect DMVs to the ER, thereby supporting lipid flux and membrane remodeling [66].

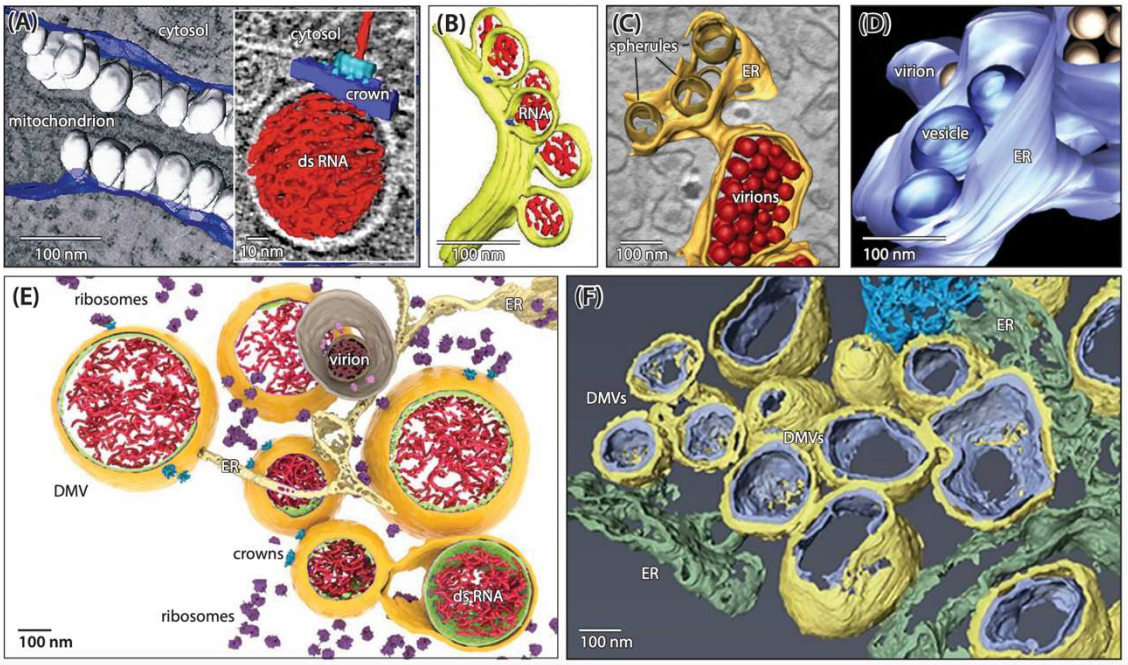

Figure 7: Cryo-electron microscopy (cryo-EM) tomographic 3D reconstructions of RNA replication organelles. (A) Flock House nodavirus spherules (white) on the mitochondrial outer membrane (blue). In the inset, RNA is colored red and the replication complex crown structure light blue. (B) Chikungunya alphavirus spherules invaginating from the plasma membrane (yellow) with RNA content (red). (C) Dengue virus and (D) Zika virus (flaviviruses) spherules invaginating into the

endoplasmic reticulum (ER). Virus particles in proximity can be seen in red and white, respectively. (E) Mouse hepatitis coronavirus ER-derived DMV (yellow surrounding green), with RNA in red and DMV pore complexes in blue. An intracellularly budding new virus particle is seen in the center top of the image inside the tan-colored vesicle. (F) Middle East respiratory syndrome coronavirus DMV in yellow and purple. Other virus-induced membrane rearrangements are colored green and blue [61].

DNA viruses, such as HSV-2, do not rely on cytoplasmic organelles but instead establish nuclear replication compartments. These are membrane-less condensates formed *via* liquid–liquid phase separation inside the nucleus, where viral DNA synthesis and transcription occur. They concentrate viral proteins and genomes, ensuring efficient replication while co-opting nuclear architecture [67]. However, as an exception, a DNA virus family, the Poxviridae, never reaches the nucleus during replication. This family is made up of viruses that encode their own machinery to transcribe RNA and therefore do not require nuclear factors. VACV belongs to this family, and for this reason it was included in this work. As other members of the family, it replicates in the cytoplasm, independent of the host nucleus. To achieve this, it forms ER-derived "mini-nuclei" and cytoplasmic viroplasm-like structures, which mimic nuclear environment and provide compartmentalization for DNA replication and transcription [68]. Thus, VACV illustrates how large cytoplasmic DNA viruses solve the problem of replication organization outside the nucleus.

Similarly to how *Herpesviridae* modify the nucleus, ssRNA- viruses create membrane-less condensates in the cytosol of infected cells without altering the ER [69]. VSV, a prototype rhabdovirus, replicates in the cytoplasm without forming organelles. Its replication complexes are diffuse and transient, relying on rapid kinetics and local concentration of the nucleocapsid protein, polymerase, and template RNA. Unlike DENV or VACV, VSV does not remodel host membranes into protective structures, making its replication more exposed to immune surveillance

but also highly dynamic and efficient [70]. IAV is an unusual ss-RNA virus because it replicates in the nucleus rather than in the cytoplasm. It does not build membranous organelles; instead, it imports its segmented genome into the nucleus, hijacking host transcription and splicing machinery to amplify viral RNA. This reliance on nuclear processes avoids the need for ROs but necessitates intricate trafficking of viral ribonucleoproteins across the nuclear envelope [71].
Together, these examples illustrate the diversity of viral replication strategies: the presence or absence of replication organelles reflects the evolutionary solution for each virus to balance efficiency, genome protection, and control of the host environment.

3.5.1. Host proteins involved in RO biogenesis

The formation of ROs largely relies on the recruitment and manipulation of host factors. These proteins contribute to membrane remodeling, lipid metabolism, and the creation of microenvironments that favor viral replication. Viruses often hijack host proteins that naturally generate membrane curvature, such as reticulons and other ER-shaping factors including atlastins (ATLs), receptor expression-enhancing proteins (REEPs), and ADP-ribosylation factors (ARF) GTPases, a family of small regulatory GTP-binding proteins that belong to the Ras superfamily of GTPase.
For example, enteroviruses redirect host curvature-stabilizing factors like reticulons (RTN) to bend ER membranes into vesicle-linked replication tubules, while coronavirus replication depends on both reticulons and ER sheets. Viruses such as ZIKV and SARS-CoV-2 recruit reticulons, ATLs, and other ER-shaping GTPases to RO sites mainly through the action of their membrane-integrated nonstructural proteins. These viral proteins insert into the endoplasmic reticulum, where they directly interact RTNs or manipulate ER lipid composition to favor their accumulation. ATLs, normally responsible for ER membrane fusion, are co-opted to remodel ER tubules into vesicles, while RTNs help stabilize the high curvature of the forming double membranes. In this way, viral proteins act as molecular anchors that

selectively concentrate these host factors at RO sites, ensuring efficient bending, scission, and stabilization of the membranes needed for viral RNA replication [66].

3.5.2. The reticulon family (RTNs)

RTNs are a family of highly conserved membrane-associated proteins found across eukaryotes, from vertebrates to some invertebrates. In vertebrates, there are four main genes: RTN1, RTN2, RTN3, and RTN4 (also known as Nogo). All members share a C-terminal reticulon homology domain, composed of two hydrophobic segments separated by a hydrophilic loop and followed by a terminal tail. This domain is crucial for their function, as it allows RTNs to shape membranes and generate highly curved tubular structures in the ER (Table 1). RTNs play key roles in shaping and maintaining the ER, acting as structural proteins that stabilize its tubular network. By assembling into stable oligomers within the membrane, they generate positive curvature that drives the formation and preservation of ER tubules and their junctions. Beyond this structural role, RTNs also contribute to ER trafficking and homeostasis by cooperating with other ER-shaping proteins. Among these are REEPs, small membrane proteins that insert hairpin-like domains to promote high curvature, and ATLs, GTPases that remodel ER membranes through fusion events [72]. RTN1 is primarily expressed in neurons, where it regulates axon growth, neuronal development, and ER morphology, while RTN2 is enriched in muscle tissues and contributes to ER organization and protein trafficking, particularly in skeletal and cardiac muscle. Although less studied in viral replication, both proteins share the curvature-inducing properties of RTNs, making them potential contributors to membrane remodeling processes exploited by viruses [73]. RTN3 is involved in various cellular processes, including membrane trafficking and the formation of ER tubules. It has been implicated in neuroprotection and synaptogenesis within the adult nervous system. Additionally, RTN3 plays a role in the degradation of ER tubules through a selective autophagy pathway known as ER-phagy, where it acts as a receptor for the turnover of ER tubules. RTN3 is involved in

various cellular processes, including membrane trafficking and the formation of ER tubules. It has been implicated in neuroprotection and synaptogenesis within the adult nervous system. Additionally, RTN3 plays a role in the degradation of ER tubules through a selective autophagy pathway known as ER-phagy, where it acts as a receptor for the turnover of ER tubules. RTN3 has two isoforms, L and S, due to different splice variants of the RTN3 gene. The long isoform (L) contains additional N-terminal sequences that contribute to its ability to oligomerize and induce ER tubule fragmentation. In contrast, the short isoform (S) lacks these extended regions, resulting in distinct functional properties. The differential expression and functional roles of these isoforms suggest that they may have tissue-specific functions and could be differentially regulated in response to various physiological conditions [74]. RTN4 is also expressed in several isoforms generated through alternative splicing, each with distinct functions and tissue distributions. All isoforms share a conserved reticulon homology domain responsible for inducing and stabilizing ER curvature, but differ in their N-terminal regions, which determine their specialized functions and tissue specificity [75]. RTN4A (Nogo-A) is predominantly expressed in the central nervous system and is well known for inhibiting neurite outgrowth and axonal regeneration, acting through specific receptor interactions, while also contributing to ER tubule structure and neuronal plasticity. RTN4B (Nogo-B) is more widely expressed across various tissues and plays an important role in ER morphology in non-neuronal cells, without inhibiting neurite growth. RTN4C (Nogo-C) is less well characterized but is believed to regulate ER shape and may influence cell cycle progression, particularly in cancer cells.

Table 1 summarizes the RTNs functions and localization in the ER:

RTN Member	Localization	Main Functions	Role in Virology / ROs
RTN1	Endoplasmic reticulum (neurons)	Involved in neuronal development, axon growth regulation, and synaptic signaling.	Less studied in viral infections; may contribute to membrane remodeling in infected neuronal cells
RTN2	Endoplasmic reticulum (skeletal and cardiac muscle)	Regulates protein trafficking and ER organization in muscle tissues; implicated in myopathies	Not well characterized in viral infection
RTN3	Endoplasmic reticulum (ubiquitous expression)	Modulates autophagy, protein degradation, and ER morphology; linked to neurodegeneration	Recruited by flaviviruses (e.g., ZIKV) and coronaviruses (e.g., SARS-CoV-2) to stabilize membrane curvature during RO formation
RTN4 (Nogo)	Endoplasmic reticulum (ubiquitous, highly expressed in CNS)	Controls neurite outgrowth (Nogo-A), shapes ER membranes, involved in neuronal regeneration	Involved in SARS-CoV-2 DMV formation: interacts with nsp3/nsp4 and contributes to ER remodeling for viral replication

Table 1: Localization and functions of RTN members.

3.5.3. Other proteins involved in ER remodeling

An important protein in ER balance is FAM134B, an ER-resident protein that maintains ER homeostasis by driving ER-phagy, selectively fragmenting and degrading damaged or excess ER through autophagosomes. Its role is especially critical in neurons, where loss-of-function mutations cause hereditary sensory and autonomic neuropathy type II due to impaired ER turnover and axonal degeneration. FAM134B is also a target flaviviruses like ZIKV and DENV that degrade or suppress it to block ER-phagy, ensuring a stable ER platform for replication and enhancing

pathogenicity. Overall, FAM134B acts both as an architect of ER structure and a defender against cellular stress and viral exploitation, linking basic cell biology with neurodegeneration and infectious disease [76].

Another essential protein in the ER shaping is the transmembrane protein TMEM41B, it emerged as a key host factor in the replication of diverse ssRNA(+) viruses [77]. TMEM41B is involved in autophagosome formation and lipid mobilization. Although the exact mechanisms remain to be elucidated, TMEM41B might contribute to ROs formation by regulating lipid flux and membrane remodeling via its scramblase activity, facilitating membrane fluidity and curvature necessary for ROs formation [78]. Finally, ATLs are large dynamin-related GTPases that form dimers in both *cis* and *trans* configurations to mediate the fusion of adjacent ER membranes. In humans, three ATL isoforms exist (ATL1, ATL2, ATL3) which share overlapping functions but display different expression levels across cell types. Mutations in ATL1, ATL3, or other ER-shaping proteins are linked to neurological disorders such as hereditary sensory neuropathy and spastic paraplegia, conditions marked by impaired axon and dendrite growth. Moreover, ATLs have been shown to act after viral entry by increasing the levels of viral RNA and proteins. In the absence of ATL, the amounts of infectious virus released into the supernatants are strongly reduced, and it is therefore likely that ZIKV and other flaviviruses compensate for the absence of ATL by replicating in viral factories that form in a much less efficient manner compared to when these proteins are present (Fig. 8) [79,80].

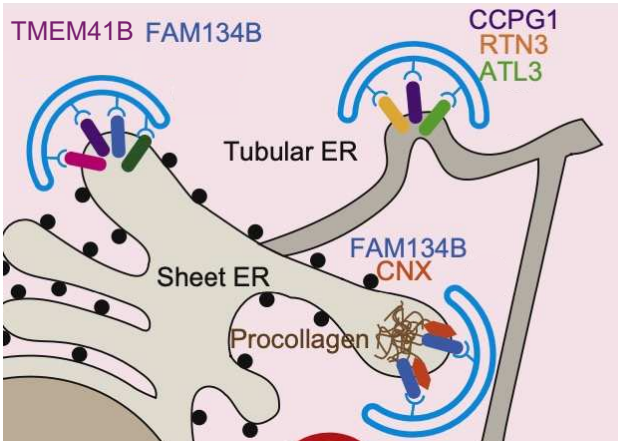

Figure 8: Endoplasmic reticulum proteins localized in different compartments [80].

3.6. Viruses and autophagy

In addition to ER-modeling and nuclear replicative proteins, viruses frequently exploit other cellular processes to support their replication, including autophagy and the unfolded protein response (UPR), a stress pathway triggered when the ER accumulates unfolded or misfolded proteins [81]. They can also interfere with ER-associated protein degradation, the quality control system that targets defective proteins for proteasomal destruction. During flaviviral infection, activation of the UPR sensors IRE1 (ERN1) and ATF6 causes expansion of ER membranes [82], while inflammatory signaling is dampened through proteasomal degradation of immune factors. To stabilize ROs, flaviviruses promote lipophagy, the autophagic breakdown of lipid droplets, while suppressing ER-phagy, the degradation of ER membranes [83]. By contrast, coronavirus-induced double-membrane vesicles rely on non-lipidated LC3 proteins, an autophagy marker, but bypass the canonical autophagy machinery [84].

3.7. Antiviral therapy

The development of antiviral therapy has always been hindered by the fact that viruses replicate in cells and use their same metabolic machinery. However, recently antiviral therapy has advanced significantly with the introduction of directly acting antivirals (DAAs) and host-targeted antivirals (HTAs). These two classes of drugs differ fundamentally in their mechanisms of action, therapeutic applications, and implications for resistance development.

DAAs are designed to target specific viral proteins essential for replication. This is usually achieved after the crystal structure of the target protein has been carefully defined, allowing design of specific compounds that bind critical amino acid residues [85]. In the treatment of hepatitis C virus (HCV), for example, they inhibit viral enzymes such as protease, polymerase, or bind the NS5A, thereby disrupting the viral life cycle at multiple stages [86]. The arrival of DAAs has revolutionized

chronic hepatitis C management, offering high efficacy rates, shorter treatment duration, and improved tolerability compared to earlier interferon-based therapies. Among them, sofosbuvir (SOF), a uridine nucleotide analog that inhibits the HCV RdRp, is considered the backbone of present therapy. By acting at the catalytic site of the polymerase, SOF potently suppresses viral replication and demonstrates a high genetic barrier to resistance. It is effective across all HCV genotypes and remains a cornerstone of interferon-free regimens [87]. Unfortunately, the specificity of DAAs to viral targets can often lead to the rapid emergence of resistance mutations, particularly in the absence of complete adherence to treatment regimens [88].

In contrast, HTAs aim to modulate host cell factors that viruses exploit for replication. By targeting host proteins or cellular pathways, each HTA can inhibit a broad range of viruses, including those with high mutation rates. This approach reduces the likelihood of resistance development, as targeting host factors essential for viral replication is considered less prone to select for mutation than targeting viral proteins. However, the development of HTAs presents challenges, first toxicity due to the interference with normal host cell functions [89,90].

To sum up, whereas the primary advantage of DAAs lies in their high specificity and potency against viral targets, leading to rapid viral suppression, their effectiveness is contingent upon strict adherence to prescribed regimens, and the emergence of resistance remains a significant concern. On the other hand, HTAs offer a broader spectrum of activity and a lower risk of resistance; however, their development is hindered by concerns over safety and the complexity of targeting host pathways without disrupting normal cellular functions [90].

3.7.1. Antiflaviviral compounds

Flavivirus infections continue to pose significant global health challenges, having caused tens of millions of infections annually and more than one hundred thousand estimated deaths worldwide over the past three years. Despite decades of research,

there remains a conspicuous absence of approved antiviral therapies, highlighting a critical gap in the management of these infections. Current strategies under investigation encompass all stages of the viral life cycle, including viral entry, RNA replication, polyprotein processing, assembly, and egress. For instance, inhibitors targeting the envelope glycoprotein E have demonstrated the ability to impede viral attachment and fusion [91], while compounds directed against the viral RpRd, such as favipiravir and remdesivir, induce lethal mutagenesis or generate defective viral particles, thereby curtailing replication. Similarly, protease inhibitors targeting NS2B–NS3 have shown promise in interfering with polyprotein processing, although the emergence of drug-resistant variants continues to represent a significant limitation. Beyond these classical enzymatic targets, increasing attention has turned to non-structural proteins that orchestrate the formation of viral replication complexes. In this regard, the small-molecule inhibitor of DENV, JNJ-A07, exemplifies a promising therapeutic strategy: by binding to NS4B and its precursor NS4A-2K-NS4B, it disrupts the interaction with the NS2B–NS3 protease–helicase complex, thereby preventing the *de novo* formation of vesicle packets, the membrane-bound ROs essential for DENV RNA synthesis, while leaving already established complexes largely unaffected [92]. In addition to virus-directed approaches, host-targeted strategies are increasingly being explored, including the modulation of host proteins co-opted during replication, such as STIM1, as well as the application of artificial microRNAs and exosome-based therapeutics to disrupt viral propagation and enhance host antiviral responses. In the case of possibly pandemic viruses, such as Flaviviruses, the advantage of an indirect approach inhibiting a common pathway used by the genus members, as opposed to one specific species, would allow preparedness for future epidemics. Collectively, these observations underscore the urgent need for continued research into flavivirus pathogenesis and antiviral development, with an emphasis on integrative approaches that consider both viral targets and host cellular factors, to identify safe, effective, and broadly applicable therapeutic strategies [93].

3.7.2. Antiviral compound repurposing

As discussed in the previous chapters, increasing globalization and the geographic expansion of flaviviruses, together with the recent COVID-19 pandemic, have dramatically highlighted the urgent need for broad-spectrum antiviral drugs capable of responding rapidly to emerging health crises. In this context, one of the most widely adopted strategies in antiviral research, particularly during emergencies, is drug repurposing. This approach involves testing drugs already approved for other purposes (e.g. anticancer or antidiabetic drugs) or compounds whose clinical development is in phase II or III, for antiviral activity. The main advantage of this strategy lies in the availability of established pharmacokinetic and safety profiles, allowing for a faster transition to clinical application compared to entirely novel compounds [94]. A prominent example is represented by HIV protease inhibitors, such as lopinavir, which have been investigated for repurposing against SARS-CoV-2 [95]. These examples demonstrate how drug repurposing can provide rapid solutions in response to emerging viral threats. Building on this rationale, the present study investigates a series of chemically diverse molecules previously shown to inhibit other RNA viruses, with the aim of assessing their potential efficacy against flaviviruses.

4. AIM OF THE STUDY

The main aim of this study was to identify and characterize novel antiviral compounds active against RNA viruses of medical relevance, with a particular focus on flaviviruses. To this purpose, a library of 24 chemically diverse molecules, previously reported to inhibit other RNA viruses, such as BVDV and CV-B5, was screened for antiviral activity against ZIKV, chosen as a representative member of the *Flaviviridae* family and a major emerging pathogen [96–100]. This initial screening led to the identification of PS1097 and PS1240, two pyrido[2,3-g] quinoxalinone derivatives, as the most active and promising compounds within the tested series, showing potent antiviral activity coupled with low cytotoxicity.

Once PS1097 was identified as the lead compound due to its selectivity index, subsequent experiments were designed to further characterize its antiviral profile and elucidate its mechanism of action. This part of the study aimed to determine the breadth of its antiviral spectrum across different virus families, to define its effective concentration 50% (EC_{50}) and cytotoxic concentration (CC_{50}), and to establish its selectivity index (SI) under various experimental conditions. The SI represents the ratio between CC_{50} and EC_{50}, it indicates how far apart the toxic concentration is from the effective concentration: the higher the ratio, the greater the difference between the two, and therefore, the better the compound. The mechanism of action of PS1097 was investigated after defining its pharmacological properties. Time-of-addition (TOA) assays, virucidal tests, and protein interaction analyses were performed to pinpoint the specific stage of the viral life cycle affected by PS1097 and to clarify whether its mode of action was direct, targeting viral proteins, or indirect, through the modulation of host cellular pathways. In parallel, particular attention was devoted to defining the pathway that PS1097 might affect if it were to work as HTA.

A close look was directed to the role of ER-associated host proteins, especially those involved in the formation of viral replication organelles, such as members of the RTNs family. Since flaviviruses rely heavily on ER remodeling for replication, the

hypothesis was that PS1097 could exert its antiviral activity by altering the expression or stability of these host proteins. Therefore, the study also investigated the effects of PS1097 on ER-shaping factors including RTN3, RTN4, FAM134B, and TMEM41B. The purpose of the study was therefore not only to describe a novel antiviral compound but also to use it to possibly discover and describe novel cellular pathways hijacked by the viruses affected by the antiviral activity of PS1097.

Building upon these findings, future work will focus on dissecting the molecular relationship between RTN3 modulation and PS1097 antiviral activity. In particular, the next step will involve the generation of stable cell lines overexpressing RTN3 to evaluate whether increased levels of this protein can counteract the inhibitory effects of PS1097 on flavivirus replication. Conversely, RTN3 knockout cell lines will be established using CRISPR/Cas9 technology to assess whether the absence of RTN3 mimics or enhances the antiviral phenotype observed during PS1097 treatment. Comparing the infection dynamics and drug responsiveness of RTN3-overexpressing and RTN3-deficient cells will clarify whether RTN3 downregulation is directly responsible for the compound antiviral effect or represents a secondary cellular response.

Ultimately, this combined approach provided a deeper understanding of the host–virus interaction network centered on ER remodeling and to validate RTN3 as a potential therapeutic target. These studies will also contribute to defining PS1097 precise mechanism of action and evaluating its potential as a lead compound for the development of novel host-directed, broad-spectrum antiviral agents.

5. MATERIALS AND METHODS

5.1. Chemical compounds

Compound synthetic routes and characterization are reported in Briguglio et al [100] and Carta et al [99]. Starting materials were purchased from Merck-Sigma-Aldrich and Fluorochem. Ribavirin[1-(b-D-ribofuranosyl)-1H-1,2,4-triazole-3-carboxamide, RBV), β-D-N4-hydroxycytidine (EIDD-1931, Merck) and Sofosbuvir (SOF; GS-7977; MedChemExpress) [101] were used as reported by manufacturers.
All compounds were stored at 10 mM in dimethyl sulfoxide (DMSO) at room temperature for 1 month. For longer storage, aliquots were kept at -20°C.

5.2. Cell lines

A549, Huh-7 [102], and Vero E6 cells were cultured in DMEM (Gibco), 1 mM glutamine, 1 mM sodium pyruvate, 7% fetal bovine serum (FBS, Gibco). Vero-TMPRSS [103] were cultured like Vero-E6 cells, with 1 mg/mL of G418 (Merck) added once a month. Mosquito C6/36 cells (ATCC, CCL-1660) were cultured at 28°C (no CO_2) in Leibovitz's medium, 1% non-essential aminoacids, 1 mM glutamine, 1 mM sodium pyruvate, 10% FBS. MDCK cells (ATCC) were grown in Ex-cell serum-free medium (Merck), 1 mM glutamine. HMC3 (a gift by Barbara Costa, University of Pisa) were grown in EMEM, 1 mM glutamine, 1 mM sodium pyruvate, 10% FBS. All cells were cultured without antibiotics and checked for *Mycoplasma* as described [104].

5.3. Viruses

ZIKV (family *Flaviviridae*, genus *Orthoflavivirus*, species *Orthoflavivirus zikaense*) strain Brazil/2016/INMI1 ($ZIKV^{Br}$) (National Institute for Infectious Diseases Spallanzani, Roma, Italy), ZIKV strain MP1751 ($ZIKV^{Ug}$), WNV strain B956, USUV catalog number 105081v (Public Health England), CHIKV (family *Togaviridae*, genus

Alphavirus, species *Alphavirus chikungunya*) strain UVE/CHIKV/2006/RE/LR2006_OPY1(001v-EVA83) (European Virus Archive) were propagated on Huh-7 cells.

Influenza A virus (family *Orthomyxoviridae*, genus *Alphainfluenzavirus*, species *Alphainfluenzavirus influenzae*, IAV) strain A/PR/8/34 (ATCC) was propagated on MDCK cells.

VSV (family *Rhabdoviridae*, genus *Vesiculovirus*, species *Vesiculovirus indiana*,) (courtesy of Guido Antonelli, University La Sapienza, Rome) and VACV-IND-G (family *Poxviridae*, genus *Orthopoxvirus*, species *Orthopoxvirus vaccinia*), (courtesy of Rolf Zinkernagel, University of Zurich, Switzerland) [105] were propagated on Vero E6 cells.

CV-B5 (Unit of Virology, AOUP Pisa, Italy) was propagated on HeLa cells.

TOSV (family *Bunyaviridae*, genus *Phlebovirus*, species *Phlebovirus toscanaense*), clinical isolate courtesy of Grazia Cusi, University of Siena, Italy) was propagated on C6/36.

SARS-CoV-2 VR PV10734 (GISAID EPI_ISL_2544194) (family *Coronaviridae*, genus *Betacoronavirus*, species *Betacoronavirus pandemicum*, SARS-CoV2-^{Mi}), courtesy of University San Raffaele, Milan, Italy, was propagated on VERO-TMPRSS cells.

5.4. Determination of compound cytotoxicity and Cytotoxic Concentration 50% (CC_{50})

Cytotoxic/cytostatic effects were evaluated in uninfected cells by WST-8 (Orangu, Cell Guidance Systems): 1×10^4 cells/well in a 96-well plate were incubated in the presence of 3-fold serial dilutions of compounds, from 0.30 to 218 µM, for 48h. Medium was replaced with 50 µl of 10% WST-8, in DMEM, 2% FBS. Following a 1-h incubation at 37°C, optical density (OD) in wells was measured at 450 nm using Varioskan LUX (ThermoFisher Scientific). CC_{50} was calculated using the formula:

% viability = $100 \times (OD_{compound}/OD_{untreated\ control})$

where $OD_{compound}$ and $OD_{untreated}$ are the OD of the cells treated with compound or DMSO, respectively.

The cytostatic effect was assessed by crystal violet, cells were exposed to the same concentrations and incubation times as previously described. After 48 h, cells were fixed and stained with crystal violet, air-dried for 24 h, and the dye was solubilized in 30% acetic acid diluted in distilled water. Absorbance was measured at 595 nm using a Varioskan LUX, and values were normalized to the untreated control, as described before [106].

5.5. Determination of viral yield reduction and Effective Concentration 50% (EC_{50})

The virus yield reduction assay was performed as described by Prichard [107] (Table 1). A primary 96-well plate with 1 × 10^4 Huh-7 cells/well was infected with ZIKV at a multiplicity of infection (MOI) of 1 for 2 h at 37°C, 5% CO_2. The inoculum was replaced with 100 µl 1:2 dilutions of each compound in DMEM, 2% FBS, starting from 100 µM. Cells were incubated for 48 h then viral yields in supernatants were titrated. For ZIKV, supernatants were diluted 1:3 and added onto Vero E6 monolayers and removed after 2 h at 37°C post infection (p.i.). The inoculum was replaced with 100 µl of 1% Carboxymethyl cellulose (CMC, Merck) in complete medium. After 72 h, cells then fixed with 4% buffered formalin solution (Merck) and stained with 1% crystal violet (Merck). Titres were calculated as follows:

PFU/ml = $\frac{number\ of\ plaques \times 3^n}{vol\ of\ infection}$ where *n*: dilution where plaques were counted.

For plaque reduction assays, A549, Vero E6 or Huh-7, 3×10^4 cells, were seeded in 48-well plates and infected with virus at 25 PFU/well for 1.5 h at 37 °C, 5% CO_2. The inoculum was replaced with 1:2 dilutions of the compound to be tested in 1% CMC in DMEM, 2% FBS. Cells were incubated for 3 days then were fixed and stained as

described above. For IAV, viral yield was evaluated by Tissue Culture Infectious Units $(TCID)_{50}$/ml [108].

EC_{50} values for each compound were calculated by determining viral titres (pfu/ml or $TCID_{50}$/ml) in supernatants of cells infected in the presence of compounds at different concentrations and compared with the DMSO-treated control; the % inhibition *vs* log drug concentration was plotted on a graph (Fig. 9) and EC_{50} values were obtained by nonlinear regression analysis [107].

SI was obtained by dividing CC_{50} by EC_{50} for each drug/virus/cell line. Compounds with SI values ≥ 10 were considered to be active in vitro.

5.6. Western blotting

Western blot (WB) was performed to evaluate the cellular content of viral and cellular proteins in infected cells, treated or not with compounds. Cells were washed in PBS and lysed using RIPA lysis buffer (Merck) added with protease and phosphatase inhibitors (Thermo Fisher Scientific). Lysates were added with Laemmli 4x Sample Buffer (0.25 M TRIS base, 8% SDS, 40% glycerol, 20% β-mercaptoethanol, 1% bromophenol blue) then were sonicated, incubated for 10 min at 70 °C and then placed back on ice. Subsequently, electrophoresis was performed on a polyacrylamide gel 12% in running buffer (TRIS, glycin and SDS). The run was carried out at a constant voltage of 200 V for about 40 min. The marker used was the PageRuler Prestained Protein Ladder 250 kDa (ThermoFisher).

At the end of the run, proteins were transferred onto a nitrocellulose membrane (0.22 µm, Merck). The transfer buffer used was Trans-Blot Turbo 5x Transfer Buffer (Bio-Rad), diluted in H_2O and ethanol. The transfer was performed with Trans-Blot Turbo instrument (Bio-Rad) with the standard protocol up to 1A and 25 V for 30 minutes.

Once the transfer was completed, the nitrocellulose membrane was immersed in Ponceau Red stain (Sigma) to verify the efficiency of the transfer. After several washes to remove the stain, incubation in blocking buffer was carried out. The

blocking solution consisted of PBS-0.1% Tween 20 (Sigma) and 5% Skim Milk (Sigma) and was kept under agitation at room temperature (RT) for 1 h. Afterwards, it was removed and the primary antibody, diluted in fresh blocking solution, was added. In this case, incubation was overnight at 4°C. The antibodies used are schematically represented in Table 2. After incubation, three washes of 5 min each in PBS-0.1% Tween 20 were performed. Then, secondary antibodies conjugated with horseradish peroxidase were added and incubated for 1 h under agitation at RT. The secondary antibodies used were goat anti-rabbit IgG (Sigma) and anti-mouse IgG (Sigma), both diluted 1:20.000 in blocking solution.

Table 2: Antibodies used in this study

Antigen	Host species	Manufacturer	Use	Cat. #	Dilution
ZIKV Capsid	rabbit	GeneTex	WB/IF	GTX133317	1:1000
ZIKV NS5	rabbit	GeneTex	WB	GTX 133328	1:1000
ZIKV NS3	rabbit	GeneTex	WB	GTX133309	1:1000
ZIKV NS2B	rabbit	GeneTex	WB	GTX133318	1:1000
GAPDH	mouse	Invitrogen	WB	MA5-15738	1:1000
RTN3-L	rabbit	Genetex	WB	GTX131091	1:1000
RTN3-S	mouse	Santa Cruz	WB	sc-374599	1:1000
RTN4	mouse IgM	Santa Cruz	WB	sc-271878	1:1000
FAM134B	rabbit	Proteintech	WB	21537-1-AP	1:1000
TMEM41B	rabbit	My Biosource	WB	MBS154820	1:1000
rabbit IgG	Goat, HRPO	Merck	WB	A0545	1:20.000
mouse IgG	Rabbit, HRPO	Merck	WB	A9044	1:20.000
rabbit IgG	Rabbit, Alexa Fluor®	Invitrogen	IF	A-11008	1:1000

5.7. Immunostaining

Cultured cells were fixed in 4% paraformaldehyde (PFA) for 12 min at RT. After two 3-minutes washed with Phosphate Buffered Saline-Triton X-100 (PBSX) [0.1% Triton

X-100 in PBS] cells were permeabilized for 10 min with permeabilization solution [0.5% Triton X-100 in PBS] and blocked for 1 h with blocking solution [5% fetal bovine serum, 0.3% Triton X-100 in PBS]. Cells were incubated with primary antibodies against ZIKV capsid protein (Genetex, GTX133317 1:1000), diluted in antibody solution [3% fetal bovine serum, 0.2% Triton X-100 in PBS] at 4°C overnight. The next day, cells were washed with PBSX three times for 3 minutes and then incubated for 1h at RT with Alexa Fluor® 488 anti-rabbit secondary antibodies (Invitrogen, ThermoScientific, A-11008, 1:1000) and DAPI (D1306, Invitrogen, 1 µg/ml) diluted in antibody solution. After two washes of 3 minutes with PBSX all images were acquired using Operetta CLS confocal microscope.

5.8. Quantitative reverse transcriptase PCR (qRT-PCR)

Viral RNA was extracted from infected cells with Trizol (Qiagen). qRT-PCR was performed on ZIKV^{Br} NS1 gene following the instructions of One Step PrimeScript™ III RT-PCR Kit (Takara Bio), with 0.5 µM primers: **NS1**-FW 5'-TGAGATCAACCACTGCAAGY-3', **NS1**-REV 5'-GCCTTATCTCCATTCCATACCA-3'; and 0.1 µM probe 5-FAM/ATCGAGGAATGGTGCTGCAGGGA/3-BHQ. The mixtures were run in a CFX Connect Real-Time PCR (Bio-Rad Laboratories, Hercules, CA, USA) using previously standardized conditions (52°C for 5 min, 95°C for 10 s, 40 cycles of 5 s at 95°C, and 57°C for 30 s). For absolute quantification, standard curves were generated using 10-fold dilutions of a homemade plasmid at known concentrations. For the relative quantification of RTN3, RTN4, and FAM134B mRNA, normalized to GAPDH, the Power SYBR™ Green RNA-to-CT™ 1-Step Kit (Thermo Fisher) was used with the following primers:

RTN3 FW-5'-CTTACCTCATCCTGGCTCTTCTC-3'

RTN3 REV-5'-GACAGAGTAATGTCTACGTCCAG-3'

RTN4 FW-5'- TCTTSSTGCTGCATCTGAGCCT-3'

RTN4 REV-5'- GCAGTTTCAAGCAGGACAGATGG-3'

FAM134B FW-5'-GTCTCAGAGGTATCCTGGACTG-3'

FAM134B REV-5'- TTCCTCACTGGGTCGGTCAAGA-3'

GAPDH FW-5'-GTCTCCTCTGACTTCAACAGCG- 3'

GAPDH REV-5'-ACCACCCTGTTGCTGTAGCCAA -3'

5.9. Time-of-addition (TOA) experiments

Huh-7 cells, 12 × 10^4 per well in a 12-well plate, were infected with $ZIKV^{Br}$ (MOI:1) for 2 h. PS1097 was added at 6 µM at 0, 2, 6, 12, 24, 36 h p.i. [109]. SOF was used as a reference compound at 15 µM. At 48 h p.i., viral proteins were determined by western blot or by qRT-PCR in cell lysates.

To monitor intracellular viral RNA production kinetics in untreated cells, these were infected as described above for 2 h. After removing the inoculum, assay medium was added, then cells were collected at the time points of the TOA assay. Viral RNA replication was monitored as described above in cell lysates.

5.10. Co-immunoprecipitation assay

Huh7 cells, 3 × 10^5 cells per well, were seeded in three wells of a six-well plate. Two wells were infected with $ZIKV^{Br}$ (MOI:5) while the remaining received 500 µL of serum-free medium as a mock-infected control. After 1.5 h incubation, the inoculum was replaced with medium containing 2% FBS, and cells were further incubated for 24 h. At this time point, one infected well was treated with 2 µM PS1097 for 3 h, while the other was left untreated. Cells were then washed with ice-cold PBS and lysed in 1 mL of freshly prepared lysis buffer composed of 150 mM NaCl, 50 mM Tris-HCl (pH 7.5), and 0.5% NP-40, supplemented with protease and phosphatase inhibitors. After a 5 min incubation on ice, cells were collected by scraping, passed through a syringe, and divided into two fractions of 500 µL each. One aliquot was immediately frozen, while the other was incubated at 4 °C under rotation for 1 h, followed by centrifugation at maximum speed for 10 min at 4 °C. The supernatant was collected, and 150 µL were stored at −80 °C.

For immunoprecipitation, magnetic beads were first resuspended and 50 µL were transferred into a 1.5 mL microcentrifuge tube per sample. Beads were washed twice with 1 mL of wash buffer (PBS supplemented with 0.5% Tween-20) using magnetic separation. To functionalize the beads, antibody (anti-NS5) was diluted to a final concentration of 10 µg/mL in 200 µL of wash buffer and incubated with the beads for 45 min at room temperature under rotation. Beads were then washed three times and incubated with 400 µL of lysate for 45 min at room temperature with rotation to allow antigen–antibody binding. After magnetic separation, beads were washed four times with 1 mL of wash buffer, resuspended in 350 µL of wash buffer, and stored at −80 °C until further use.

For Western blot analysis, frozen samples were thawed, mixed with loading buffer containing β-mercaptoethanol, and heated at 70 °C for 10 min. Approximately 15 µL of each sample were loaded per well. Membranes were probed with antibodies against NS3, NS2B, and GAPDH, as well as with secondary antibody alone as a control [110].

5.11. Virucidal effect assessment

The virucidal potential of PS1097 was assessed by comparing residual infectivity after pre-exposure of virus to the compound *vs* appropriate controls on a permissive cell line. Briefly, infectious ZIKV^{Br} suspensions were incubated for 1h at 37°C alone or with PS1097 or SOF prior to quantification of infectious virus by plaque assay on VeroE6 cells. The only ZIKV^{Br}, without treatments, pre-incubated is a control of temperature inactivation. To discriminate true virucidal activity from immediate assay interference, parallel samples consisting of ZIKV^{Br} alone or with compounds that were not pre-incubated with PS1097 or SOF, but the compounds were added, and the virus titrated immediately. An additional specificity control employed is HSV-2 treated in an identical manner, as PS1097 is not demonstrated to affect this virus.

5.12. Cellular Thermal Shift Assay (CETSA) assay

CETSA allows to evaluate the potential binding between the compound PS1097 and the RdRp of $ZIKV^{Br}$, also called NS5 to explain its inhibitory activity [111].

For the preliminary setup of the assay, 1×10^6 Huh-7 cells were grown into two T75 flasks so that they reached to 80% confluence. They were then infected with $ZIKV^{Br}$ (MOI:1) the following day, and after 48 h of incubation at 37°C and 5% CO_2, one flask was treated with 50 µM SOF and the other with DMSO, as a control, for 1 h. After this incubation, the cells from each treatment were detached and counted to distribute 10^6 cells, resuspended in 100 µl of PBS in 6 tubes. Each tube of each treatment was exposed to 6 different temperatures ranging from 43°C to 63°C, with intervals of 4°C, for 3 min. Subsequently, the samples were placed on ice, and through three rapid freeze-thaw cycles with liquid N_2 (snap freeze), cellular lysis was performed. After cellular lysis, the samples were centrifuged at 20000 *g* for 20 min, and the soluble fraction was recovered for WB analysis. The next step was using the same protocol with 30 µM PS1097 and the DMSO as control. Then CETSA was performed as before, but the range of analyzed temperatures was narrowed to focus on the temperature range at which ZIKV CV and NS5 typically denature and precipitate. Each tube for each treatment was exposed to a series of six temperatures, ranging from 45°C to 60°C in around 4°C increments. Finally, a WB analysis was performed to evaluate the ability of PS1097 to bind to ZIKV NS5 or CV.

5.13. Synergism between PS1097 and SOF

Huh-7 cells were infected with $ZIKV^{Br}$, MOI:1, as described above and treated with serial twofold dilutions of the PS1097 and SOF combinations (PS1097 2.0-0.125 µM; SOF (5.0-0.39 µM). At 48 h p.i., antiviral activities of each combination were evaluated in supernatants as described [107]. Percent inhibition of viral replication was plotted, and drug interaction analysed by SynergyFinder (https://synergyfinder.fimm.fi) or MatLab (mathworks.com). Synergy scores less

than −10 indicated an antagonistic interaction, scores between −10 and 10 an additive effect, and scores greater than 10 a synergistic effect between drugs. The analysis was performed using the Loewe additivity model, an algorithm that evaluates drug interactions by comparing the observed combined effect with the effect expected if the two drugs acted as dilutions of each other.

5.14. Selection of viral mutants

Huh-7 cells, 6×10^4 per well in a 24-well plate, were infected with $ZIKV^{Br}$ (MOI:1) for 2 h at 37 °C. Virus was then removed and cells were further incubated with 0.6 μM and 1.2 μM PS1097 for 2 days at 37 °C. The supernatants were then titrated by plaque assay and used to infect freshly seeded cells at MOI:1. The remaining supernatant was stored at –80 °C. During weekly passaging of the virus, the starting concentration of the compound was gradually increased. In parallel, wild-type $ZIKV^{Br}$ was passaged using Huh-7 cells in a similar way to compound-treated virus [112].

5.15. Proteasome inhibition assay to study RTN3 stability

Huh-7 cells were seeded at a density of $1{,}2 \times 10^5$ cells per well in 12-well plates and allowed to adhere under standard culture conditions. To explore the possible involvement of the proteasomal pathway, MG132 was administered at 1 μM either 24h or 42h after PS1097 (or DMSO) treatment, corresponding respectively to 24-h and 6-h exposures before the end of the 48-hour experiment. Appropriate control groups were also included, consisting of cells treated with either MG132 or PS1097 alone, as well as untreated cells, to allow a direct comparison and to exclude unspecific effects. PS1097 was administered at 6 μM.

Protein expression levels were subsequently analyzed by WB, with the aim of monitoring specific markers of proteasomal degradation. Anti-FAM134B antibody was used as a positive control to validate the effectiveness of proteasome

inhibition, RTN3 was probed as the protein of interest to determine whether its degradation is enhanced by treatment with our compound, and GAPDH served as a housekeeping protein for normalization of protein loading.

5.16. Determination of RTN3, RTN4, FAM134B and GAPDH half-life

For protein half-life evaluation, Huh-7 cells were seeded in 12-well plates at a density of 1,2 × 10^5 cells per well. After 24 h, all experimental conditions were treated with cycloheximide (10 µg/ml) to inhibit de novo protein synthesis. Cells were harvested by lysis in RIPA buffer at 6-, 12-, 24-, and 48-h post-treatment. For each time point, an untreated control sample was collected in parallel to assess basal protein expression levels. Analysis was performed on the proteins of interest RTN3, RTN4, FAM134B, and GAPDH by WB. The obtained values were normalized to GAPDH and plotted as a function of time, allowing the calculation of each protein half-life through exponential decay regression of the signal.

5.17. Graphics and statistic

Graphs and statistical analyses were performed using GraphPad Prism 7 software. Data are presented as mean ± SD or as 95% confidence intervals to provide an estimate of variability and the precision of the measurements. Statistical significance was assessed using a one-way ANOVA test followed by Tukey–Kramer post-hoc correction or t-test. The one-way ANOVA allows the comparison of the means across multiple experimental groups simultaneously. When the ANOVA indicates a significant effect, the Tukey–Kramer post-hoc test is applied to identify which specific pairs of groups differ from each other. The unpaired t-test, instead, compares the means of two independent groups to evaluate whether they are significantly different.

6. RESULTS

6.1. Antiviral activity against ZIKV by a selection of compounds

With the aim of a possible repurposing of known antiviral compounds, this study began by evaluating 24 compounds with known antiviral activity against various viral agents (Tab. 3). A group of compounds from an in-house library synthesized by researchers at the University of Sassari and that have been found to be active against BVDV and CVB5 were tested against ZIKV because the viruses belong to the same family *Flaviviridae* as BVDV [100]. Specifically, $ZIKV^{Br}$, considered one of the most pathogenic strains, was used [113]. Human hepatoma Huh-7 cells were infected, and antiviral activity was tested at a concentration range of 100-1.5 μM by viral yield reduction assays. SOF, a potent HCV inhibitor exerting antiviral activity against other members of the *Flaviviridae* family, and Ribavirin (RBV) were used as controls [101]. In parallel, compound toxicity was evaluated on the same cells and at the same compound concentrations.

Several compounds exhibited anti-flaviviral activity (Tab. 3), while others exhibited no activity at all. Figure 9 shows the graphs obtained by plotting antiviral activity and cytotoxicity values for the 2 most active compounds. The data show that the thiophen-derivatives PS1097: 5-chloro-3-(thiophen-2-yl) pyrido[2,3-*g*] quinoxalin-2(1*H*)-one and, to a lesser extent, its analogue substituted on N-1 with a methyl group (PS1240) had marked inhibitory activity against $ZIKV^{Br}$ (EC_{50} 0.6 and 2.06 μM, respectively) (Fig. 9 and Tab. 3). RBV did not seem to be active against $ZIKV^{Br}$ at nontoxic concentrations (Fig. 9) while SOF exhibited an EC_{50} of 1.5 μM and was used as the only reference drug thereafter.

Thus, PS1097 showed the highest antiviral activity against $ZIKV^{Br}$ and was prioritized for further experiments. Being structurally related to PS1240, we assumed that the activity of the two compounds would be relying on the same mechanisms (Tab. 3).

Table 3: Anti-BVDV and -CVB5/CVB2 activity (EC_{50}) and cytotoxicity (CC_{50}) values of 24 molecules selected from an in-house library and their newly tested antiviral activity against $ZIKV^{Br}$ and cytotoxicity in Huh-7 cells. Selectivity Index (SI) was calculated as CC_{50}/EC_{50}.

Label (previously published as)	Previously published data					This paper data		
	CC_{50} Vero76 (μM)	EC_{50} BVDV (μM)	EC_{50} CVB5 (μM)	EC_{50} CVB2 (μM)	Ref.	CC_{50} Huh-7 (μM)	EC_{50} $ZIKV^{Br}$ (μM)	SI
PS462 – (4h)	>100	5	Na	Na	[99]	294	100	3
PS1000 – (2h)	>100	1.2	Na	Na	[99]	393.4	1.4	271
PS1001 – (2i)	>100	10	Na	Na	[99]	126.5	1.3	94
PS1067 – (3e)	>100	18	Na	Na	[99]	150.1	5.5	27
PS1076 – (6b)	>100	0.3	Na	Na	[100]	86.1	2.6	32
PS1086 – (16)	30	25	Na	2	[114]	Na	Na	Na
PS1097 – (4)	>100	5	Na	Na	[100]	228.9	0.6	331.7
PS1100 – (18)	35	Na	Na	2	[114]	Na	Na	Na
PS1101 – (19)	90	9	Na	Na	[114]	Na	Na	Na
PS1240 – (18)	>100	2	Na	Na	[100]	293.1	2	142.3
SMA14 – (5h)	>100	Na	Na	4	[115]	Na	Na	Na
SMA19 – (5i)	>100	Na	Na	11	[115]	Na	Na	Na
SMA20 – (5j)	>100	Na	Na	9	[115]	178.8	2.6	69
SMA87 – (4c)	>100	Na	9	Na	[116]	183.4	7.8	23
SMA115 – (5g)	>100	Na	8	Na	[116]	110.4	21.1	5
SMA187 – (100b)	>100	Na	50	Na	[97]	72.8	10.5	7
SMA189 – (99b)	>100	Na	16	Na	[97]	Na	Na	Na
SMA292 – (43a)	>100	Na	9	Na	[97]	115.6	57.1	2
SMA305 – (41a)	>100	Na	18.5	Na	[97]	85.5	39.5	2
SMA332 – (9a)	>100	Na	23	Na	[117]	Na	Na	Na
SMA352 – (48a)	3.1	Na	52	Na	[97]	31.51	5.2	6
SMA353a – (4c)	37	Na	37	Na	[117]	Na	Na	Na
SMA363a – (4d)	>100	Na	10	Na	[117]	57.1	7	8
SMA364a – (4a)	90	Na	13	Na	[117]	Na	Na	Na
EIDD-1931						147.7	1.7	87
RBV						144	8.8	16
SOF						281.7	1.5	184

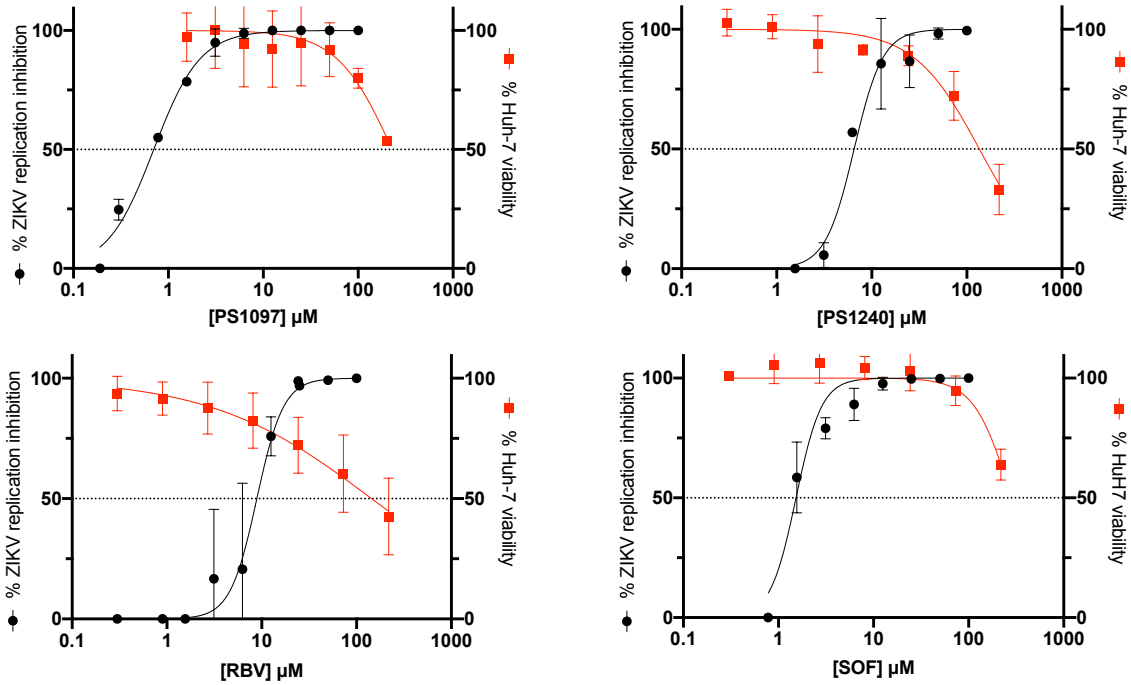

Figure 9: Curves of viral inhibition and cell viability of PS1097, PS1240, SOF and RBV. Dose-response curves of the % ZIKV^{Br} replication inhibition (black line) and % cell viability (red line) of the compounds tested and of control drugs SOF and RBV. The antiviral activity of each compound was evaluated on Huh-7 cells infected with ZIKV^{Br} in the presence of 1:2 dilutions of compounds, starting from 100 µM. Viral yields were determined by titrating supernatants on Vero E6 cells.

6.2. Antiviral activity of PS1097 on different cell lines

To confirm the antiviral activity of PS1097, it was tested on other permissive cell lines, including simian Vero E6, Vero TMPRSS, human HMC3, A549, and *Aedes albopictus* C6/36. Experiments were performed as described for Huh-7 in the paragraph above, and viral yield assays were used as a read out if not specified otherwise. EC_{50} values were comparable on human and monkey cells, while slightly lower SI values were obtained on Vero E6 cells, mostly due to lower CC_{50} values. PS1097 also inhibited ZIKV in insect C6/36 cells (Tab. 4). However, values of SI were roughly 10 times lower, due to both higher toxicity and lower EC_{50} of the compound on these cells.

Table 4: Antiviral activity of PS1097 against ZIKV^{Br} in various cell lines

Cell line	EC_{50} (µM)	CC_{50} (µM)	SI [a]
Huh-7	0.6 (0.6 to 0.8)[b]	228.9 (150.2 to 348.7) [b]	331.7
VeroE6	1.3 (0.9 to 1.8)[b]	126.5 (63.6 to 252.5)[b]	94.4
Vero TMPRSS	2.6 (1.2 to 6.1)[b]	86.1 (72.6 to 102.2)[b]	32.4
HMC3	>100	294 (186 to 464.8)[b]	< 2.9
C6/36	5.5 (4.5 to 6.8)[b]	150.1 (124.9 to 180.4)[b]	27.2
A549	44.5 (32.1 to 64.5)[b]	130 (100.2 to 184.8)[b]	2.9

EC_{50}: effective Concentration 50%; CC_{50}: cytotoxic concentration 50%

[a] Selectivity index (SI) was calculated by dividing CC_{50} by EC_{50}

[b] 95% Confidence Interval

6.3. Antiviral activity of PS1097 on different viruses

To investigate the activity range of PS1097, it was tested against another ZIKV strain and other viral species to determine whether it had broad antiviral effects. Other flaviviruses tested were ZIKV^{Ug}, USUV, WNV on Huh-7 cells and the results are shown in Table 5. PS1097 showed an EC_{50} of 1.29 against the African ZIKV Uganda strain (ZIKV^{Ug}), comparable to the one against ZIKV^{Br}. It was also effective against other *Flaviviridae* members, including USUV and WNV, with an EC_{50} comparable to ZIKV (Tab. 5). PS1097 also showed an inhibitory effect against SARS-CoV-2^{Mi}, an early COVID-19 pandemic variant (B.1.177 Pangolin lineage), though with a higher SI than against *Flaviviridae* (Fig. 10). Antiviral activity was further tested on viruses from families different from *Flaviviridae* and *Coronaviridae* by plaque reduction assays. The viruses tested were CHIKV, VSV, VV-IND-G, HSV-2, IAV and TOSV, everyone on its corresponding reference cell line, as presented in Table 5. PS1097 exhibited activity against CVB5, CHIKV, and VV-IND-G (DNA virus), but no significant activity was observed against ssRNA$^-$ viruses like VSV, TOSV, IAV or another DNA virus such as HSV-2. IAV was evaluated by $TCID_{50}$ reduction (Tab. 5).

Table 5: Antiviral activity of PS1097 against ZIKV^{Ug} and against other viral species and strains.

Virus strain (cell line)	**EC_{50} (µM)**	**CC_{50} (µM)**	**SI [a]**
ZIKV^{Ug} (Huh-7)	1.2 (1.1 to 1.5)[b]	228.9 (150.2 to 348.7)[b]	177.4
USUV (Huh-7)	0.8 (0.5 to 1.4)[b]	228.9 (150.2 to 348.7)[b]	266.2
WNV (Huh-7)	1.1 (1 to 1.5)[b]	228.9 (150.2 to 348.7)[b]	199
SARS-CoV-2 ^{Mi} (Vero TMPRSS)	0.1 (0.02 to 0.4)[b]	436.1 (113.7 to 1674)[b]	4361
CVB5 (A549)	4.4 (2.8 to 7.6)[b]	218.2 (200 to 241.4)[b]	48.8
CHIKV (Huh-7)	4.4 (3.3 to 5.9)[b]	228.9 (150.2 to 348.7)[b]	52
VSV (Huh-7)	>50	228.9 (150.2 to 348.7)[b]	na[c]
VV-IND-G (Huh-7)	1.7 (0.6 to 4.3)[b]	228.9 (150.2 to 348.7)[b]	132.3
HSV-2 (A549)	>50	218.2 (200 to 241.4)[b]	na[c]
IAV (MDCK)	>50	nd [d]	na[c]
TOSV (VeroE6)	>50	574.6 (195.8 to 1678)[b]	na[c]

CHIKV: Chikungunya virus; CVB5: Coxsackie B virus, serotype 5; HSV-2: Herpes Simplex Virus 2; IAV: Influenza A virus; TOSV: Toscana virus; USUV: Usutu virus; VV-IND-G: Vaccinia virus recombinant for VSV-Indiana G protein; VSV: vesicular stomatitis virus; WNV: West Nile virus; ZIKV: Zika virus.

EC_{50}: effective Concentration 50%; CC_{50}: cytotoxic concentration 50%

[a] Selectivity index (SI) was calculated by dividing CC_{50} by EC_{50}

[b] 95% Confidence Interval

[c] na: no antiviral activity

[d] nd: not determined

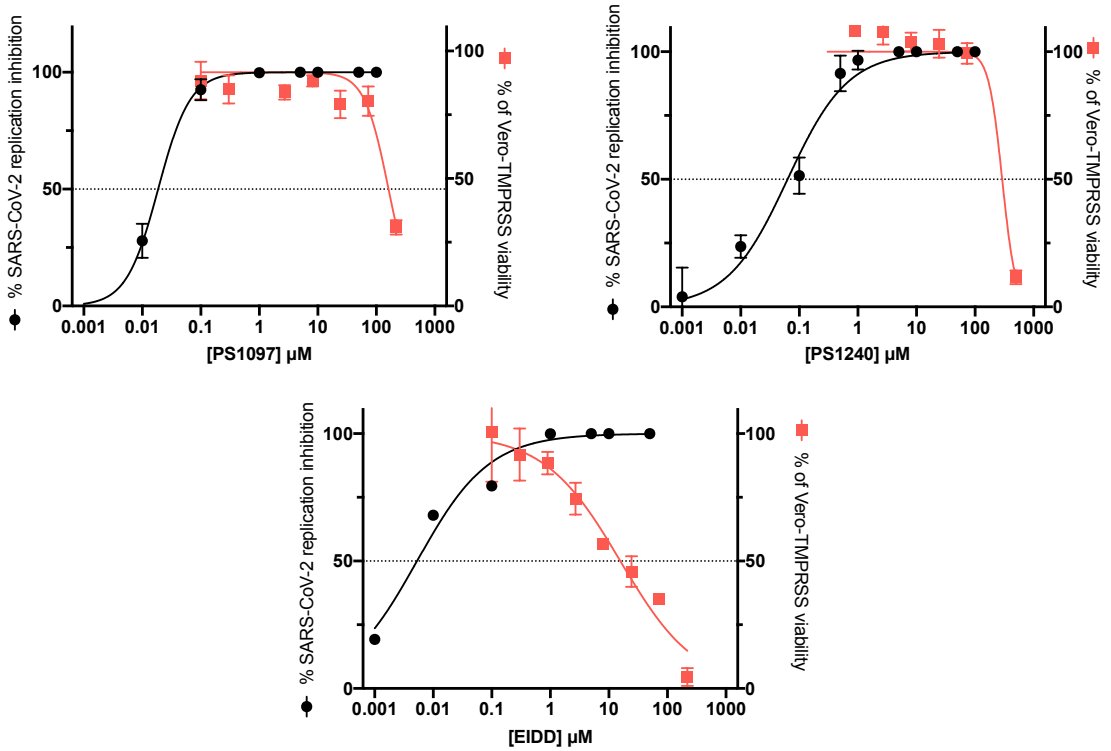

Figure 10: Dose-response curves of the % SARS-CoV-2^{Mi} replication inhibition (black line) and % cell viability (red line) of the compounds tested. The antiviral activity of each compound was evaluated on Vero-TMPRSS cells infected with SARS-CoV-2^{Mi} in the presence of 1:2 dilutions of compounds, starting from 100 µM. Viral yields were determined by titrating supernatants on Vero-TMPRSS cells.

Data represent mean values ± SD from at least three independent experiments.

6.4. Determination of viral protein synthesis during treatment with PS1097

Once determined that PS1097 is endowed with antiviral activity against a wide range of viral species, we attempted to define its mode of action.

To determine whether the reduction in ZIKV yield by PS1097 was due to inhibiting viral protein synthesis, or downstream events in viral replication such as viral release, Huh-7 and Vero E6 cells were infected with ZIKV^{Br} and treated with PS1097 or SOF at 1×, 5×, and 10× their EC_{50} (0.6, 3, 6 µM and 1.5, 7.5, 15 µM, respectively). Viral protein levels in cell lysates were analyzed by immunoblotting (Fig. 11A, B), while virion release was assessed by quantifying ZIKV RNA in supernatants (Fig.

11C). PS1097 downregulated viral protein expression in Huh-7 cells but did not fully suppress it, whereas SOF completely abolished protein synthesis at 7.5 µM (5× EC_{50}) (Fig. 11A, B). Interestingly, in Vero E6 cells, SOF had no effect on viral protein content, as previously reported [118], while PS1097 consistently reduced protein levels, as in Huh-7 cells. Viral RNA levels in supernatants closely mirrored intracellular viral protein quantification (Fig. 11B, C).

These findings indicate that, in both cell lines, PS1097 reduced ZIKV yield primarily by impairing viral protein synthesis, rather than by blocking virion release.

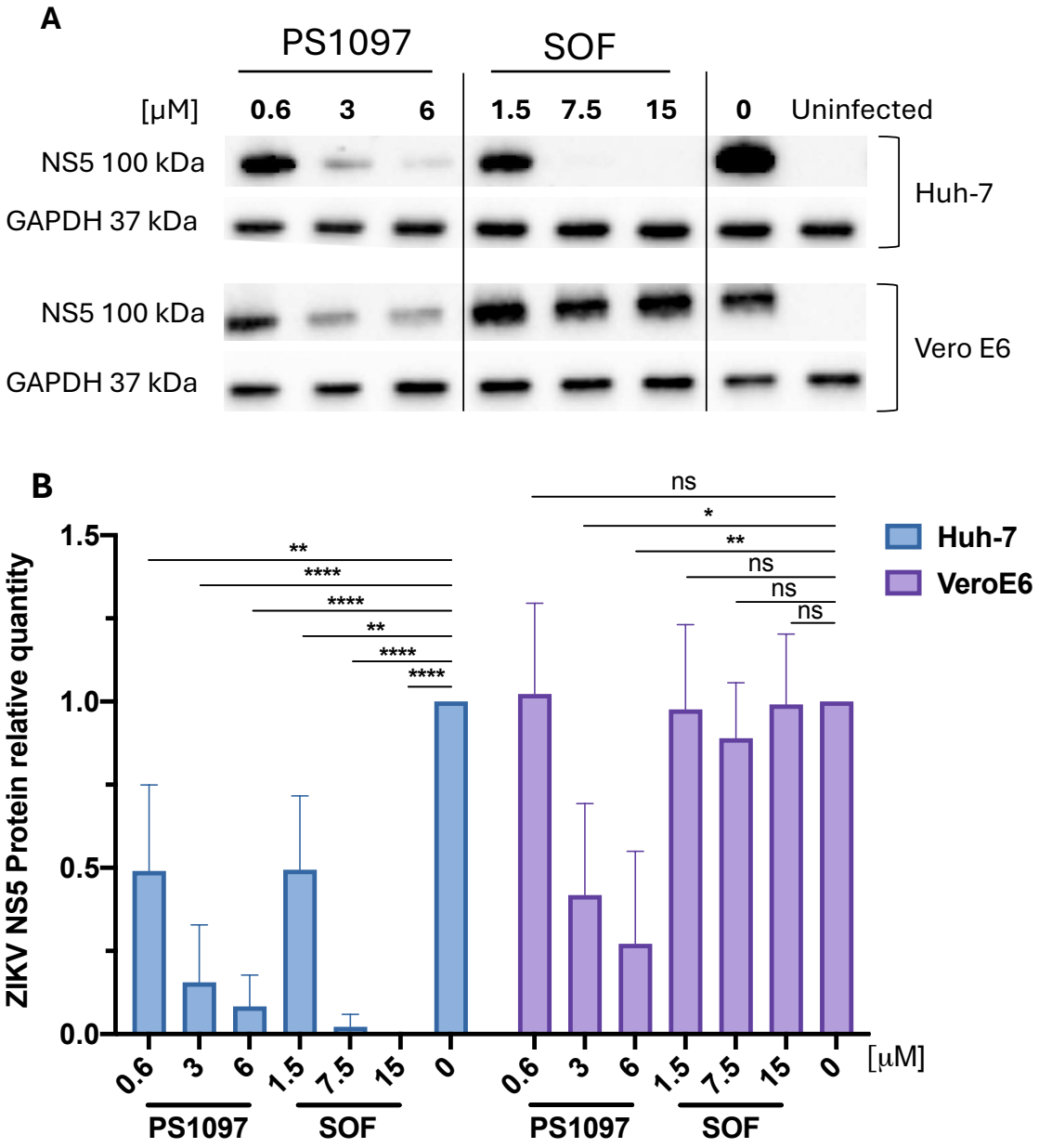

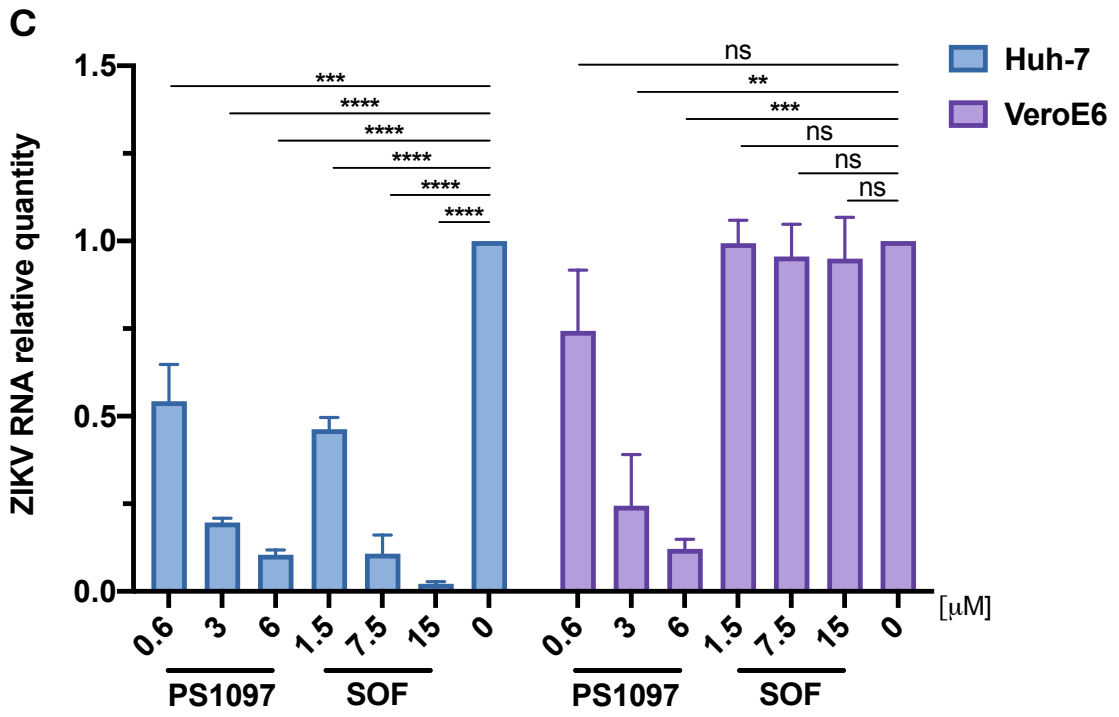

Figure 11: Viral protein quantification after treatment with PS1097 or SOF by WB and qRT-PCR. ***A)*** *Huh-7 cells (2 upper panels) or Vero E6 (2 lower panels) were infected with ZIKV, MOI:1, and treated with PS1097 or SOF at the concentrations shown (EC_{50} × 1, × 5 and × 10) for 48 h. Impact of treatment on ZIKV protein synthesis was evaluated on cell extracts analysed by western blot using anti- ZIKV NS5, or anti-GAPDH as a housekeeping control.* ***B)*** *Quantitative analysis of the results in A.* ***C)*** *Viral yield determination by qRT-PCR. ZIKV genome content was determined on supernatants taken from the cells used in A and quantified relative to untreated infected cells.*

Statistical analysis was performed using One-Way Anova followed by Tukey–Kramer post-hoc correction ($p<0.01$; $\alpha = 0.05$) with all groups compared against each other in the multiple-comparison analysis. Data are expressed as mean ± 95% confidence interval, N=4. Antibodies used are shown in Table 2.

Next, to assess viral protein expression in another way, through confocal microscopy, Huh-7 and Vero E6 cells were infected with ZIKV at MOI:1 and subsequently treated with increasing concentrations of PS1097, ranging from 0.18

to 15 µM. Viral expression was analyzed by confocal microscopy through immunofluorescence staining, using an anti-Capsid antibody (Genetex, GTX133317, 1:1000) in combination with DAPI (D1306, Invitrogen, 1 µg/ml) and visualized with Alexa Fluor 488-conjugated anti-rabbit secondary antibodies (Invitrogen, ThermoScientific, A-11008, 1:1000) (Fig. 12). As can be seen in Figure 12A and C, PS1097 itself exhibited intrinsic orange fluorescence, detectable at 568 nm even in the absence of additional staining, which facilitated the monitoring of compound distribution within the cells. In particular, the fluorescence signal was much more evident in Huh7 cells (Fig. 12A), likely due to their higher permeability to the compound compared to Vero E6 cells (Fig. 12C). Since Huh7 cells are known to be rich in intracellular lipids, this observation suggests that PS1097 may possess lipophilic properties, promoting its accumulation in these cells. At the highest concentrations tested, PS1097 exhibited a certain degree of cytotoxicity, which restricted its use under those conditions. However, when applied at non-toxic concentrations (≤5 µM), the compound still showed a pronounced antiviral effect. This inhibitory activity persisted even at lower concentrations, with significant efficacy observed down to 0.6 µM (Fig. 12A, C). The analysis of viral replication inhibition and cytotoxicity was performed by calculating the percentage of infected cells relative to the total number of nuclei, and the number of nuclei in treated cells relative to untreated controls, respectively (Fig. 12B, D). These results confirm that PS1097 is active against ZIKV and that protein production by the virus is halted during treatment.

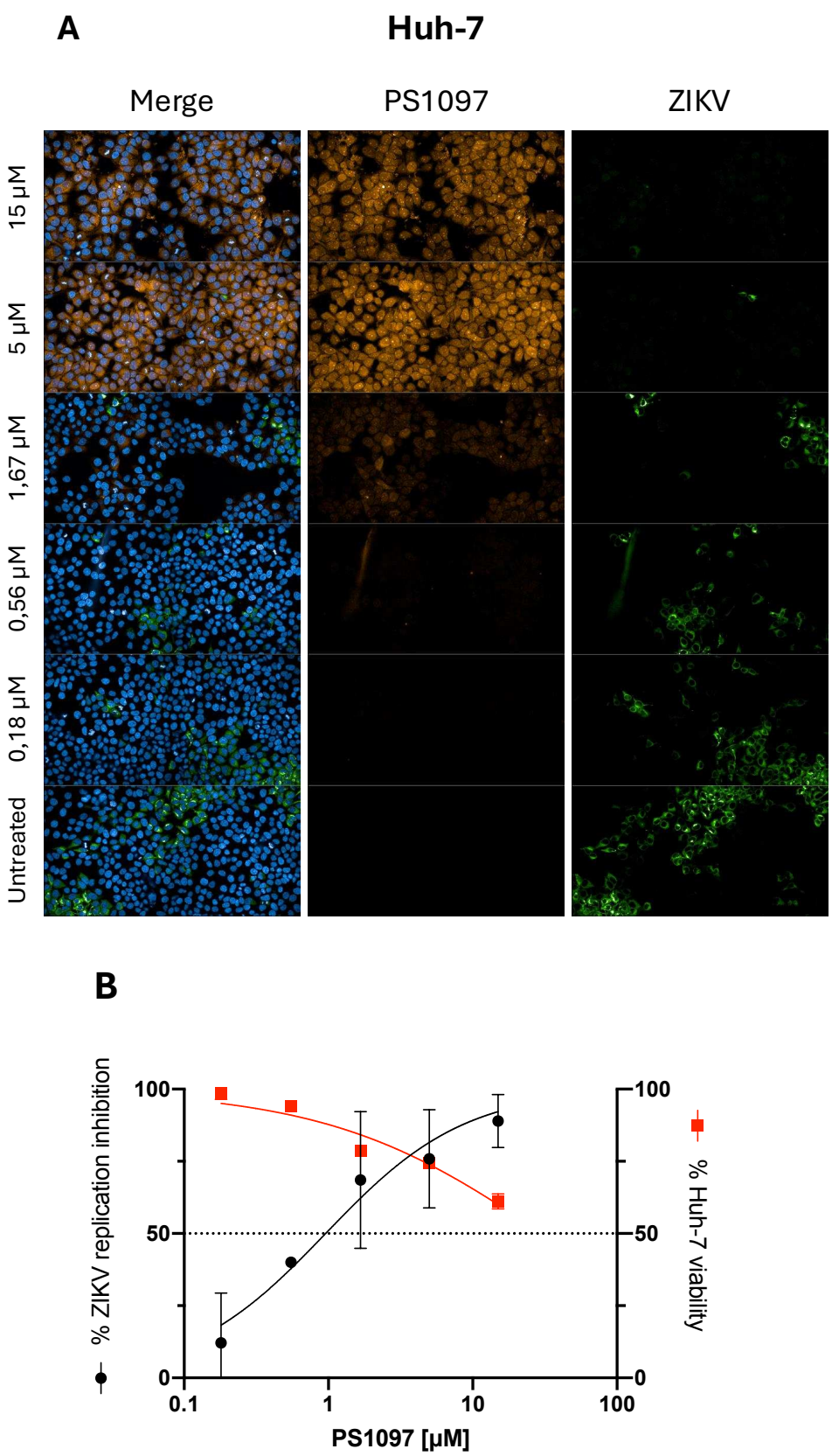
A
Huh-7
Merge
PS1097
ZIKV
15 µM
5 µM
1,67 µM
0,56 µM
0,18 µM
Untreated
B
% ZIKV replication inhibition
% Huh-7 viability
100
50
0
0.1
1
10
100
PS1097 [µM]

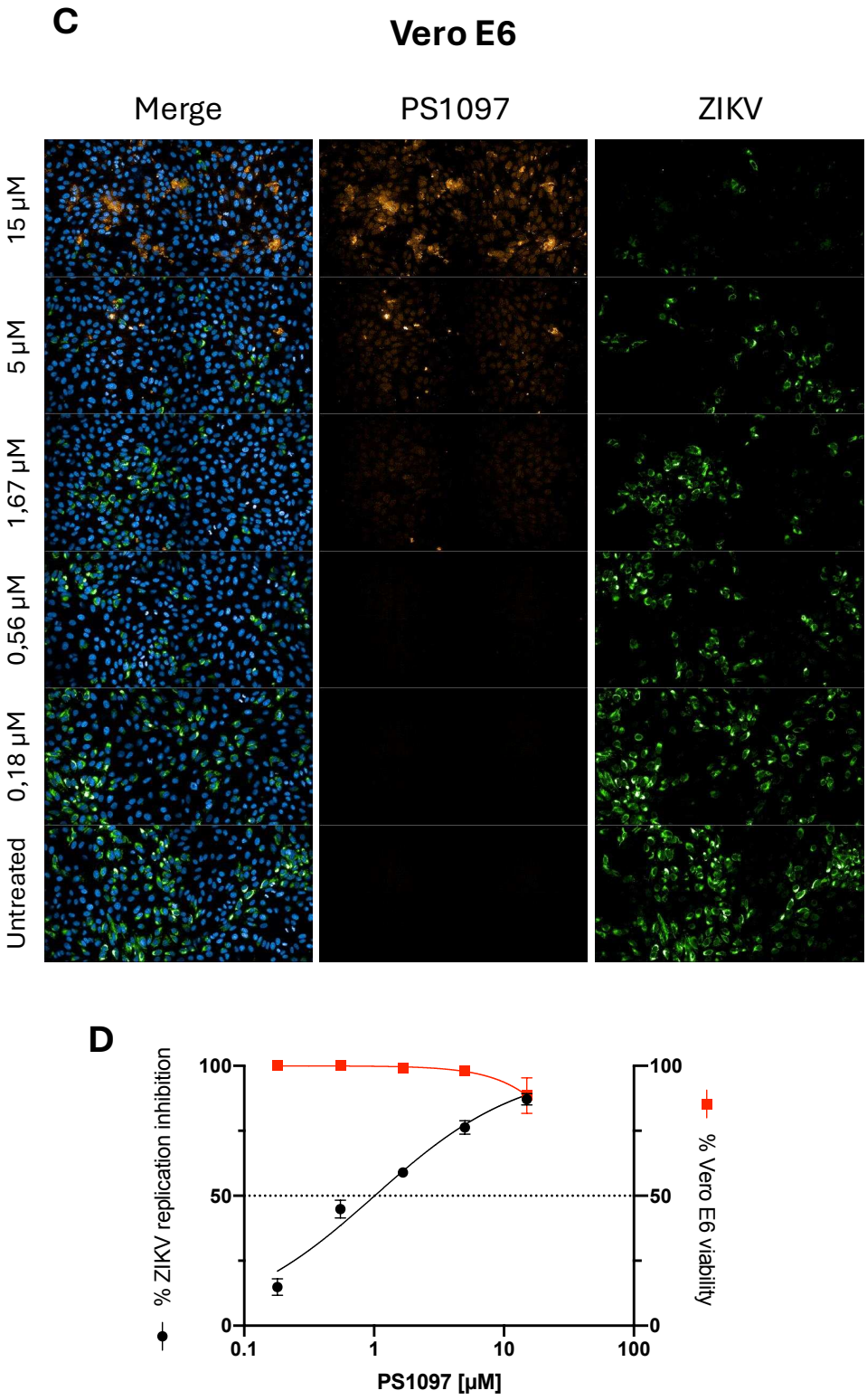

Figure 12: Viral protein quantification after treatment with PS1097 or SOF by immunofluorescence. ***A)*** *Confocal microscopy analysis of Huh-7 cells infected with ZIKV (MOI:1) and treated with increasing concentrations of PS1097 (0.18–15 µM).*

Viral protein expression was detected by immunofluorescence staining using an anti-Capsid antibody (green, Alexa Fluor 488), while nuclei were counterstained with DAPI (blue). PS1097 displayed intrinsic fluorescence detectable at 568 nm (orange). At high concentrations, the compound induced cytotoxic effects, whereas at non-toxic concentrations (≤5 μM) it strongly reduced viral expression, with efficacy maintained down to 0.6 μM. ***B)*** *Dose-response curves of the % ZIKV replication inhibition (black line) and % cell viability (red line) of the compound tested. The antiviral activity and cytotoxicity of PS1097 was evaluated on Huh-7 cells analyzed on Operetta CLS microscope calculating the percentage of infected cells relative to the total number of nuclei.* ***C)*** *Confocal microscopy analysis of Vero E6 cells infected with ZIKV (MOI:1) and treated with increasing concentrations of PS1097 (0.18–15 μM). Viral protein expression was detected by immunofluorescence staining using the same antibodies used on Huh-7 cells.* ***D)*** *Dose-response curves of the % ZIKV replication inhibition (black line) and % cell viability (red line) of the compound tested on Vero E6 cells.*

6.5. TOA experiments

To further elucidate the mechanism of PS1097 antiviral action, TOA experiments were conducted to shed light into the replication phase that might be inhibited by PS1097 (Fig. 14A). ZIKV^{Br} replication kinetics was first assessed by quantifying viral genomic RNA and protein inside Huh-7 cells at the times post infection (p.i.) shown in Figure 13A. Viral RNA was detectable as from ~12 h p.i. (Fig. 13C), whereas viral protein was visible by WB beginning from 24 h p.i. (Fig. 13B, C).

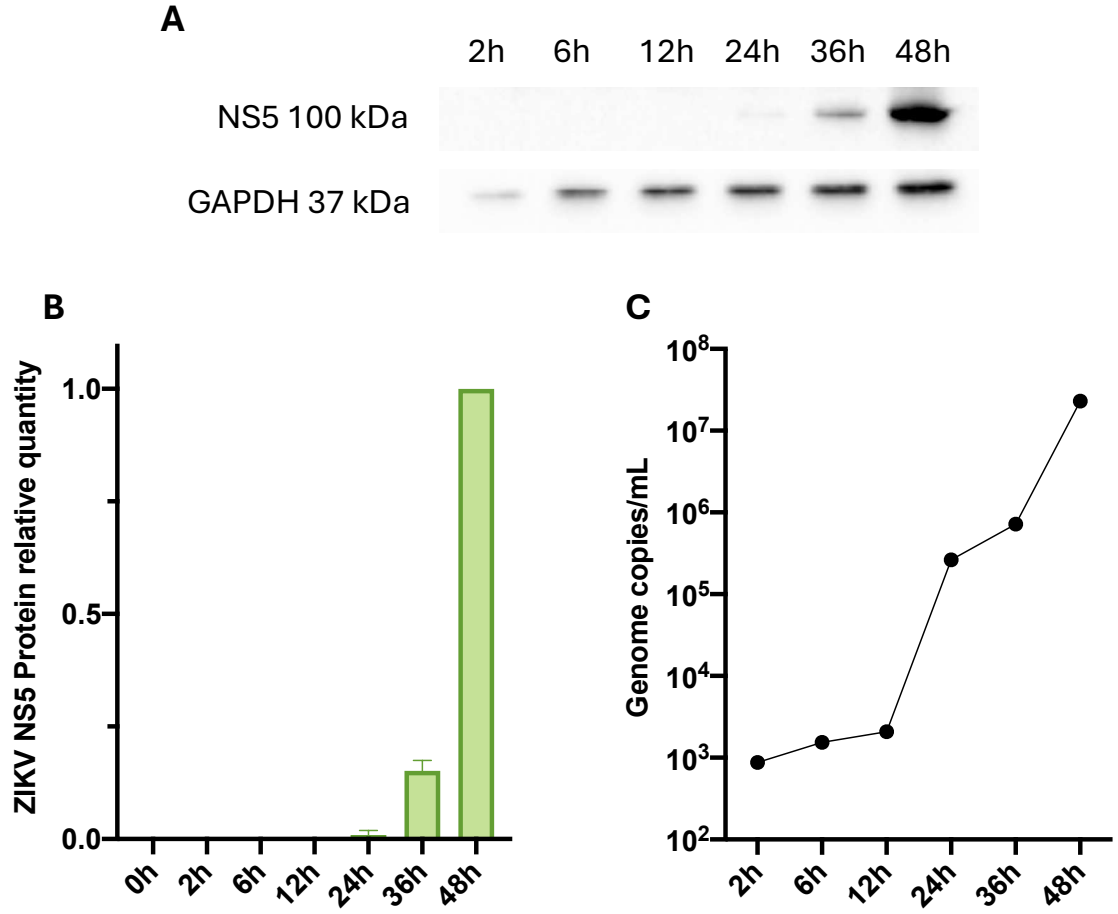

Figure 13: ZIKV replication kinetics. ***A)*** *ZIKV replication kinetics was determined on Huh-7 cells infected at MOI 1 for 2 h by WB cell lysates harvested at the times post infection shown. ZIKV NS5 and GAPDH were monitored with the antibodies in Table S1.* ***B)*** *Quantitative analysis of the results in A).* ***C)*** *qRT-PCR quantification of ZIKV RNA was carried out in ZIKV-infected cells lysed at the times post infection indicated on the x axis.*

In parallel, for TOA, cells were exposed to viral inoculum for 2 h. PS1097 or SOF were added at 10× EC_{50} together with the viral inoculum (0 h p.i.) or immediately after virus inoculum removal (2 h p.i.) or at the times p.i. shown in Figure 14A. Then, they were harvested at 48 h p.i. Viral RNA in cells was measured by qRT-PCR and inhibition relative to DMSO-treated cells was calculated, as described by [112] (Fig. 14D). Viral protein quantification revealed PS1097 suppressed viral protein expression when added up to 12 h p.i. in a time-dependent way (Fig. 14B, C): both

PS1097 and SOF demonstrated the strongest inhibition when added between o and 6 h p.i., indicating that PS1097 is likely to target the early phase of ZIKV replication, with similar kinetics as SOF.

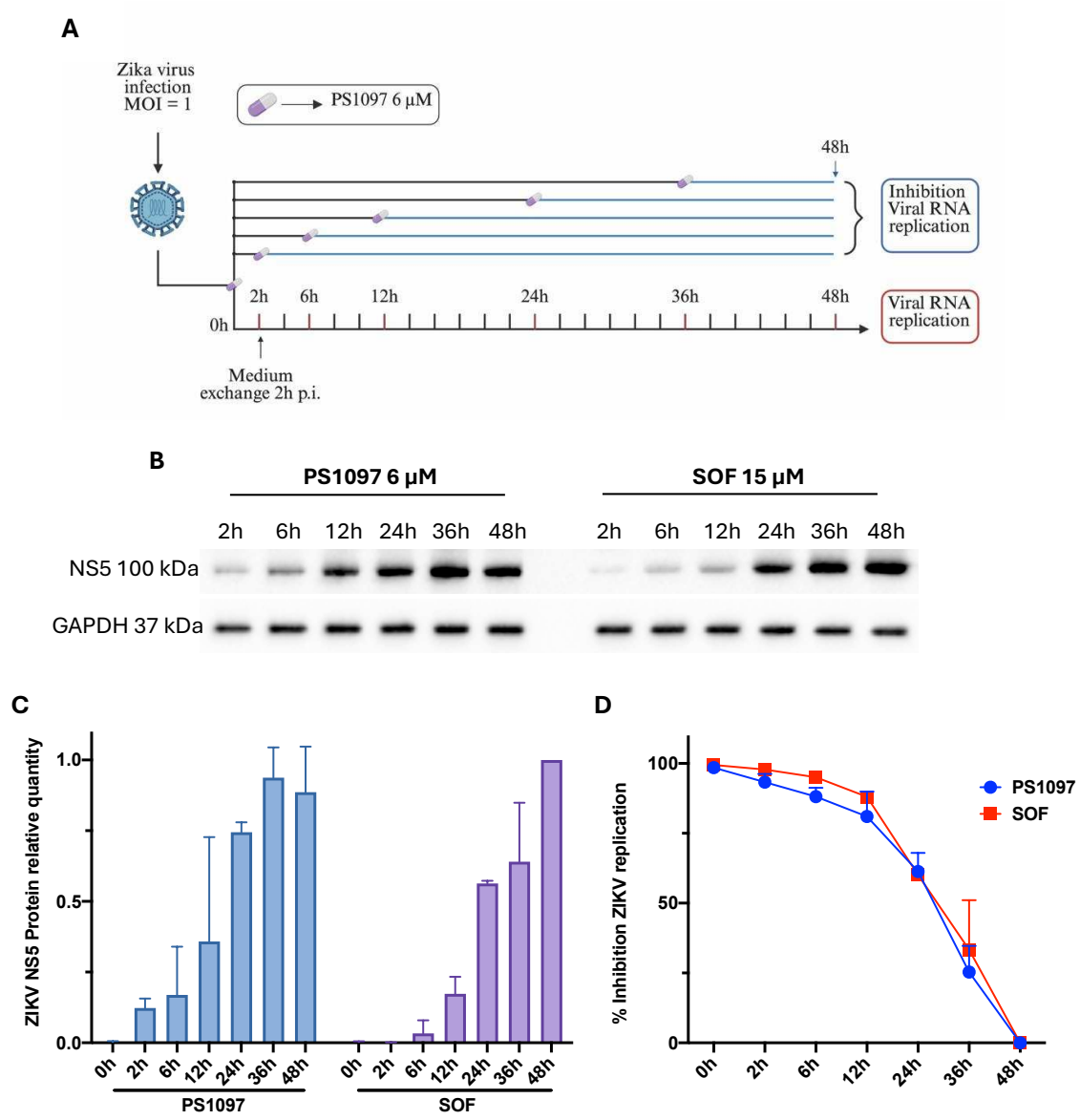

Figure 14: TOA assay and antiviral activity of PS1097 and SOF against ZIKV ***A)*** *Experimental design of the TOA assay for PS1097 and SOF.* ***B)*** *WB of lysates of Huh-7 cells harvested at 48 h p.i. where treatment with PS1097 or SOF was started as by A).* ***C)*** *Quantitative analysis of the results in B).* ***D)*** *ZIKV RNA was quantified in lysates of cells harvested at 48 h p.i. where treatment with PS1097 (blue line) or SOF (red line) was started at the times p.i. indicated on the x axis.*

6.6. Co-immunoprecipitation of ZIKV protein NS3 and NS2B

In the literature, a highly potent antiviral compound against DENV, JNJ-A07, described by Kaptein [112], exerts its activity by preventing the formation of the NS3–NS4B complex, a critical step in the viral replication cycle, without disrupting pre-existing interactions. To assess whether PS1097 might also interfere with the interaction between the viral protease NS3 and NS2B, co-immunoprecipitation experiments were carried out in ZIKV-infected Huh7 cells. Following infection and PS1097 treatment (6 μM), NS3-containing complexes were immunoprecipitated from cell lysates and analyzed by Western blot. In the precipitated fractions, NS2B was consistently detected together with NS3, confirming the expected physical association between the two proteins. Importantly, no difference was observed between untreated and PS1097-treated samples, indicating that the compound does not impair the stability of the NS3–NS2B complex (Fig.15).

As technical controls, western blots of the immunoprecipitated material were also probed with secondary antibody alone, which revealed the characteristic heavy chain of the immunoglobulins bound to the beads, thereby excluding non-specific cross-reactivity. In parallel, non-immunoprecipitated lysates (input fractions) were loaded in the gel and probed for NS3, NS2B, and GAPDH, confirming the presence of intact viral and cellular proteins in all conditions. Moreover, to obtain a quantitative evaluation of viral protein precipitation, densitometric analysis was performed and the ratio of NS2B to NS3 was calculated. This analysis showed that comparable NS2B/NS3 ratios were precipitated under all experimental conditions, further supporting the conclusion that PS1097 does not alter the formation or stoichiometry of the NS3–NS2B complex. Taken together, these results demonstrate that PS1097 does not interfere with the interaction between NS3 and its cofactor NS2B, suggesting that the antiviral activity of the compound is mediated through a different mechanism.

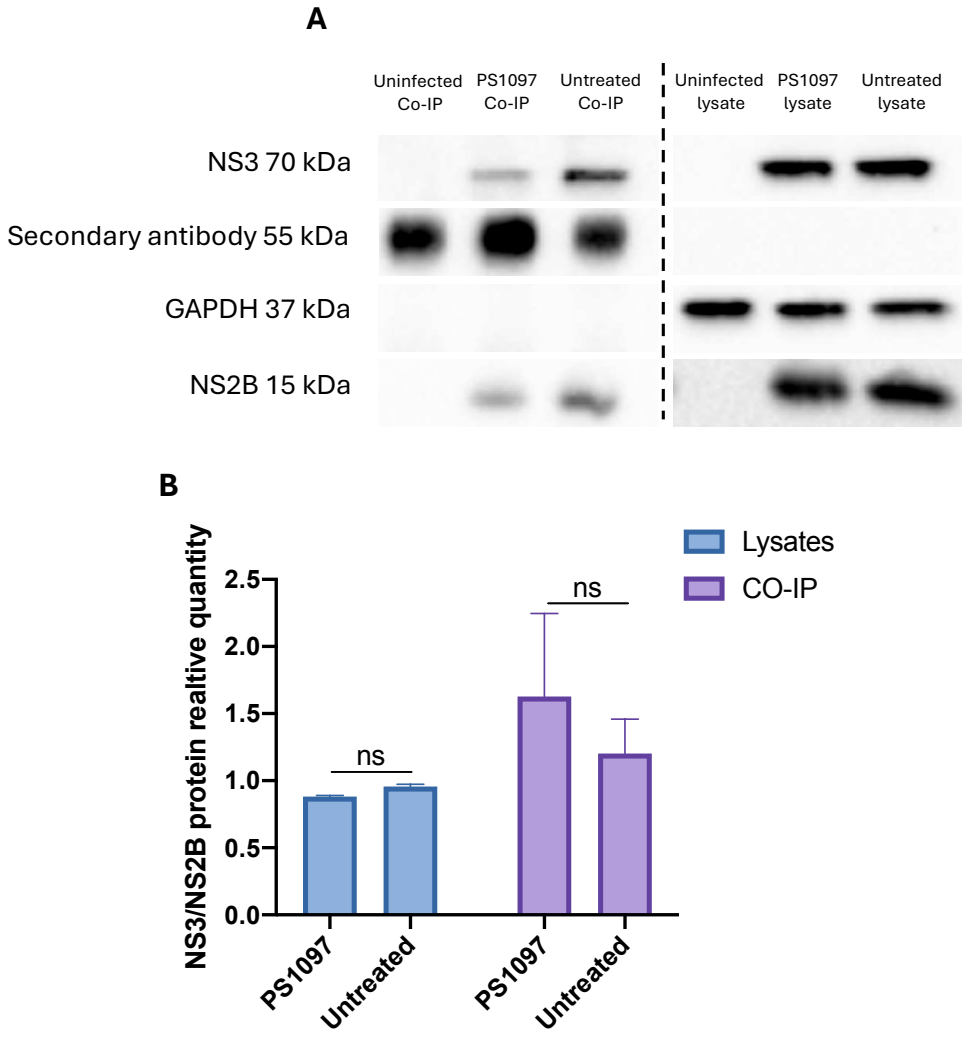

Figure 15: Co-immunoprecipitation of NS3 and NS2B in ZIKV-infected Huh7 cells. ***A)*** *Huh-7 cells were infected with ZIKV (MOI:1) and either left untreated or treated with 0.6 µM PS1097 for 48h. Cell lysates were subjected to immunoprecipitation using magnetic beads coupled with anti-NS3 antibody and analyzed by WB.* ***B)*** *Quantification of results in A) through the ratio between the amounts of NS2B protein to NS3 for each treatment.*

Statistical analysis was performed using paired t-test. Data are expressed as mean ± SD, N=2. Antibodies used are shown in Table 2.

6.7. Does PS1097 have a virucidal effect?

To evaluate a potentially virucidal activity of PS1097, infectious ZIKV^{Br} suspensions were incubated for 1 h at 37 °C either in the absence of compound (temperature stability control) or in the presence of PS1097 or SOF, before titration on Vero E6 cells by plaque assay. In parallel, control samples were processed in which ZIKV^{Br} was mixed with the compounds immediately prior to titration, omitting the pre-incubation step. This control was designed to rule out potential assay interference resulting from compound carryover, ensuring that any observed antiviral effect was not attributable to residual compound activity during the titration phase. HSV-2 suspensions treated under identical conditions were also included as an additional specificity control, since PS1097 has not been shown to affect this virus.

The results in Figure 16 clearly demonstrated that pre-incubation of ZIKV^{Br} with PS1097 did not reduce viral infectivity. The number of plaques obtained from PS1097-pretreated samples was indistinguishable from that observed in untreated virus or in virus incubated with SOF, and comparable to the corresponding non–pre-incubated controls (Fig. 16). Similarly, no differences were observed in the HSV-2 samples. These findings indicate that PS1097 does not exert any direct virucidal effect on ZIKV particles, but rather requires intracellular conditions to inhibit replication.

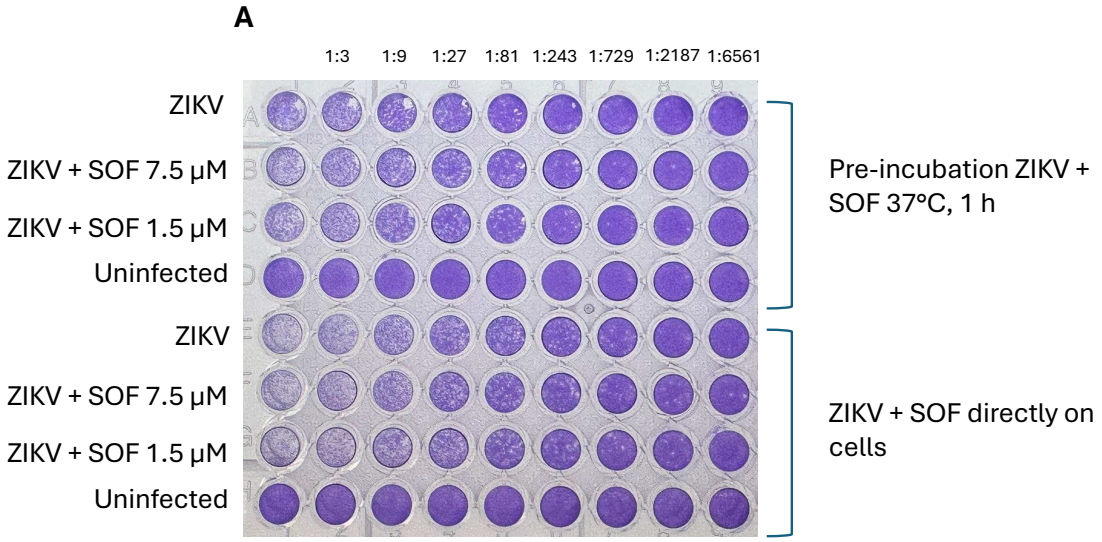

B

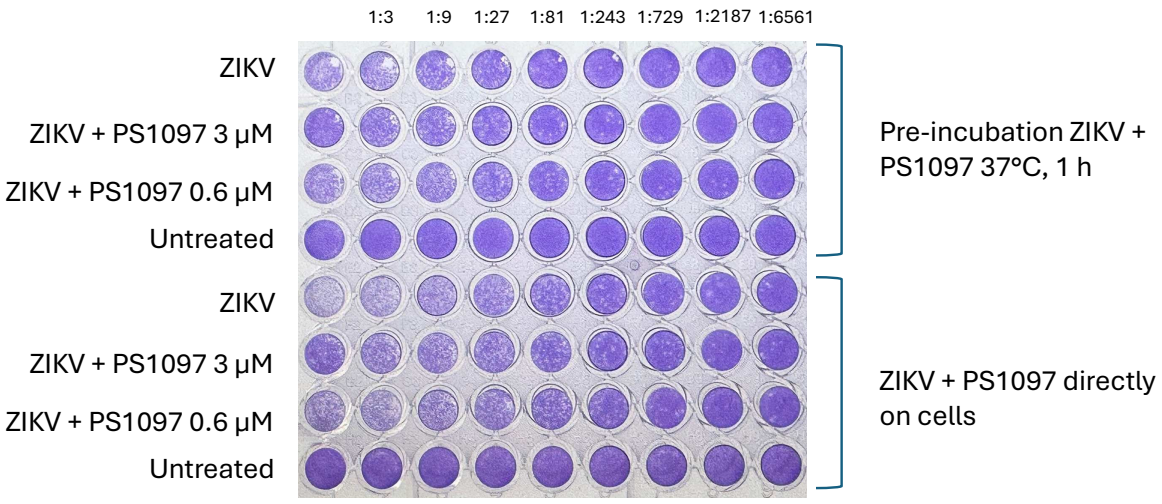
1:3 1:9 1:27 1:81 1:243 1:729 1:2187 1:6561
ZIKV
ZIKV + PS1097 3 µM
ZIKV + PS1097 0.6 µM
Untreated
ZIKV
ZIKV + PS1097 3 µM
ZIKV + PS1097 0.6 µM
Untreated
Pre-incubation ZIKV + PS1097 37°C, 1 h
ZIKV + PS1097 directly on cells

C

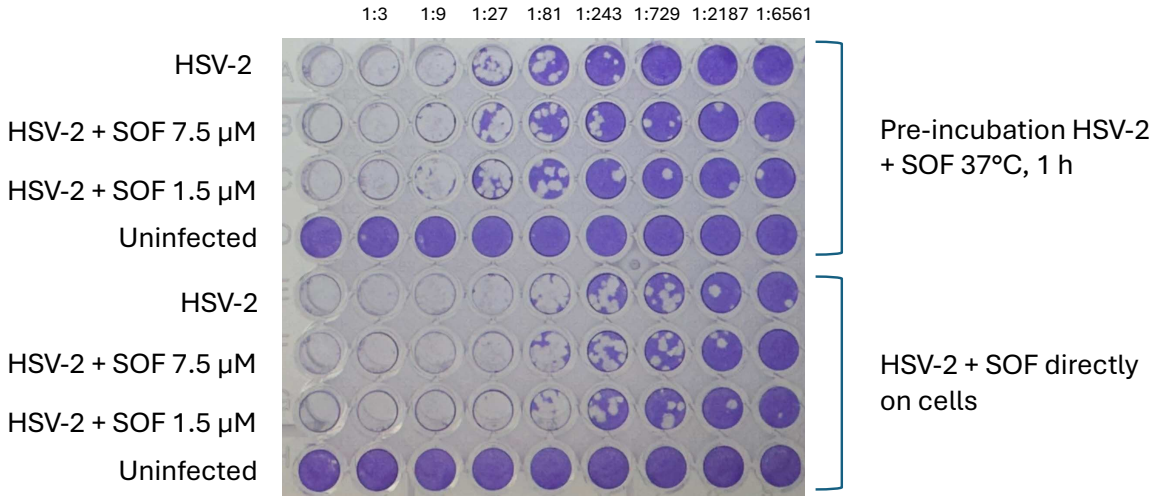
1:3 1:9 1:27 1:81 1:243 1:729 1:2187 1:6561
HSV-2
HSV-2 + SOF 7.5 µM
HSV-2 + SOF 1.5 µM
Uninfected
HSV-2
HSV-2 + SOF 7.5 µM
HSV-2 + SOF 1.5 µM
Uninfected
Pre-incubation HSV-2 + SOF 37°C, 1 h
HSV-2 + SOF directly on cells

D

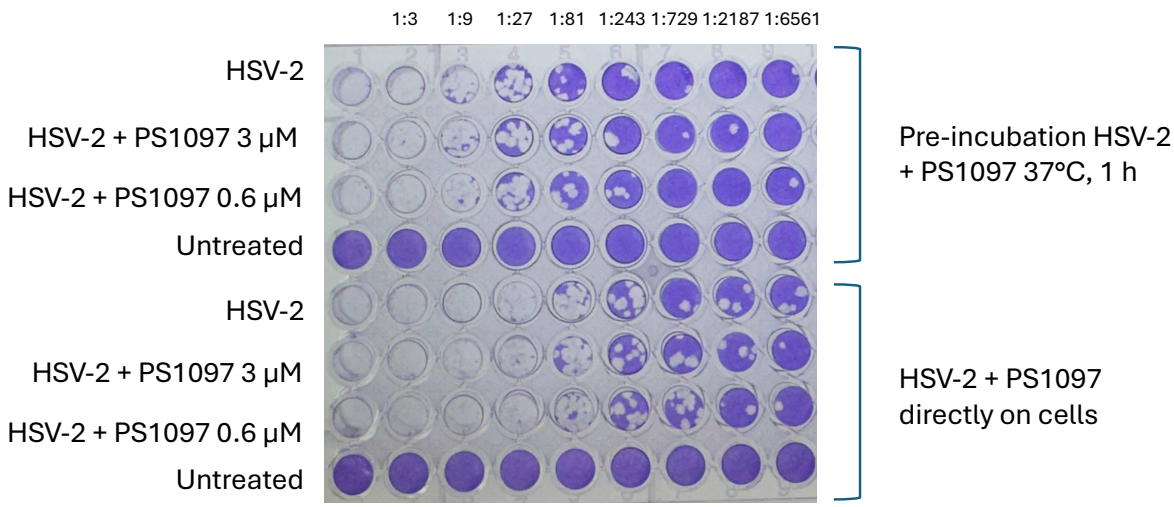
1:3 1:9 1:27 1:81 1:243 1:729 1:2187 1:6561
HSV-2
HSV-2 + PS1097 3 µM
HSV-2 + PS1097 0.6 µM
Untreated
HSV-2
HSV-2 + PS1097 3 µM
HSV-2 + PS1097 0.6 µM
Untreated
Pre-incubation HSV-2 + PS1097 37°C, 1 h
HSV-2 + PS1097 directly on cells

Figure 16: Evaluation of the potential virucidal activity of PS1097. Infectious ZIKV^{Br} suspensions (MOI:1) were incubated for 1 h at 37 °C either in the absence of compound (temperature stability control) or in the presence of PS1097 or SOF, followed by titration on Vero E6 cells by plaque assay. In parallel, control samples without pre-incubation (virus mixed with compounds immediately before titration) were included to rule out assay interference due to compound carryover. HSV-2 suspensions treated under identical conditions were used as an additional specificity control.

6.8. CETSA assay

To investigate whether PS1097 or SOF were able to interact with ZIKV NS5 or CV, and stabilize them to heat denaturation, we applied the CETSA assay, which relies on monitoring protein stability across a temperature gradient as an indirect measure of compound binding. This assay is based on the observation that protein binding increases protein stability to temperature.

In this setup, infected Huh-7 cells were treated with either DMSO, SOF, or PS1097 prior to being exposed to increasing temperatures. Cells were then lysed and centrifuged, and the soluble fractions of the proteins were subsequently analyzed by WB. The result expected in case any compound bound to NS5 (RdRp) or capsid was an increased presence of soluble proteins in compound-treated sample as compared to untreated ones. As shown in Figure 17A, in all conditions NS5 and CV progressively denatured and precipitated as the temperature increased. However, the comparison of the thermal profiles across treatments revealed no appreciable differences between the samples: the degradation pattern of the viral proteins analyzed were comparable in cells treated with DMSO, SOF, or PS1097, with band intensities decreasing in the same manner across the full temperature range tested. Even when the analysis was refined to focus specifically on the temperature window at which NS5 typically unfolds, no evidence of stabilization was observed. Overall,

the CETSA results indicate that neither PS1097 nor SOF induced detectable changes in the thermal stability of NS5 or CV protein, suggesting that under the experimental conditions used, these compounds do not exert a measurable binding effect on the protein (Fig. 17).

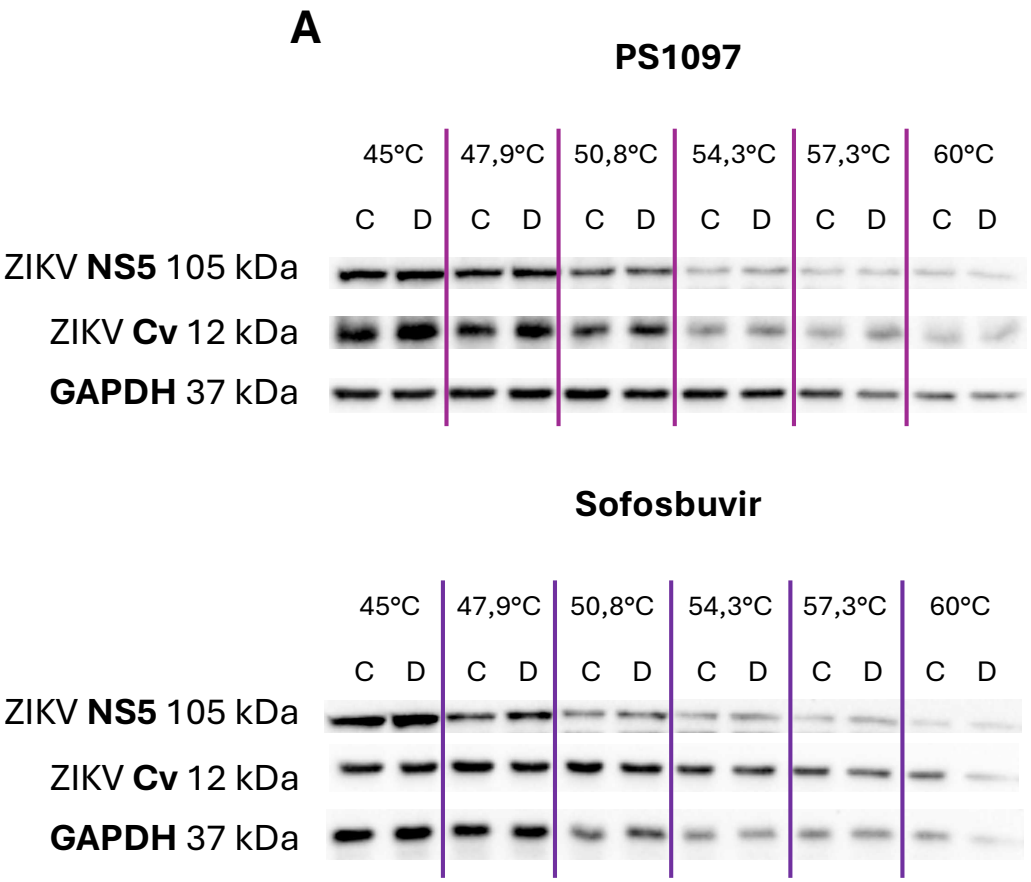

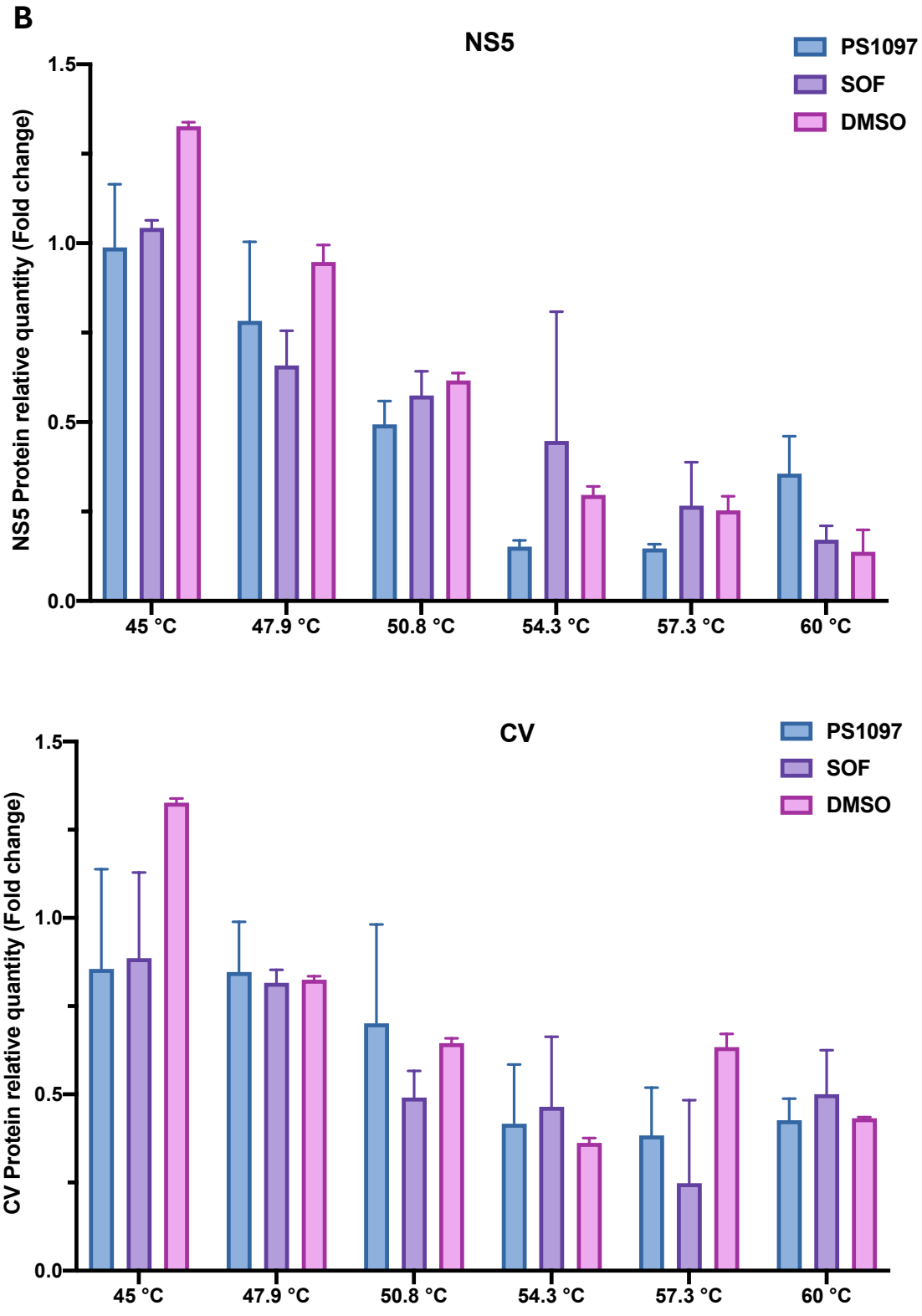

Figure 17: Thermal stability analysis of NS5 and CV proteins in cells treated with PS1097 or SOF. ***A)*** *WB analysis of soluble protein fractions after heat treatment*

across a temperature gradient (43–63 °C) showed progressive denaturation of NS5 and CV viral proteins (C = compound; D = DMSO). No differences were observed between DMSO-, SOF-, or PS1097-treated cells, indicating that neither compound altered the thermal stability of NS5 and CV under the experimental conditions tested. ***B)*** *Densitometric quantification of NS5 and CV band intensities normalized to the GAPDH housekeeping protein confirmed the absence of detectable stabilization or protection by SOF or PS1097 (or DMSO), with degradation profiles overlapping across treatments. Data are expressed as mean ± SD, N=2.*

6.9. Determination of synergistic effects

To continue in the effort to provide knowledge on PS1097 mechanism of action, interaction between PS1097 and SOF was investigated. If PS1097 and SOF produced similar effects on viral infection, their interaction could suggest whether they acted at the same pathway (additive or synergistic effect) by enhancing each other's effects. In contrast, independent or complementary effects would suggest action at different sites; competitive antagonism would suggest that both drugs acted on the same receptor site, whereas noncompetitive antagonism might indicate that they act on different sites but affect the same pathway.

To explore potential interactions between PS1097 and SOF, combined treatments were systematically tested under different experimental conditions. Cells were infected with $ZIKV^{Br}$, MOI:1 and treated with serial twofold dilutions of the PS1097 and SOF combinations (PS1097 2.0-0.125 µM; SOF 5.0-0.39 µM). Overall, no clear synergistic effects could be detected, indicating that the simultaneous administration of the two compounds does not enhance their antiviral activity beyond the effect observed with each drug alone. Interestingly, at the highest concentrations tested, a slight but reproducible antagonistic effect was observed (Fig. 18A). This finding suggests that PS1097 may interfere, either directly or indirectly, with the mechanism of action of SOF, potentially by competing for similar molecular targets or by modulating cellular pathways that influence SOF activity.

Their combined use does not appear to provide therapeutic advantages; on the contrary, it points toward a possible functional interference and supports the hypothesis that PS1097 acts through a mechanism distinct from that of SOF (Fig. 18). This observation not only underscores the importance of evaluating drug–drug interactions in the early phases of antiviral development but also highlights the need for further mechanistic studies to clarify the molecular basis of the observed antagonism and to define whether PS1097 may represent a viable candidate for combinatorial regimens or should instead be considered for stand-alone therapeutic strategies.

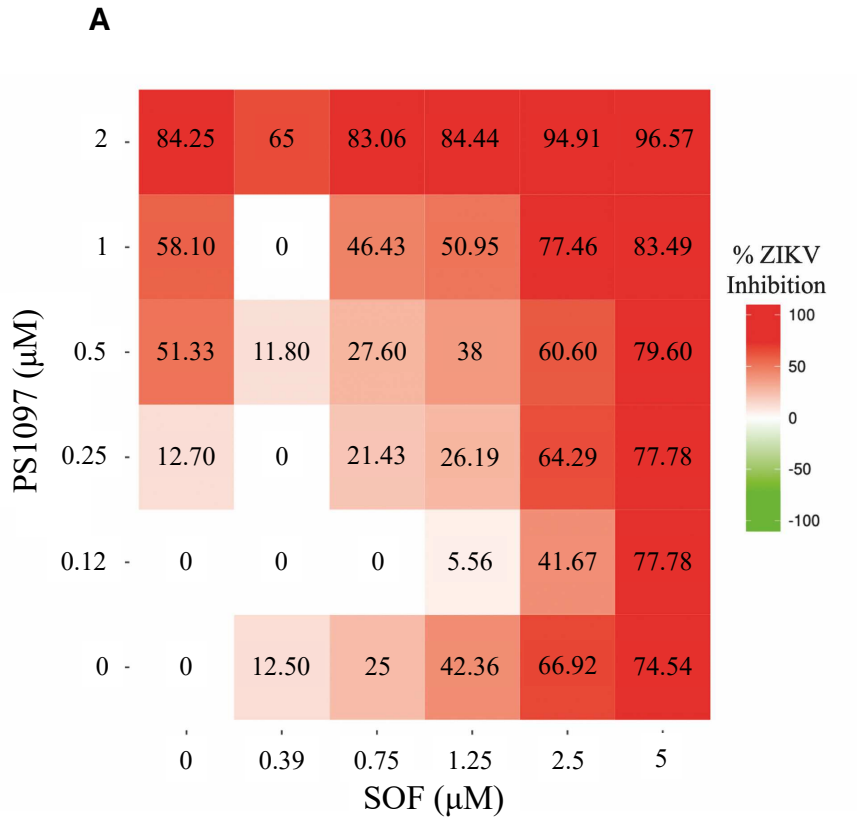

B

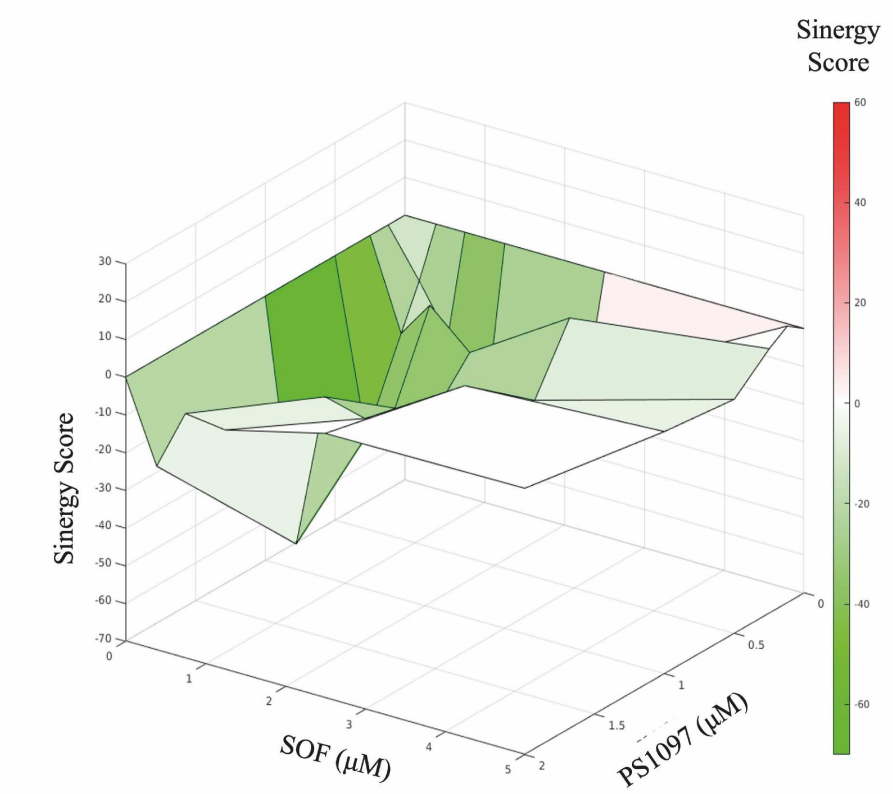

Figure 18: Combined antiviral activity of PS1097 with SOF against ZIKV. ***A****) Huh-7 cells were infected with ZIKV then treated with PS1097 or SOF, alone or in combination, at the indicated concentrations. After 48 h p.i., supernatants were harvested and titrated for ZIKV yield. Two-dimensional representation of dose-response interaction matrix was determined in synergyfinder.org (Loewe algorithm). Color gradient indicates viral yield inhibition score (red-highest score).* ***B)*** *Three-dimensional surface plot representing synergy score (Z axis) for each compound combination. X axis: SOF up to 5 µM, Y axis: PS1097 up to 2 µM. Green: antagonistic effect, red: synergistic effect.*

6.10. Selection of PS1097-resistant variants

To identify a viral protein possibly acting as a target for PS1097 antiviral activity, the possibility to select for PS1097-resistant variants was explored. Indeed, by selecting viral variants capable of replicating in the presence of a drug, one can sequence the

resistant strains to identify mutations in viral proteins that confer resistance to the drug. To this aim, $ZIKV^{Br}$ was passaged in the presence of an initial concentration of 0.6 μM, as graphically described in Figure 19, with the intention of gradually increasing it [112].

At least four independent attempts were performed, each starting from wild type virus; however, no resistant strains of ZIKV ever adapted to the presence of PS1097. Instead, viral yield progressively decreased until no infectious virus could be detected at the 9^{th} passage (corresponding to 9 weeks), when the passaging procedure had to be interrupted because the virus could not be retrieved any longer. This behavior strongly suggests that the mechanism targeted by PS1097 is indispensable for viral replication and that, once inhibited, the virus cannot easily acquire compensatory mutations to bypass the block. Therefore, PS1097 appears to exhibit a high genetic barrier to resistance, a feature of relevance for potential therapeutic development.

In parallel, additional experiments are currently being conducted to include a control condition with SOF, a drug known from the literature to readily generate resistant mutants under similar passaging conditions [119]. The introduction of this parallel control is intended to serve as a proof of concept, demonstrating that the experimental setup is indeed capable of supporting the selection of resistant variants when feasible, and thereby strengthening the conclusion that the absence of resistant strains in the case of PS1097 is due to its unique mode of action and not to technical limitations of the assay.

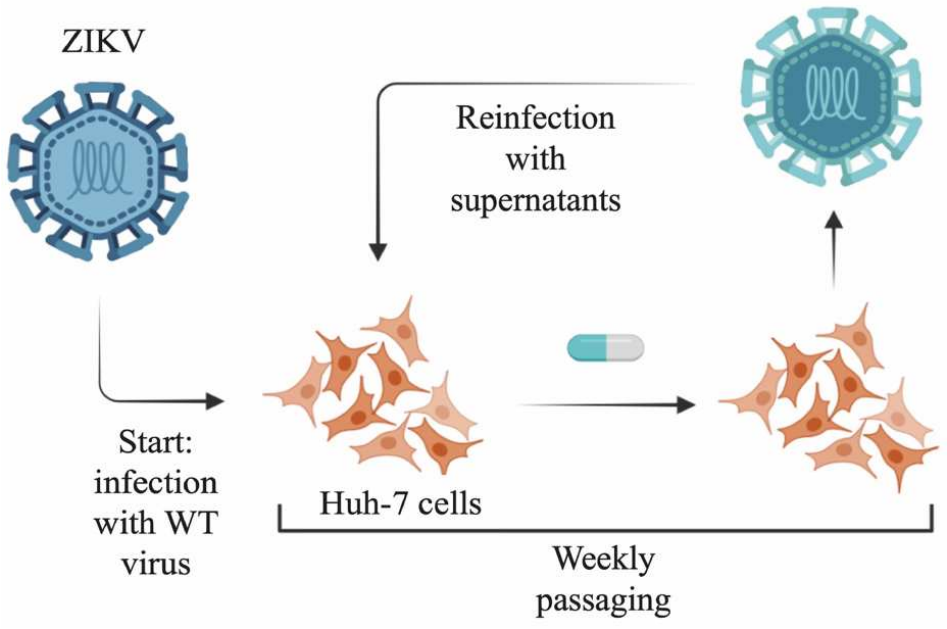

Figure 19: Experimental design for selection of compound-resistant viral mutants. Huh-7 cells were infected with ZIKV^{Br} (MOI:1) for 2 h at 37°C, then added with 0.6 μM of PS1097 for 48 h at 37 °C. The supernatants were then titrated and used to infect freshly seeded cells at MOI:1. During passaging of the virus, the starting concentration of the compound was increased every week.

6.11. PS1097 causes potent downregulation of RTN3 protein

Given the broad range of antiviral activity of PS1097 (Tab. 4), it was considered unlikely that the compound could block proteins from totally different viral species. Instead, an indirect activity of PS1097 acting on a cellular protein important in the replication of a variety of viruses was hypothesized. A common feature of the viruses sensitive to PS1097 is that most of them cause ER rearrangement during the first phases of their replication, with the notable exception of CHIKV, that rearranges its ROs at the plasma membrane [120].

In this part of the experimental work, attempts were made to determine whether several ER resident proteins were affected by treatment of cells with PS1097. The proteins selected, mentioned in Par. 1.5 of the Introduction, were:

- RTN3, placed on the tips of ER tubules [121,122], can induce or stabilize membrane curvature binding the flaviviral nonstructural protein NS4B, which is required for formation of membranous webs, the sites of viral replication [123];
- RTN4 that is likely a supporting ER membrane-shaping factor aiding in the morphological changes in the ER required for flavivirus replication complexes [124];
- FAM134B that mediates ER-phagy, removing excess or damaged ER, including possibly parts of viral-altered ER, thereby acting as a restriction factor limiting the membrane resources available for viral replication [125].
- TMEM41B interacts (or colocalizes) with viral nonstructural proteins (NS4A, NS4B) in infected cells, and is recruited to viral RNA replication complexes, presumed to help with membrane curvature in the ER for forming replication organelles [126].

Huh-7 cells were treated with 6 μM PS1097 or, as a negative control, SOF, 15 μM, for 48 h, then they were lysed for WB. The results, shown in Figure 20, demonstrate that treatment with PS1097 caused a significant decrease in RTN3 content, whereas FAM134B, RTN4 and TMEM41B were virtually unchanged. To exclude that the effect was due to the antibody used, or to differential splicing of the RTN3 mRNA that might cause the elimination of an epitope recognized by the other antibody, two different antibodies were used, one detecting the N-terminus (RTN3L) and the other the C-terminus of RTN3 (RTN3S) and similar results were obtained (Fig. 20A, B).

To evaluate whether a reduction in RTN3 mRNA transcription possibly caused by treatment with PS1097 contributes to the observed decrease in RTN3 protein levels, qRT-PCR was performed on cell lysates to quantify mRNA levels for RTN3, RTN4, and FAM134B following treatment with PS1097 or SOF. As shown in Figure 19C, PS1097 treatment led to an approximately 50% reduction in RTN3 mRNA, while SOF treatment resulted in a roughly 25% decrease. However, since the modest reduction in RTN3 mRNA following SOF treatment did not affect RTN3 protein levels, it is unlikely that the 50% decrease in RTN3 mRNA alone accounts for the marked

reduction in protein levels observed with PS1097 treatment. Nonetheless, this decrease may contribute to the antiviral activity of PS1097, as RTN3 has been shown to be essential for ZIKV replication [127].

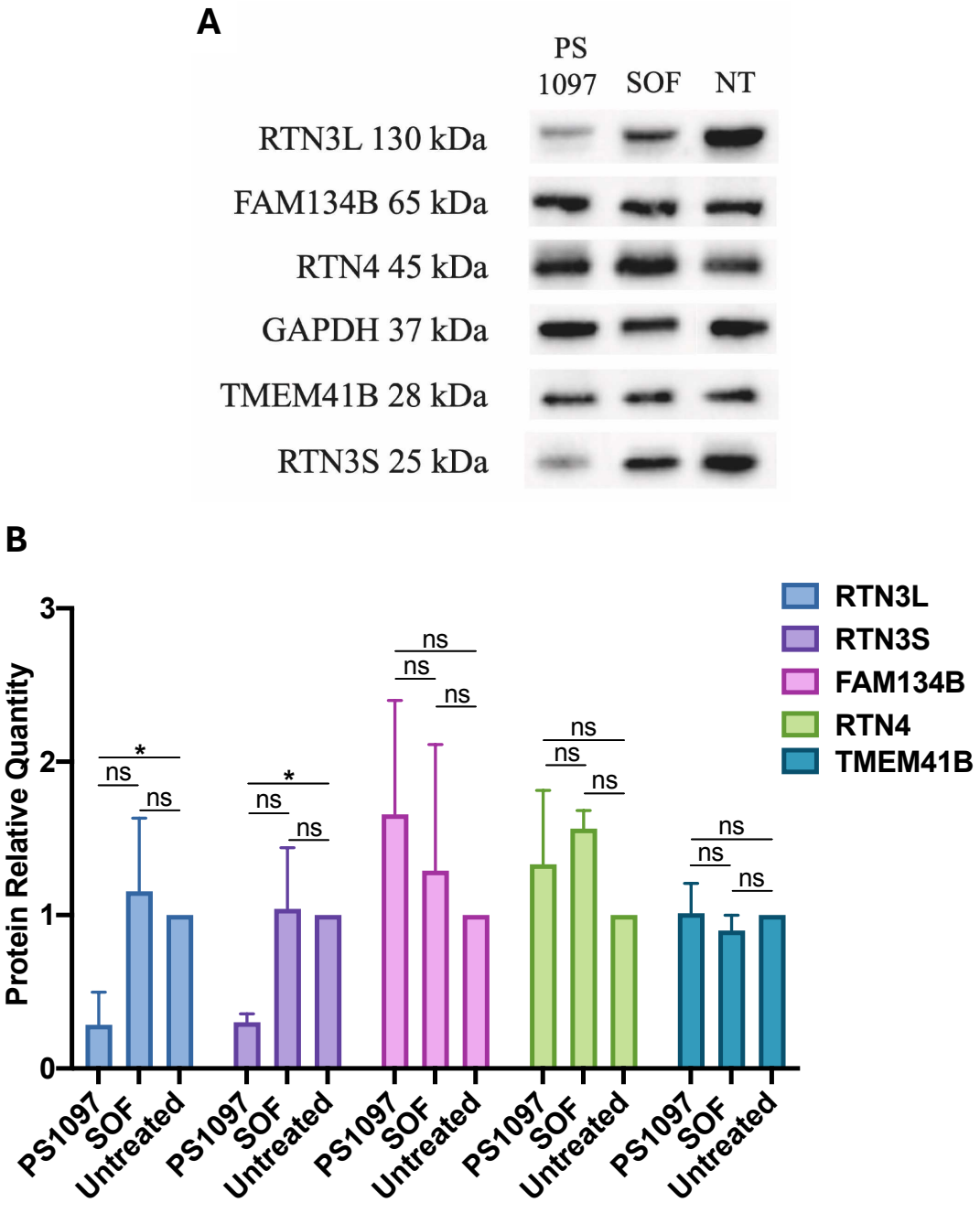

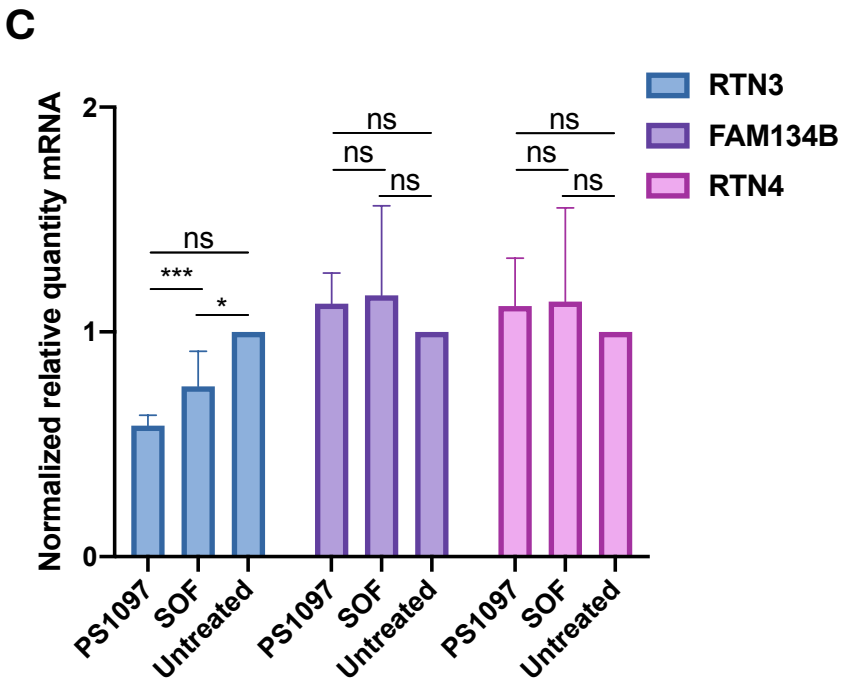

Figure 20: Effect of PS1097 and SOF on ER protein expression and mRNA levels in Huh-7 cells. ***A)*** *Western blot of Huh-7 lysed 48 h after treatment with 6 μM PS1097 or 15 μM SOF developed with antibodies against the ER proteins shown on the left or GAPDH as a control.* ***B)*** *Quantitative analysis of the results in A).* ***C)*** *qRT-PCR of RTN3 or RTN4 or FAM134B mRNA in extracts of cells treated with 6 μM PS1097 or 15 μM SOF for 48 h.*

Statistical analysis was performed using One-Way Anova followed by Tukey–Kramer post-hoc correction ($p<0.01$; $\alpha = 0.05$) with all groups compared against each other in the multiple-comparison analysis. Data are expressed as mean ± SD, N=3. Antibodies used are shown in Table 2.

6.12. Does PS1097 promotes RTN3 degradation through the proteasomal pathway?

To clarify whether RTN3 is directed towards proteasomal degradation in response to PS1097, we designed experiments based on the use of the proteasome inhibitor MG132. Huh-7 cells were treated or not with PS1097 (6 μM). After 24 h, or 42 h (i.e., 24 h or 6 h before the end of the 48-h incubation, respectively), cells were treated

with MG132 (1 μM). WB analysis was performed using antibodies against RTN3, FAM134B, and GAPDH. FAM134B served as a positive control for proteasome inhibition, as it is known to be degraded *via* this pathway [128]; accordingly, its accumulation was observed in wells treated with MG132 (Fig. 21). If RTN3 were also degraded *via* the proteasome, its accumulation would be expected under the same conditions. Instead, in cells treated with MG132, RTN3 levels remained comparable to the untreated control, while RTN3 expression continued to decrease in PS1097-treated cells (Fig. 21). These findings suggest that RTN3 degradation upon PS1097 treatment does not occur through the proteasomal pathway but likely involves an alternative degradation mechanism.

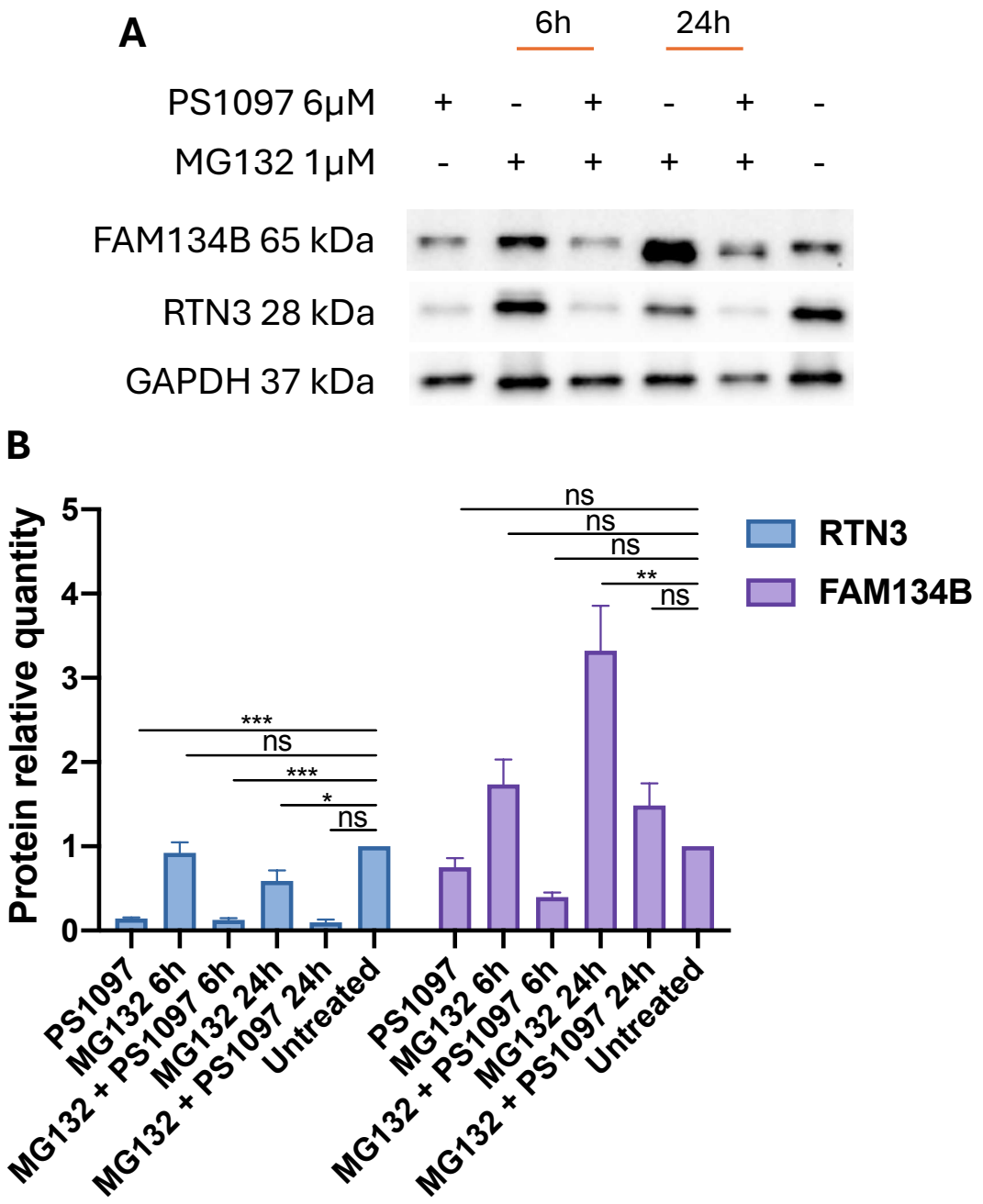

Figure 21: Role of the proteasome in RTN3 decrease. ***A)*** *WB analysis of RTN3, FAM134B, and GAPDH in Huh-7 cells treated with PS1097 (6 μM) and/or MG132 (1 μM) as indicated. FAM134B accumulation confirms effective proteasome inhibition by MG132. RTN3 levels decrease upon PS1097 treatment and are not restored by proteasome inhibition.* ***B)*** *Quantification of RTN3 protein levels normalized to GAPDH. Statistical analysis was performed using One-Way Anova followed by Tukey–Kramer post-hoc correction ($p<0.01$; $\alpha = 0.05$) with all groups compared*

against each other in the multiple-comparison analysis. Data are expressed as mean ± SD, N=2. Antibodies used are shown in Table 2.

6.13. Protein half-life determination using cycloheximide chase assay

To evaluate the stability of selected proteins, Huh-7 cells were treated with cycloheximide (10 µg/ml) to inhibit *de novo* protein synthesis, and protein levels were monitored over time. Huh-7 cells were treated with cycloheximide or not and were harvested at 0-, 6-, 12-, 24-, 36-, 48h post treatment and analyzed by WB. The expression of RTN3, RTN4, and FAM134B progressively declined at 6-, 12-, 24-, and 48-h post-treatment. Quantification of band intensities normalized to GAPDH revealed distinct degradation kinetics among the proteins analyzed. Nonlinear regression of the decay curves allowed the calculation of protein half-lives, which were estimated to be approximately 21h for RTN3, > 48h for RTN4, and 15h for FAM134B.

These results confirm that the cycloheximide chase assay provides a reliable readout of protein turnover dynamics in Huh-7 cells and highlight differences in protein stability that may underlie their cellular functions. RTN3 and FAM134B displayed very similar half-lives, suggesting that, under basal conditions, the two proteins undergo degradation with comparable kinetics (Fig. 22). This observation is relevant in the context of PS1097 treatment. Indeed, while RTN3 levels were affected, no reduction in FAM134B was observed upon exposure to PS1097. Given that FAM134B and RTN3 have a similar intrinsic half-life, the absence of a decrease in FAM134B following treatment argues against the hypothesis that PS1097 primarily acts by blocking *de novo* protein synthesis. Instead, these data suggest that the compound might influence protein levels through a more selective or pathway-specific mechanism rather than a global inhibition of translation.

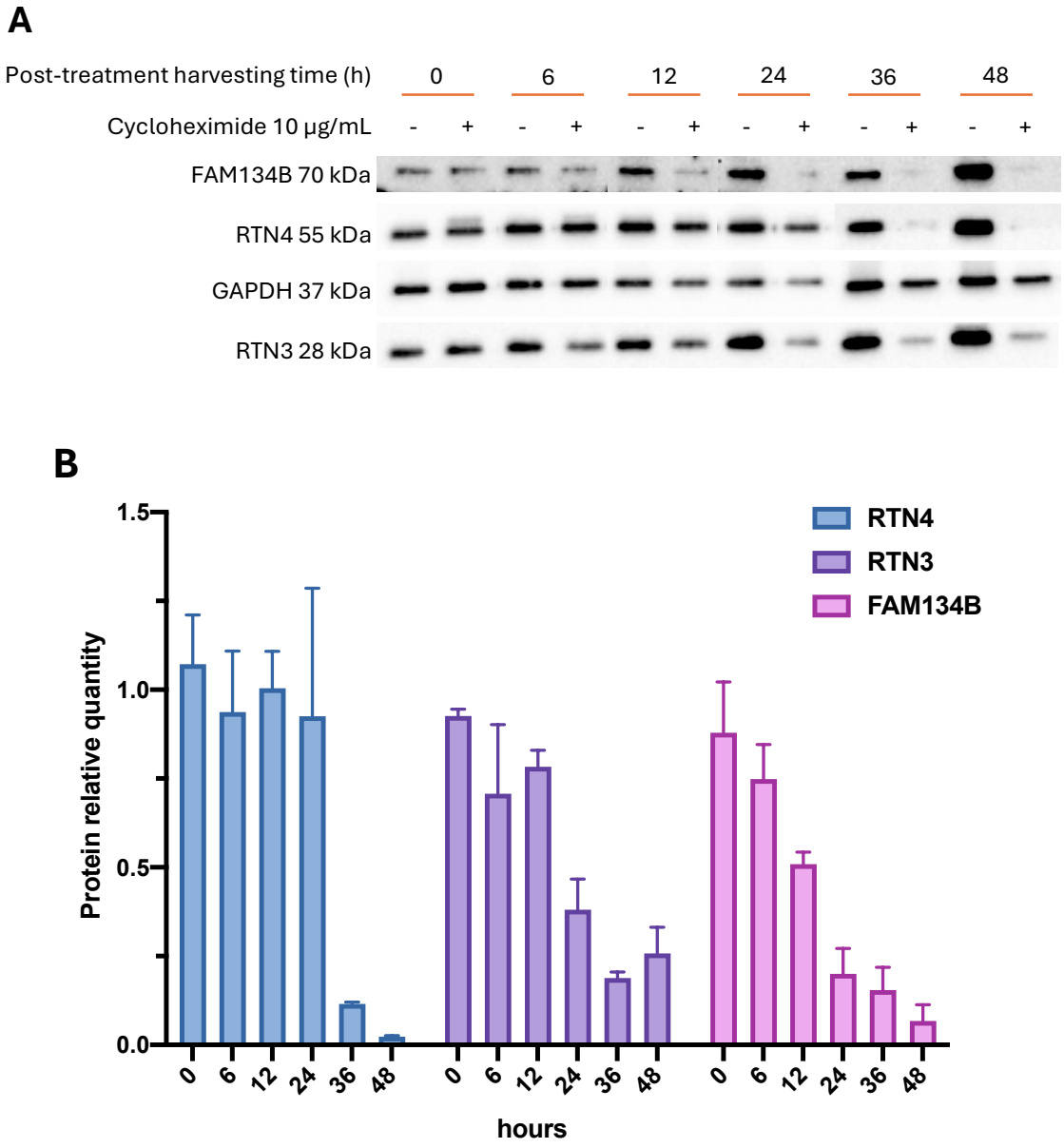

Figure 22: Protein half-life determination. ***A)*** *Western blot analysis of RTN3, RTN4, and FAM134B expression in Huh-7 cells treated with cycloheximide (10 µg/ml) and collected at the indicated time points post-treatment (6, 12, 24, and 48 h).* ***B)*** *Quantification of protein levels normalized to GAPDH and plotted as a function of time. Data were fitted by nonlinear regression (one-phase exponential decay) to calculate protein half-lives.*

7. DISCUSSION AND CONCLUSION

Emerging and re-emerging viral infections continue to pose a significant threat to global health, as exemplified by recent outbreaks of ZIKV, DENV, and other arboviruses. The rapid spread and unpredictable nature of these pathogens highlight the urgent need for effective antiviral therapeutics. However, the traditional development of new drugs is a lengthy and resource-intensive process, often incompatible with the immediacy of epidemic responses. In this context, drug repurposing, the strategy of identifying new antiviral uses for compounds already developed or approved for other diseases, has emerged as a powerful complementary approach to the *de novo* synthesis of novel molecules. Repurposed drugs offer several advantages, including known safety profiles, established pharmacokinetics, and accelerated clinical translation. This strategy is particularly relevant for emerging viruses, for which time-efficient identification of effective treatments is essential. The present study aimed 1) to test anti ZIKV activity of an in-house library of compounds originally identified for their inhibitory effects on BVDB (Tab. 3) [129]; 2) to characterize compound PS1097, a pyrido[2,3-g] quinoxalinone, the compound with the highest efficacy, for its antiviral properties and mechanism of action.

Initial screening across a panel of RNA and DNA viruses revealed that PS1097 exhibited potent inhibitory effects against ZIKV, with EC_{50} values in the low micromolar range (approximately 0.6 µM in Huh-7 cells), while maintaining a favorable SI (Fig. 9). It was demonstrated to possess broad-spectrum antiviral activity, particularly against members of the *Flaviviridae* family, including ZIKV, WNV, and USUV. Activity against unrelated viruses, such as CHIKV, HSV-2 and IAV, was minimal or absent. This selective pattern supports the hypothesis that PS1097 acts on a cellular process specifically exploited by flaviviruses during replication, rather than on a universal viral function (Tab. 5). These findings position PS1097 as a promising lead compound for further development of host-targeted antiviral therapeutics.

In both Huh-7 and Vero E6 cells, PS1097 substantially reduced viral RNA and protein synthesis, confirming that the compound interferes with intracellular replication rather than virion release or entry (Fig. 11 and 12). In line with this conclusion, virucidal assays demonstrated that PS1097 does not directly inactivate viral particles, as viral infectivity remained unchanged after incubation with the compound in cell-free conditions (Fig. 16). Thus, the antiviral effect clearly depends on the intracellular environment, pointing toward a host-targeted mechanism.

TOA experiments indicated that PS1097 acts during the early stages of the ZIKV replication cycle, displaying a temporal inhibition profile similar to that of SOF. When administered up to 12 h post-infection, PS1097 maintained strong antiviral activity, suggesting interference with viral genome replication or the initial formation of replication complexes (Fig. 14). However, no direct interaction between PS1097 and viral enzymes could be detected, since CETSA assay revealed no detectable binding or stabilization of the viral RNA-dependent RNA polymerase NS5 or CV proteins (Fig. 17). Also, co-immunoprecipitation assays demonstrated that the NS3–NS2B protease complex remained stable in the presence of PS1097, excluding inhibition of protease assembly as a potential mechanism (Fig. 15). Together, these results indicate that PS1097 does not act as a classical direct-acting antiviral (DAA), but rather through modulation of host pathways essential for viral replication. An additional and significant observation emerged from the long-term passaging experiments conducted to select PS1097-resistant ZIKV variants. Despite multiple independent attempts, no resistant strains could be isolated, and viral replication progressively declined until complete extinction by the ninth passage. This contrasts sharply with the behavior observed for DAAs such as SOF, which readily induce resistance mutations under comparable conditions. The inability of the virus to develop resistance strongly suggests that PS1097 targets a cellular factor that is indispensable for viral replication and cannot be easily compensated by genetic adaptation. This feature constitutes a key advantage for therapeutic development, as it implies a high genetic barrier to resistance (Fig. 19).

Combination assays between PS1097 and SOF did not reveal any synergistic enhancement of antiviral activity. On the contrary, at higher concentrations, a mild antagonistic effect was consistently observed (Fig. 18). This suggests a possible functional interference between the two compounds, potentially due to overlapping or convergent modulation of host factors or metabolic pathways. The lack of synergy further supports the notion that PS1097 operates *via* a distinct, host-mediated mechanism and should therefore be considered primarily as a standalone therapeutic candidate rather than in combination with polymerase inhibitors.

The hypothesis of modulation by PS1097 of a host pathway was substantiated by its pronounced impact on ER-associated proteins. Among the ER-resident proteins analyzed, PS1097 induced a significant and selective downregulation of RTN3, a key structural component of ER tubule curvature and dynamics. Other ER proteins, such as RTN4, FAM134B, and TMEM41B, remained unaffected, indicating a specific rather than global disruption of ER homeostasis. RTN3 downregulation occurred at both the protein and transcript levels, with approximately a 50% reduction in mRNA abundance, although the magnitude of protein loss exceeded that explained by transcriptional effects alone. This suggests that PS1097 may enhance RTN3 degradation or inhibit its synthesis through post-transcriptional mechanisms (Fig. 20). The observed downregulation of RTN3 is particularly relevant in the context of flavivirus biology, as RTN3 has been implicated in the formation of replication organelles and the remodeling of ER membranes, a process critical for viral RNA replication [127]. Thus, the inhibition of RTN3 expression by PS1097 is likely to contributes to the disruption of viral replication sites and provides a plausible mechanistic explanation for its antiviral activity. Further experiments demonstrated that PS1097-induced RTN3 degradation does not occur via the canonical proteasomal pathway. Treatment with the proteasome inhibitor MG132 failed to restore RTN3 levels, indicating the involvement of an alternative degradation route, possibly autophagy-related or mediated by ER-associated quality control systems (Fig. 21). Cycloheximide chase assays revealed that RTN3 and FAM134B display comparable intrinsic half-lives under basal conditions, but only RTN3 was

destabilized following PS1097 exposure (Fig. 22). These findings reinforce the idea that PS1097 acts selectively on RTN3 turnover rather than globally suppressing protein synthesis.

Taken together, these findings establish PS1097 as a potent and selective antiviral compound with a novel host-targeted mechanism. By modulating the stability of RTN3, PS1097 may interferes with a cellular process that is essential for the replication of flaviviruses and potentially other ER-dependent RNA viruses. The absence of resistant mutants highlights the robustness of its antiviral effect and underscores its potential as a lead compound for future therapeutic development.

Nonetheless, further studies will aim to clarify the causal relationship between RTN3 downregulation and the antiviral activity of PS1097. To this end, experimental approaches involving RTN3 overexpression and gene knockout will be employed to assess whether modulation of RTN3 levels directly impacts viral replication efficiency. Comparing infection outcomes and RTN3 abundance in cells treated or not with PS1097 will provide critical insights into whether the compound's antiviral effect depends on RTN3 suppression or occurs through parallel host pathways. These experiments will be essential to validate RTN3 as a mechanistic determinant of PS1097 activity and to establish its potential as a novel host-targeted antiviral target. In addition, more research is necessary to elucidate the precise molecular mechanism underlying RTN3 modulation. Key questions remain regarding whether PS1097 directly binds to RTN3 or acts indirectly through regulatory pathways affecting ER homeostasis. Transcriptomic and proteomic analyses, combined with advanced imaging and functional assays, will be instrumental in clarifying this aspect. Additionally, in vivo studies are necessary to evaluate the pharmacokinetic properties, safety profile, and antiviral efficacy of PS1097 in animal models of flavivirus infection.

From a broader perspective, the identification of RTN3 as a host factor susceptible to pharmacological modulation opens new avenues in antiviral research. Targeting host factors involved in ER remodeling may represent a generalizable strategy to combat diverse viral pathogens that rely on the ER for replication, including

flaviviruses and coronaviruses. However, because such pathways are tightly intertwined with essential cellular functions, a detailed understanding of drug selectivity and cytotoxicity will be critical to balance efficacy and safety.

This work contributes to the growing body of evidence supporting host-directed antivirals as a viable alternative to classical, virus-targeted approaches. PS1097 exemplifies the potential of this strategy: it combines broad-spectrum activity, high potency, and a strong resistance barrier, while unveiling a previously underexplored host pathway as an antiviral target. Although still at an early stage of characterization, PS1097 represents a promising scaffold for further chemical optimization and mechanistic exploration. Its study not only advances our understanding of flavivirus–host interactions but also provides a conceptual framework for the development of next-generation antivirals aimed at essential host processes exploited by viruses.

8. BIBLIOGRAPHY

[1] Pielnaa P, Al-Saadawe M, Saro A, et al. Zika virus-spread, epidemiology, genome, transmission cycle, clinical manifestation, associated challenges, vaccine and antiviral drug development. Virology 2020;543:34–42. https://doi.org/10.1016/j.virol.2020.01.015.

[2] Brown CM, DeMaria A. The Resurgence of West Nile Virus. Ann Intern Med 2012;157:823–4. https://doi.org/10.7326/0003-4819-157-11-201212040-00543.

[3] Habarugira G, Suen WW, Hobson-Peters J, et al. West Nile Virus: An Update on Pathobiology, Epidemiology, Diagnostics, Control and "One Health" Implications. Pathogens 2020;9:589. https://doi.org/10.3390/pathogens9070589.

[4] https://www.genetex.com/Research/Overview/infectious_diseases/zika_virus?srsltid=AfmBOoqm-7d9bso9_r-He1SljlmEmdWzi_SxZSyoWqZQPsD5OSaT3dZ7 n.d.

[5] Kellman EM, Offerdahl DK, Melik W, et al. Viral Determinants of Virulence in Tick-Borne Flaviviruses. Viruses 2018;10:329. https://doi.org/10.3390/v10060329.

[6] Suthar MS, Diamond MS, Gale Jr M. West Nile virus infection and immunity. Nat Rev Microbiol 2013;11:115–28. https://doi.org/10.1038/nrmicro2950.

[7] Metsky HC, Matranga CB, Wohl S, et al. Zika virus evolution and spread in the Americas. Nature 2017;546:411–5. https://doi.org/10.1038/nature22402.

[8] MacNamara FN. Zika virus : A report on three cases of human infection during an epidemic of jaundice in Nigeria. Trans R Soc Trop Med Hyg 1954;48:139–45. https://doi.org/10.1016/0035-9203(54)90006-1.

[9] Duffy MR, Chen T-H, Hancock WT, et al. Zika Virus Outbreak on Yap Island, Federated States of Micronesia. New England Journal of Medicine 2009;360:2536–43. https://doi.org/10.1056/NEJMoa0805715.

[10] Fauci AS, Morens DM. Zika Virus in the Americas — Yet Another Arbovirus Threat. New England Journal of Medicine 2016;374:601–4. https://doi.org/10.1056/NEJMp1600297.

[11] Nicolas Calderon K, Fabian Galindo J, Bermudez-Santana CI. Evaluation of Conserved RNA Secondary Structures within and between Geographic Lineages of Zika Virus. Life (Basel) 2021;11. https://doi.org/10.3390/life11040344.

[12] Dick GWA, Kitchen SF, Haddow AJ. Zika Virus (I). Isolations and serological specificity. Trans R Soc Trop Med Hyg 1952;46:509–20. https://doi.org/10.1016/0035-9203(52)90042-4.

[13] Olson JG, Ksiazek TG, Suhandiman, et al. Zika virus, a cause of fever in Central Java, Indonesia. Trans R Soc Trop Med Hyg 1981;75:389–93. https://doi.org/10.1016/0035-9203(81)90100-0.

[14] Oehler E, Watrin L, Larre P, et al. Zika virus infection complicated by Guillain-Barré syndrome – case report, French Polynesia, December 2013. Eurosurveillance 2014;19. https://doi.org/10.2807/1560-7917.ES2014.19.9.20720.

[15] Musso D, Nilles EJ, Cao-Lormeau V-M. Rapid spread of emerging Zika virus in the Pacific area. Clinical Microbiology and Infection 2014;20:O595–6. https://doi.org/10.1111/1469-0691.12707.

[16] Ioos S, Mallet H-P, Leparc Goffart I, et al. Current Zika virus epidemiology and recent epidemics. Med Mal Infect 2014;44:302–7. https://doi.org/10.1016/j.medmal.2014.04.008.

[17] Boorman JPT, Porterfield JS. A simple technique for infection of mosquitoes with viruses transmission of zika virus. Trans R Soc Trop Med Hyg 1956;50:238–42. https://doi.org/10.1016/0035-9203(56)90029-3.

[18] Oliveira Melo AS, Malinger G, Ximenes R, et al. Zika virus intrauterine infection causes fetal brain abnormality and microcephaly: tip of the iceberg? Ultrasound in Obstetrics & Gynecology 2016;47:6–7. https://doi.org/10.1002/uog.15831.

[19] Besnard M, Lastère S, Teissier A, et al. Evidence of perinatal transmission of Zika virus, French Polynesia, December 2013 and February 2014. Eurosurveillance 2014;19. https://doi.org/10.2807/1560-7917.ES2014.19.13.20751.

[20] Musso D, Roche C, Robin E, et al. Potential Sexual Transmission of Zika Virus. Emerg Infect Dis 2015;21:359–61. https://doi.org/10.3201/eid2102.141363.

[21] Musso D, Nhan T, Robin E, et al. Potential for Zika virus transmission through blood transfusion demonstrated during an outbreak in French Polynesia, November 2013 to February 2014. Eurosurveillance 2014;19. https://doi.org/10.2807/1560-7917.ES2014.19.14.20761.

[22] Diallo D, Sall AA, Diagne CT, et al. Zika Virus Emergence in Mosquitoes in Southeastern Senegal, 2011. PLoS One 2014;9:e109442. https://doi.org/10.1371/journal.pone.0109442.

[23] Plourde AR, Bloch EM. A Literature Review of Zika Virus. Emerg Infect Dis 2016;22:1185–92. https://doi.org/10.3201/eid2207.151990.

[24] http://www.who.int/emergencies/zika-virus/situation-report/5- february-2016/en/ n.d.

[25] http://www.cdc.gov/zika/pdfs/denvchikvzikv-testing-algorithm.pdf n.d.

[26] Gourinat A-C, O'Connor O, Calvez E, et al. Detection of Zika Virus in Urine. Emerg Infect Dis 2015;21:84–6. https://doi.org/10.3201/eid2101.140894.

[27] Musso D, Roche C, Nhan T-X, et al. Detection of Zika virus in saliva. Journal of Clinical Virology 2015;68:53–5. https://doi.org/10.1016/j.jcv.2015.04.021.

[28] Petersen LR, Brault AC, Nasci RS. West Nile Virus: Review of the Literature. JAMA 2013;310:308. https://doi.org/10.1001/jama.2013.8042.

[29] Gould C V., Staples JE, Guagliardo SAJ, et al. West Nile Virus: a review. JAMA 2025;334:618. https://doi.org/10.1001/jama.2025.8737.

[30] Reisen W. Ecology of West Nile Virus in North America. Viruses 2013;5:2079–105. https://doi.org/10.3390/v5092079.

[31] Nash D, Mostashari F, Fine A, et al. The Outbreak of West Nile Virus Infection in the New York City Area in 1999. New England Journal of Medicine 2001;344:1807–14. https://doi.org/10.1056/NEJM200106143442401.

[32] https://www.epicentro.iss.it/westnile/bollettino n.d.

[33] Dauphin G, Zientara S, Zeller H, et al. West Nile: worldwide current situation in animals and humans. Comp Immunol Microbiol Infect Dis 2004;27:343–55. https://doi.org/10.1016/j.cimid.2004.03.009.

[34] SBRANA E, TONRY JH, XIAO S-Y, et al. ORAL TRANSMISSION OF WEST NILE VIRUS IN A HAMSTER MODEL. Am J Trop Med Hyg 2005;72:325–9. https://doi.org/10.4269/ajtmh.2005.72.325.

[35] Clé M, Beck C, Salinas S, et al. Usutu virus: A new threat? Epidemiol Infect 2019;147:e232. https://doi.org/10.1017/S0950268819001213.

[36] Andersen KG, Rambaut A, Lipkin WI, et al. The proximal origin of SARS-CoV-2. Nat Med 2020;26:450–2. https://doi.org/10.1038/s41591-020-0820-9.

[37] Xiao K, Zhai J, Feng Y, et al. Isolation of SARS-CoV-2-related coronavirus from Malayan pangolins. Nature 2020;583:286–9. https://doi.org/10.1038/s41586-020-2313-x.

[38] Wang MY, Zhao R, Gao LJ, et al. SARS-CoV-2: Structure, Biology, and Structure-Based Therapeutics Development. Front Cell Infect Microbiol 2020;10. https://doi.org/10.3389/fcimb.2020.587269.

[39] Sternberg A, Naujokat C. Structural features of coronavirus SARS-CoV-2 spike protein: Targets for vaccination. Life Sci 2020;257. https://doi.org/10.1016/j.lfs.2020.118056.

[40] Jafarzadeh A, Nemati M, Jafarzadeh S. Contribution of STAT3 to the pathogenesis of COVID-19. Microb Pathog 2021;154:104836. https://doi.org/10.1016/j.micpath.2021.104836.

[41] Canedo-Marroquín G, Saavedra F, Andrade CA, et al. SARS-CoV-2: Immune Response Elicited by Infection and Development of Vaccines and Treatments. Front Immunol 2020;11. https://doi.org/10.3389/fimmu.2020.569760.

[42] Park KS, Sun X, Aikins ME, et al. Non-viral COVID-19 vaccine delivery systems. Adv Drug Deliv Rev 2021;169:137–51. https://doi.org/10.1016/j.addr.2020.12.008.

[43] Mascellino MT, Di Timoteo F, De Angelis M, et al. Overview of the Main Anti-SARS-CoV-2 Vaccines: Mechanism of Action, Efficacy and Safety. Infect Drug Resist 2021;Volume 14:3459–76. https://doi.org/10.2147/IDR.S315727.

[44] de Lima Cavalcanti TYV, Pereira MR, de Paula SO, et al. A Review on Chikungunya Virus Epidemiology, Pathogenesis and Current Vaccine Development. Viruses 2022;14:969. https://doi.org/10.3390/v14050969.

[45] Fontana S, Fiore S, Buttinelli G, et al. Molecular Characterization of Coxsackievirus B5 Isolates from Sewage, Italy 2016–2017. Food Environ Virol 2019;11:440–5. https://doi.org/10.1007/s12560-019-09395-z.

[46] Green J, Casabonne D, Newton R. Coxsackie B virus serology and Type 1 diabetes mellitus: a systematic review of published case-control studies. Diabetic Medicine 2004;21:507–14. https://doi.org/10.1111/j.1464-5491.2004.01182.x.

[47] Sin J, Mangale V, Thienphrapa W, et al. Recent progress in understanding coxsackievirus replication, dissemination, and pathogenesis. Virology 2015;484:288–304. https://doi.org/10.1016/j.virol.2015.06.006.

[48] Yang P, Shi D, Fu J, et al. Atomic Structures of Coxsackievirus B5 Provide Key Information on Viral Evolution and Survival. J Virol 2022;96. https://doi.org/10.1128/jvi.00105-22.

[49] Andreoni AR, Colton AS. Coxsackievirus B5 associated with hand-foot-mouth disease in a healthy adult. JAAD Case Rep 2017;3:165–8. https://doi.org/10.1016/j.jdcr.2017.01.026.

[50] Ayhan N, Eldin C, Charrel R. Toscana virus: A comprehensive review of 1381 cases showing an emerging threat in the Mediterranean regions. Journal of Infection 2025;90:106415. https://doi.org/10.1016/j.jinf.2025.106415.

[51] Keskek Turk Y, Ergunay K, Kohl A, et al. Toscana virus – an emerging Mediterranean arbovirus transmitted by sand flies. Journal of General Virology 2024;105. https://doi.org/10.1099/jgv.0.002045.

[52] Fotakis EA, Di Maggio E, Del Manso M, et al. Human neuroinvasive Toscana virus infections in Italy from 2016 to 2023: Increased incidence in 2022 and 2023. Eurosurveillance 2025;30. https://doi.org/10.2807/1560-7917.ES.2025.30.2.2400203.

[53] Palese P. Influenza: old and new threats. Nat Med 2004;10:S82–7. https://doi.org/10.1038/nm1141.

[54] Hastie E, Cataldi M, Marriott I, et al. Understanding and altering cell tropism of vesicular stomatitis virus. Virus Res 2013;176:16–32. https://doi.org/10.1016/j.virusres.2013.06.003.

[55] Black BL, Lyles DS. Vesicular stomatitis virus matrix protein inhibits host cell-directed transcription of target genes in vivo. J Virol 1992;66:4058–64. https://doi.org/10.1128/jvi.66.7.4058-4064.1992.

[56] Ahmed MM, Okesanya OJ, Ukoaka BM, et al. Vesicular Stomatitis Virus: Insights into Pathogenesis, Immune Evasion, and Technological Innovations in Oncolytic and Vaccine Development. Viruses 2024;16:1933. https://doi.org/10.3390/v16121933.

[57] Zhu S, Viejo-Borbolla A. Pathogenesis and virulence of herpes simplex virus. Virulence 2021;12:2670–702. https://doi.org/10.1080/21505594.2021.1982373.

[58] Omarova S, Cannon A, Weiss W, et al. Genital Herpes Simplex Virus—An Updated Review. Adv Pediatr 2022;69:149–62. https://doi.org/10.1016/j.yapd.2022.03.010.

[59] Sun H, Chen X, Wang Y. Strategies for the Modification of Vaccinia Virus towards a Better Vaccine Vector. Zoonoses 2025;5. https://doi.org/10.15212/ZOONOSES-2024-0044.

[60] Mackett M, Yilma T, Rose JK, et al. Vaccinia Virus Recombinants: Expression of VSV Genes and Protective Immunization of Mice and Cattle. Science (1979) 1985;227:433–5. https://doi.org/10.1126/science.2981435.

[61] den Boon JA, Nishikiori M, Zhan H, et al. Positive-strand RNA virus genome replication organelles: structure, assembly, control. Trends in Genetics 2024;40:681–93. https://doi.org/10.1016/j.tig.2024.04.003.

[62] Klein S, Cortese M, Winter SL, et al. SARS-CoV-2 structure and replication characterized by in situ cryo-electron tomography. Nat Commun 2020;11:5885. https://doi.org/10.1038/s41467-020-19619-7.

[63] Neufeldt CJ, Cortese M, Acosta EG, et al. Rewiring cellular networks by members of the Flaviviridae family. Nat Rev Microbiol 2018;16:125–42. https://doi.org/10.1038/nrmicro.2017.170.

[64] Mazeaud C, Anton A, Pahmeier F, et al. The Biogenesis of Dengue Virus Replication Organelles Requires the ATPase Activity of Valosin-Containing Protein. Viruses 2021;13:2092. https://doi.org/10.3390/v13102092.

[65] Zhang J, Lan Y, Sanyal S. Membrane heist: Coronavirus host membrane remodeling during replication. Biochimie 2020;179:229–36. https://doi.org/10.1016/j.biochi.2020.10.010.

[66] Stancheva VG, Sanyal S. Positive-strand RNA virus replication organelles at a glance. J Cell Sci 2024;137. https://doi.org/10.1242/jcs.262164.

[67] Caragliano E, Brune W, Bosse JB. Herpesvirus Replication Compartments: Dynamic Biomolecular Condensates? Viruses 2022;14:960. https://doi.org/10.3390/v14050960.

[68] Tolonen N, Doglio L, Schleich S, et al. Vaccinia Virus DNA Replication Occurs in Endoplasmic Reticulum-enclosed Cytoplasmic Mini-Nuclei. Mol Biol Cell 2001;12:2031–46. https://doi.org/10.1091/mbc.12.7.2031.

[69] Heinrich BS, Maliga Z, Stein DA, et al. Phase Transitions Drive the Formation of Vesicular Stomatitis Virus Replication Compartments. MBio 2018;9. https://doi.org/10.1128/mBio.02290-17.

[70] den Boon JA, Diaz A, Ahlquist P. Cytoplasmic Viral Replication Complexes. Cell Host Microbe 2010;8:77–85. https://doi.org/10.1016/j.chom.2010.06.010.

[71] Shaw ML, Stone KL, Colangelo CM, et al. Cellular Proteins in Influenza Virus Particles. PLoS Pathog 2008;4:e1000085. https://doi.org/10.1371/journal.ppat.1000085.

[72] Westrate LM, Lee JE, Prinz WA, et al. Form Follows Function: The Importance of Endoplasmic Reticulum Shape. Annu Rev Biochem 2015;84:791–811. https://doi.org/10.1146/annurev-biochem-072711-163501.

[73] Yang YS, Strittmatter SM. The reticulons: a family of proteins with diverse functions. Genome Biol 2007;8:234. https://doi.org/10.1186/gb-2007-8-12-234.

[74] Li J, Abosmaha E, Coffin CS, et al. Reticulon-3 modulates the incorporation of replication competent hepatitis C virus molecules for release inside infectious exosomes. PLoS One 2020;15:e0239153. https://doi.org/10.1371/journal.pone.0239153.

[75] Chiurchiù V, Maccarrone M, Orlacchio A. The Role of Reticulons in Neurodegenerative Diseases. Neuromolecular Med 2014;16:3–15. https://doi.org/10.1007/s12017-013-8271-9.

[76] Wang X, Jiang X, Li B, et al. A regulatory circuit comprising the CBP and SIRT7 regulates FAM134B-mediated ER-phagy. Journal of Cell Biology 2023;222. https://doi.org/10.1083/jcb.202201068.

[77] Hoffmann H-H, Schneider WM, Rozen-Gagnon K, et al. TMEM41B Is a Pan-flavivirus Host Factor. Cell 2021;184:133-148.e20. https://doi.org/10.1016/j.cell.2020.12.005.

[78] Moretti F, Bergman P, Dodgson S, et al. TMEM41B is a novel regulator of autophagy and lipid mobilization. EMBO Rep 2018;19. https://doi.org/10.15252/embr.201845889.

[79] Monel B, Rajah MM, Hafirassou ML, et al. Atlastin Endoplasmic Reticulum-Shaping Proteins Facilitate Zika Virus Replication. J Virol 2019;93. https://doi.org/10.1128/JVI.01047-19.

[80] Chino H, Mizushima N. ER-Phagy: Quality Control and Turnover of Endoplasmic Reticulum. Trends Cell Biol 2020;30:384–98. https://doi.org/10.1016/j.tcb.2020.02.001.

[81] Jheng J-R, Ho J-Y, Horng J-T. ER stress, autophagy, and RNA viruses. Front Microbiol 2014;5. https://doi.org/10.3389/fmicb.2014.00388.

[82] Yu C-Y, Hsu Y-W, Liao C-L, et al. Flavivirus Infection Activates the XBP1 Pathway of the Unfolded Protein Response To Cope with Endoplasmic Reticulum Stress. J Virol 2006;80:11868–80. https://doi.org/10.1128/JVI.00879-06.

[83] BlÃ¡zquez A-B, Escribano-Romero E, Merino-Ramos T, et al. Stress responses in flavivirus-infected cells: activation of unfolded protein response and autophagy. Front Microbiol 2014;5. https://doi.org/10.3389/fmicb.2014.00266.

[84] Wong HH, Sanyal S. Manipulation of autophagy by (+) RNA viruses. Semin Cell Dev Biol 2020;101:3–11. https://doi.org/10.1016/j.semcdb.2019.07.013.

[85] Beran RK, Vijjapurapu A, Nair V, et al. Host-targeted antivirals as broad-spectrum inhibitors of respiratory viruses. Curr Opin Virol 2025;73:101492. https://doi.org/10.1016/j.coviro.2025.101492.

[86] Alazard-Dany N, Denolly S, Boson B, et al. Overview of HCV Life Cycle with a Special Focus on Current and Possible Future Antiviral Targets. Viruses 2019;11:30. https://doi.org/10.3390/v11010030.

[87] Delemos A, Noell B, Besur S. Changing the face of hepatitis C management – the design and development of sofosbuvir. Drug Des Devel Ther 2015:2367. https://doi.org/10.2147/DDDT.S65255.

[88] Geddawy A, Ibrahim YF, Elbahie NM, et al. Direct acting anti-hepatitis C virus drugs: Clinical pharmacology and future direction. J Transl Int Med 2017;5:8–17. https://doi.org/10.1515/jtim-2017-0007.

[89] Pawlotsky J-M. What are the pros and cons of the use of host-targeted agents against hepatitis C? Antiviral Res 2014;105:22–5. https://doi.org/10.1016/j.antiviral.2014.02.008.

[90] de León P, Cañas-Arranz R, Bustos MJ, et al. Inhibition of Human Coronaviruses by Combinations of Host-Targeted and Direct-Acting Antivirals. Antimicrob Agents Chemother 2023;67. https://doi.org/10.1128/aac.01703-22.

[91] Anasir MI, Ramanathan B, Poh CL. Structure-Based Design of Antivirals against Envelope Glycoprotein of Dengue Virus. Viruses 2020;12:367. https://doi.org/10.3390/v12040367.

[92] Kiemel D, Kroell A-SH, Denolly S, et al. Pan-serotype dengue virus inhibitor JNJ-A07 targets NS4A-2K-NS4B interaction with NS2B/NS3 and blocks replication organelle formation. Nat Commun 2024;15:6080. https://doi.org/10.1038/s41467-024-50437-3.

[93] Tripathi A, Chauhan S, Khasa R. A Comprehensive Review of the Development and Therapeutic Use of Antivirals in Flavivirus Infection. Viruses 2025;17:74. https://doi.org/10.3390/v17010074.

[94] Zelikin AN, Stellacci F. Broad-Spectrum Antiviral Agents Based on Multivalent Inhibitors of Viral Infectivity. Adv Healthc Mater 2021;10. https://doi.org/10.1002/adhm.202001433.

[95] Ma L, Li Q, Xie Y, et al. Repurposing of HIV/HCV protease inhibitors against SARS-CoV-2 3CLpro. Antiviral Res 2022;207:105419. https://doi.org/10.1016/j.antiviral.2022.105419.

[96] Piras S, Sanna G, Carta A, et al. Dichloro-Phenyl-Benzotriazoles: A New Selective Class of Human Respiratory Syncytial Virus Entry Inhibitors. Front Chem 2019;7. https://doi.org/10.3389/fchem.2019.00247.

[97] Ibba R, Corona P, Nonne F, et al. Design, Synthesis, and Antiviral Activities of New Benzotriazole-Based Derivatives. Pharmaceuticals 2023;16:429. https://doi.org/10.3390/ph16030429.

[98] Carta A, Briguglio I, Piras S, et al. A combined in silico / in vitro approach unveils common molecular requirements for efficient BVDV RdRp binding of linear aromatic N-polycyclic systems. Eur J Med Chem 2016;117:321–34. https://doi.org/10.1016/j.ejmech.2016.03.080.

[99] Carta A, Briguglio I, Piras S, et al. Quinoline tricyclic derivatives. Design, synthesis and evaluation of the antiviral activity of three new classes of RNA-dependent RNA polymerase inhibitors. Bioorg Med Chem 2011;19:7070–84. https://doi.org/10.1016/j.bmc.2011.10.009.

[100] Briguglio I, Loddo R, Laurini E, et al. Synthesis, cytotoxicity and antiviral evaluation of new series of imidazo[4,5-g]quinoline and pyrido[2,3-g]quinoxalinone derivatives. Eur J Med Chem 2015;105:63–79. https://doi.org/10.1016/j.ejmech.2015.10.002.

[101] Gardinali NR, Marchevsky RS, Oliveira JM, et al. Sofosbuvir shows a protective effect against vertical transmission of Zika virus and the associated congenital syndrome in rhesus monkeys. Antiviral Res 2020;182:104859. https://doi.org/10.1016/j.antiviral.2020.104859.

[102] Nakabayashi H, Taketa K, Miyano K, et al. Growth of human hepatoma cells lines with differentiated functions in chemically defined medium. Cancer Res 1982;42:3858–63.

[103] Storti B, Quaranta P, Di Primio C, et al. A spatial multi-scale fluorescence microscopy toolbox discloses entry checkpoints of SARS-CoV-2 variants in Vero E6 cells. Comput Struct Biotechnol J 2021;19:6140–56. https://doi.org/10.1016/j.csbj.2021.10.038.

[104] Lai M, Iacono E, Spezia PG, et al. A low-cost simple test for weekly detection of Mycoplasma hyorhinis and arginini contaminations in cell cultures and viral preparations. J Virol Methods 2022;299:114327. https://doi.org/10.1016/j.jviromet.2021.114327.

[105] Mackett M, Yilma T, Rose JK, et al. Vaccinia Virus Recombinants: Expression of VSV Genes and Protective Immunization of Mice and Cattle. Science (1979) 1985;227:433–5. https://doi.org/10.1126/science.2981435.

[106] Feoktistova M, Geserick P, Leverkus M. Crystal Violet Assay for Determining Viability of Cultured Cells. Cold Spring Harb Protoc 2016;2016:pdb.prot087379. https://doi.org/10.1101/pdb.prot087379.

[107] Prichard MN, Turk SR, Coleman LA, et al. A microtiter virus yield reduction assay for the evaluation of antiviral compounds against human cytomegalovirus and herpes simplex virus. J Virol Methods 1990;28:101–6. https://doi.org/10.1016/0166-0934(90)90091-S.

[108] Frias-De-Diego A, Crisci E. Use of Crystal Violet to Improve Visual Cytopathic Effect-based Reading for Viral Titration using TCID50 Assays. Journal of Visualized Experiments 2022. https://doi.org/10.3791/63063.

[109] Daelemans D, Pauwels R, De Clercq E, et al. A time-of–drug addition approach to target identification of antiviral compounds. Nat Protoc 2011;6:925–33. https://doi.org/10.1038/nprot.2011.330.

[110] Sun J, Zhao W, Zhang L, et al. Centromere protein U mediates the ubiquitination and degradation of RPS3 to facilitate temozolomide resistance in glioblastoma. Drug Resistance Updates 2025;80:101214. https://doi.org/10.1016/j.drup.2025.101214.

[111] Jafari R, Almqvist H, Axelsson H, et al. The cellular thermal shift assay for evaluating drug target interactions in cells. Nat Protoc 2014;9:2100–22. https://doi.org/10.1038/nprot.2014.138.

[112] Kaptein SJF, Goethals O, Kiemel D, et al. A pan-serotype dengue virus inhibitor targeting the NS3–NS4B interaction. Nature 2021;598:504–9. https://doi.org/10.1038/s41586-021-03990-6.

[113] Roth NM, Reynolds MR, Lewis EL, et al. Zika-Associated Birth Defects Reported in Pregnancies with Laboratory Evidence of Confirmed or Possible Zika Virus Infection — U.S. Zika Pregnancy and Infant Registry, December 1, 2015–March 31, 2018. MMWR Morb Mortal Wkly Rep 2022;71:73–9. https://doi.org/10.15585/mmwr.mm7103a1.

[114] Carta A, Loriga M, Paglietti G, et al. Design, synthesis, and preliminary in vitro and in silico antiviral activity of [4,7]phenantrolines and 1-oxo-1,4-dihydro-

[4,7]phenantrolines against single-stranded positive-sense RNA genome viruses. Bioorg Med Chem 2007;15:1914–27. https://doi.org/10.1016/j.bmc.2007.01.005.

[115] Carta A, Loriga M, Piras S, et al. Synthesis and Anti-Picornaviridae In Vitro Activity of a New Class of Helicase Inhibitors the N,N-bis[4-(1H(2H)-benzotriazol-1(2)-yl)phenyl] alkyldicarboxamides. Med Chem (Los Angeles) 2007;3:520–32. https://doi.org/10.2174/157340607782360308.

[116] Piras S, Corona P, Ibba R, et al. Preliminary Anti-Coxsackie Activity of Novel 1-[4-(5,6-dimethyl(H)- 1H(2H)-benzotriazol-1(2)-yl)phenyl]-3-alkyl(aryl)ureas. Med Chem (Los Angeles) 2020;16:677–88. https://doi.org/10.2174/1573406416666191226142744.

[117] Ibba R, Piras S, Corona P, et al. Synthesis, Antitumor and Antiviral In Vitro Activities of New Benzotriazole-Dicarboxamide Derivatives. Front Chem 2021;9. https://doi.org/10.3389/fchem.2021.660424.

[118] Mumtaz N, Jimmerson LC, Bushman LR, et al. Cell-line dependent antiviral activity of sofosbuvir against Zika virus. Antiviral Res 2017;146:161–3. https://doi.org/10.1016/j.antiviral.2017.09.004.

[119] Dragoni F, Boccuto A, Picarazzi F, et al. Evaluation of sofosbuvir activity and resistance profile against West Nile virus in vitro. Antiviral Res 2020;175:104708. https://doi.org/10.1016/j.antiviral.2020.104708.

[120] Tan YB, Chmielewski D, Law MCY, et al. Molecular architecture of the Chikungunya virus replication complex. Sci Adv 2022;8. https://doi.org/10.1126/sciadv.add2536.

[121] Wu M-J, Ke P-Y, Hsu JT-A, et al. Reticulon 3 interacts with NS4B of the hepatitis C virus and negatively regulates viral replication by disrupting NS4B self-interaction. Cell Microbiol 2014;16:1603–18. https://doi.org/10.1111/cmi.12318.

[122] Voeltz GK, Sawyer EM, Hajnóczky G, et al. Making the connection: How membrane contact sites have changed our view of organelle biology. Cell 2024;187:257–70. https://doi.org/10.1016/j.cell.2023.11.040.

[123] Wilson A, McCormick C. Reticulophagy and viral infection. Autophagy 2025;21:3–20. https://doi.org/10.1080/15548627.2024.2414424.

[124] Rämö O, Kumar D, Gucciardo E, et al. NOGO-A/RTN4A and NOGO-B/RTN4B are simultaneously expressed in epithelial, fibroblast and neuronal cells and maintain ER morphology. Sci Rep 2016;6:35969. https://doi.org/10.1038/srep35969.

[125] Khaminets A, Heinrich T, Mari M, et al. Regulation of endoplasmic reticulum turnover by selective autophagy. Nature 2015;522:354–8. https://doi.org/10.1038/nature14498.

[126] Hoffmann H-H, Schneider WM, Rozen-Gagnon K, et al. TMEM41B Is a Pan-flavivirus Host Factor. Cell 2021;184:133-148.e20. https://doi.org/10.1016/j.cell.2020.12.005.

[127] Aktepe TE, Liebscher S, Prier JE, et al. The Host Protein Reticulon 3.1A Is Utilized by Flaviviruses to Facilitate Membrane Remodelling. Cell Rep 2017;21:1639–54. https://doi.org/10.1016/j.celrep.2017.10.055.

[128] Mo J, Chen J, Zhang B. Critical roles of FAM134B in ER-phagy and diseases. Cell Death Dis 2020;11:983. https://doi.org/10.1038/s41419-020-03195-1.

[129] Briguglio I, Loddo R, Laurini E, et al. Synthesis, cytotoxicity and antiviral evaluation of new series of imidazo[4,5-g]quinoline and pyrido[2,3-g]quinoxalinone derivatives. Eur J Med Chem 2015;105:63–79. https://doi.org/10.1016/j.ejmech.2015.10.002.